NUMERICAL MODELING OF ATLANTIC HURRICANES MOVING INTO THE MIDDLE LATITUDES

by

Christopher T. Fogarty

Submitted in partial fulfillment of the requirements
for the degree of Doctor of Philosophy

at

Dalhousie University
Halifax, Nova Scotia
March 2006

Your file Votre référence
ISBN: 978-0-494-16681-9
Our file Notre référence
ISBN: 978-0-494-16681-9

DALHOUSIE UNIVERSITY

To comply with the Canadian Privacy Act the National Library of Canada has requested that the following pages be removed from this copy of the thesis:

Preliminary Pages
- Examiners Signature Page (pii)
- Dalhousie Library Copyright Agreement (piii)

Appendices
- Copyright Releases (if applicable)

TABLE OF CONTENTS

LIST OF TABLES

LIST OF FIGURES

ABSTRACT

Hurricanes that form over the Atlantic Ocean very frequently migrate into the middle latitudes where they encounter very different oceanic and atmospheric conditions than in the tropics. Cool sea surface temperatures (SSTs) cause these storms to weaken and become thermodynamically decoupled from the ocean, while baroclinic atmospheric environments often cause them to transform into extratropical storms — a process known as extratropical transition (ET). The changing structure of these storms in the middle latitudes presents many unique forecasting challenges related to the increasing asymmetry in moisture and wind fields, and their potentially destructive nature.

An examination of three such events over Eastern Canada — using a combination of observations and a numerical model — forms the foundation of this work, with an emphasis on applying the research to weather forecasting. The case studies include Hurricane Michael (2000), Hurricane Karen (2001) and Hurricane Juan (2003). Hurricane Michael intensified in a strongly-baroclinc environment and evolved into an intense extratropical storm over Newfoundland. Karen also underwent ET, but weakened quickly during its approach to Nova Scotia, while Hurricane Juan struck the province as a category-two hurricane, experiencing only marginal weakening over anomalously warm SSTs. In essence, these cases represent a cross section of the behavior of many tropical cyclones in this part of the world.

Hindcast simulations are conducted for each event using the Canadian Mesoscale Compressible Community (MC2) model with a synthetic, observationally-consistent

hurricane vortex used in the model's initial conditions. Sensitivity experiments are run for each case by modifying initial specifications of the vortex, model physics parameterizations, and surface boundary conditions like SST. In the case of Hurricane Juan, it is determined that the anomalously-warm SSTs played a significant role in the landfall intensity, while Hurricane Michael was not particularly sensitive to small anomalies of the SSTs. Experiments conducted on Hurricane Karen reveal that the storm's landfalling intensity is not particularly sensitive to its intensity prior to traversing the cool waters south of Nova Scotia. A significant improvement in the storm structure was observed in all three cases compared with numerical models that did not employ vortex insertion.

ACKNOWLEDGEMENTS

I would like to thank my supervisors, Drs. Richard Greatbatch and Hal Ritchie for their support and guidance during this project, as well as Drs. Jinyu Sheng and Tom Duck for their reviews during the preparation of this thesis. Their positive feedback and discussions are greatly appreciated. I also appreciate many of the thought-provoking and enlightening discussions with my friend and research colleague, Doug Mercer. I would like to thank those who have helped setting up the modeling system and for technical support throughout the course of this project. They include Serge Desjardins, Weiqing Zhang, Mike Casey, Stephane Chamberland, Yves Chartier, Michel Desgagne, Pierre Pellerin, Bruce Brasnett, Ron McTaggart-Cowan, and Rick Danielson. This project has received funding from the Meteorological Service of Canada (MSC), the NSERC/MARTEC/MSC Industrial Research Chair, and a project grant from the Canadian Foundation for Climate and Atmospheric Sciences. I am also grateful to the MSC for providing access to the supercomputer facility in Dorval, Quebec, where the model runs were carried out.

CHAPTER 1

Introduction

1.1 Overview

Tropical cyclones (TCs) are powerful storms that form in the tropical or subtropical latitudes of several ocean basins throughout the world, including the North Atlantic Ocean. In this basin, these storms threaten a very large area spanning the Caribbean, Gulf of Mexico, the Eastern Seaboard of the United States and eastern Canada. Figure 1 shows the tracks of all TCs of hurricane strength from 1886-1996 in the Atlantic Basin (Elsner and Kara 1999). Almost half of the TCs that form in the Atlantic Basin undergo extratropical transition (ET) to a baroclinic (frontal), mid-latitude, cyclone (Hart and Evans 2001), prolonging the overall lifespan of the storms to about 11 days (Fogarty and Gyakum 2005). These long-lived storms occasionally travel as far east as Western Europe.

When TCs move into the mid-latitudes, they generally weaken as a consequence of increasing wind shear, encountering cool sea surface temperatures (SSTs) or making landfall. However, approximately 50% of extratropically-transitioning cyclones experience some reintensification after transition (Hart and Evans 2001), but rarely become more intense than during their tropical phase. Although the absolute intensity (as measured by the maximum surface winds in the storm) typically decreases, the impact zone increases (Jones et al. 2003). During ET the wind field expands and becomes markedly asymmetric, with strongest winds typically occurring on the right-hand side of

the storm relative to its motion. Heavy rainfall often becomes displaced to the left-hand side of the storm (e.g. Atallah and Bosart 2003; Colle 2003) and can extend for hundreds of kilometers ahead of the storm if the system is interacting with a baroclinic zone. A schematic showing basic meteorological features associated with a TC undergoing ET is shown in Fig. 2.

Most TCs migrating to the mid-latitudes undergo some form of ET, but the latitude, duration and nature of the transition is highly variable and largely dependent on the synoptic scale weather pattern into which the TC is moving (e.g. McTaggart-Cowan et al. 2001; Klein et al. 2000; Ma et al. 2003). For example, Hurricane Juan in September of 2003 had migrated significantly far north of the tropics when it struck Nova Scotia (see Fig. 3 reference map) and did not undergo ET (develop fronts) until it reached ~50°N. Juan was contained within a large-scale, deep-tropospheric ridge pattern. Hurricane Michael, on the other hand, underwent rapid ET and reintensification in October 2000 between 40°N and 50°N when a mid-latitude trough merged with the hurricane. In October of 2001, rapidly weakening Tropical Storm Karen was undergoing ET as it crossed Nova Scotia well ahead of a cold front to the west. Extratropical transition for these events is objectively defined using the cyclone phase space analysis developed by Evans and Hart (2003) and applied to a cluster analysis of ETs by Arnott et al. (2004). These storms represent a sample of greatly differing intensity and structural changes occurring in TCs that move into the mid-latitudes, and are the focus of the present work.

1.2 Motivation

Since the late 1990s there has been a growing amount of research on the changing dynamics of TCs moving into the mid-latitudes and undergoing ET. Much of the interest stems from the need to improve forecasts and warnings for these events (Jones et al. 2003). Our understanding of purely tropical and purely extratropical cyclones (ECs) is well developed, but more research is necessary to improve our understanding of how TCs evolve into ECs. Numerical weather models traditionally have difficulty simulating ET because they are often tuned to either the tropical or extratropical environment. The structural evolution of a TC moving into the mid-latitudes is particularly sensitive to the movement and positioning of synoptic-scale troughs and ridges in the pressure pattern, and to the size, strength, and position of the TC (McTaggart-Cowan et al. 2001, 2004; Klein et al. 2002; Ritchie and Elsberry 2003).

Specific forecast challenges related to ET (or TCs moving into the mid-latitudes in general) are well documented by Jones et al. (2003). It is difficult to forecast when the storm is going to accelerate, which can enhance surface winds and lead to trapped fetch oceanic wave growth (Bowyer and MacAfee 2005). It is also challenging to predict the timing and rate of sea level pressure expansion. The forecast is further complicated by uncertainty in the contributions of changing energetics that fuel the storm. As the TC moves over colder SSTs, it usually weakens, but the weakening rate depends on the value of the SSTs beneath it (Fogarty et al. 2006) and whether the storm is tapping baroclinic energy that may be present in the mid-latitude environment. Very often the strong low-

level winds in the TC will become decoupled from the surface, resulting in significant low-level wind shear (Abraham et al. 2004). The magnitude and location of decoupling further complicates the wind field forecast, which in turn affects the sea state and storm surge forecasts.

Predicting rainfall associated with a TC is very difficult because TCs often merge with frontal zones in the mid-latitudes that enhance rainfall, which can lead to flooding, especially when the front becomes stationary. The forward speed of motion is important to know in order to anticipate rainfall – fast moving storms will produce less rainfall at a point than slow moving ones. Dry air entrainment or shear-induced subsidence (Zhang and Kieu 2005) in the upstream sector of these storms can lead to depletion of convection, consequently reducing rainfalls.

To improve our understanding of these events we need (a) more observations (aircraft and surface weather data), and (b) to run numerical simulations of individual storms (at various scales) to simulate and predict their behavior. The Meteorological Service of Canada (MSC) has conducted a handful of research flights since 2000 using a research aircraft to address (a). During these flights, large amounts of in-situ flight-level data and Global Positioning System (GPS) dropsonde data were collected. Abraham et al. (2004) present some unique findings from the first of these flights into Hurricane Michael in 2000. These data are used to validate numerical simulations in this study.

As of 2005, there exists no specialized numerical forecasting capacity in Canada to address the operational prediction of TCs other than the mesoscale model used in this work, running experimentally on a case-by-case basis. Operational forecasts are prepared at the Canadian Hurricane Centre (CHC) using a combination of track/intensity forecasts from numerical models operated by other agencies, as well as forecaster expertise. Operations would benefit from having an in-house numerical model. It would help forecasters visualize structural changes taking place in the storm, which could lead to refinements in the conventional intensity/track forecasts.

1.3 Approach

A state-of-the-art atmospheric model (Mesoscale Compressible Community (MC2) model) is used to conduct simulations of three cases of TCs (introduced above) moving into eastern regions of Canada. The TC initial conditions for the model are obtained from archived forecast advisories from the National Hurricane Center (NHC) including information on storm position, intensity, and size. This information is used to construct a TC vortex in gradient balance that is a reasonable representation of reality and serves as modified initial conditions for the atmospheric model. Boundary conditions for the model come from large-scale analyses or a coarser regional weather forecast model. Many numerical experiments (ensembles) are conducted to test the sensitivity of the storm simulations to initial specifications of the storm vortex, surface boundary conditions (e.g. SSTs), model-piloting fields and microphysical parameterizations. Some experiments are also run in "forecast mode" to facilitate comparison with other numerical

weather predictions and to diagnose the feasibility of the model as a forecasting tool. Special aspects of each event (as they relate to the key forecast challenge) will be highlighted. The case studies are presented in the order in which the research was carried out.

Standard variables such as storm central (minimum) sea level pressure, maximum surface winds and storm track are generated from the model output to compare simulations with one another. Various fields, such as sea level pressure, wind speed, equivalent potential temperature and rainfall that are typically used by weather forecasters, are extracted or diagnosed from model output. These fields are compared with research aircraft and surface weather data, used to evaluate model performance. The author participated in the research aircraft missions into Tropical Storm Karen and Hurricane Juan as the on-board support meteorologist, and was also involved with organizing dropsonde deployment patterns into the storms.

CHAPTER 2

Data and Methodology

Various sources of data used to conduct this work are described in this chapter followed by details on the model and the vortex construction.

2.1 Data Sources

a. Storm Vortex Parameters

The three-dimensional, idealized TC vortex used for the initial conditions in the atmospheric model is constructed using key observational data from the NHC best track (BT) archive (http://www.nhc.noaa.gov/pastall.shtml) and from NHC storm bulletin archives (http://www.nhc.noaa.gov/archive/). Additional information to determine the size of a given TC is taken from the storm archives of QuikSCAT scatterometer imagery, available online at http://manati.orbit.nesdis.noaa.gov/cgi-bin/qscat_storm.pl.

The BT for each storm provides key information on the storm every six hours (00, 06, 12, 18 UTC): 1) storm position in tens of degrees of latitude and longitude, 2) minimum sea level pressure (MSLP) in hPa (mb), 3) maximum sustained winds (MSW) speed (knots), and 4) storm status (tropical depression, tropical storm, hurricane, extratropical). Best track positions and intensities are based on post-storm assessments of all available data, and may differ from data contained in real-time storm advisories. The MSLP is either measured by reconnaissance aircraft or estimated by inferring storm intensity using the

Dvorak (1975) satellite technique. Maximum sustained winds are defined as the highest one-minute "sustained" (mean) surface winds measured or estimated within the circulation of the storm. These winds are defined at 10 m above the ocean or land surface in unobstructed exposure. The status of the storm is primarily based on the MSW and appearance of the cloud structure in satellite imagery. A tropical depression contains a MSW of 17 m s^{-1} or less. A tropical storm possesses a MSW from 18 m s^{-1} to 32 m s^{-1} while a hurricane's winds are at least 33 m s^{-1}. Other classifications exist (subtropical and extratropical storm) in the BT archive, but the tropical phase of the storm is the focus with regard to model initiation procedures in the present work.

Information gathered from the NHC storm bulletin ("forecast advisory") archive includes estimated radii of gale force winds (17.5 m s^{-1}) for each of four storm quadrants, and the uncertainty in storm position. These advisories are issued every six hours at 03, 09, 15 and 21 UTC. The wind radii are used to determine the vortex size parameter, and the positional uncertainty is used in the sensitivity experiments that will be outlined later.

Imagery from the QuikSCAT scatterometer (Katsaros et al. 2001) is available for some cases, and serves as a useful check against wind radii estimates in the storm archives. The imagery are typically available twice daily at a given location on the earth. There are some limitations with using QuikSCAT data since an overpass may not necessarily cover the TC, or not be available at the time of interest. When QuikSCAT fields are used, the mean radius of 15-m s^{-1} (~30-kt) winds used to prescribe the idealized TC vortex is simply estimated (sketched) from the image displaying the wind barbs.

b. Initial and Boundary Conditions

Tropical cyclone intensity is very sensitive to SSTs, particularly beneath the storm core (Emanuel et al. 2004), so it is important to use good quality SST analysis fields for the model surface boundary conditions. Sources of SST fields used in this work include 1/3° (37 km) resolution data compiled at the Canadian Meteorological Centre (CMC) (Bruce Brasnett, personal communication) as well as data from the Comprehensive Large Array-data Stewardship System (CLASS) electronic library located online at http://www.class.noaa.gov/nsaa/products/. The CMC data originate from the Advanced Along-Track Scanning Radiometer (A/ATSR) aboard the polar-orbiting ENVISAT satellite. The CLASS data originate from the Advanced Very High Resolution Radiometer (AVHRR), located on the National Oceanic & Atmospheric Administration (NOAA) series of satellites. The horizontal resolution of the CLASS data is 1/8° latitude (14 km) by 2/5° longitude over the western Atlantic Ocean, and is tuned to in situ data at one-meter depth. Monthly climatological SST fields taken from Geshelin et al. (1999) are also used. The data cover the northwest Atlantic Ocean (35°N to 66°N and 76°W to 30°W) with a horizontal resolution of 1/6° (~18.5 km) (see Fig. 4).

Initial and boundary conditions for the large-scale meteorological fields are extracted from the CMC regional data assimilation system (Chouinard et al. 1994) for most numerical experiments. Some experiments are conducted using boundary conditions from the Global Environmental Multiscale (GEM) regional weather forecast model (Cote

et al. 1998) archives. The standard fields consist of geopotential height (GZ), air temperature (TT), dew point depression (ES), zonal wind speed (UU) and meridional wind speed (VV) at 16 pressure levels (1000, 925, 850, 700, 500, 400, 300, 250, 200, 150, 100, 70, 50, 30, 20, 10 hPa). Surface fields include sea level pressure (PN), air temperature (TS), dew point depression, sea surface temperature (TM), and other characteristics such as soil temperature and albedo. The fields are available every six hours at 00, 06, 12 and 18 UTC.

The regional data assimilation system consists of a blend of six-hour CMC global model forecasts (trial fields) and weather observations valid at the time of interest. These fields are optimally interpolated and weighted to produce the *analyses* used as initial and boundary conditions for the mesoscale model.

c. Observational Data

A wealth of meteorological data is used to evaluate model simulations and establish best tracks for the storms. These data include surface weather observations from stations owned and operated by the MSC, land-based radar imagery, satellite imagery and aircraft dropsonde data from the Convair-580 aircraft (Wolde et al. 2001, Abraham et al. 2004). Land-based weather stations measure standard parameters such as 5-m air temperature, 5-m relative humidity, 10-m wind speed and direction, and precipitation. Offshore buoy sites measure wind speed at the 5-m level, temperature, relative humidity, wave heights, and SST at approximately 1-m depth. Three key radar sites sampled the rainfall and wind

patterns in the storms in this study. One is located at Gore, Nova Scotia, approximately 50 km north of Halifax. This radar is dopplerized and provided valuable information of the 3D wind field during Hurricane Juan and Tropical Storm Karen. The second radar is located at Chipman, New Brunswick and the third is located at Holyrood, Newfoundland which provided information on the structure of Hurricane Michael when it made landfall on the south coast of that province. The locations of the radar sites are shown in Fig. 3.

Imagery from the Geostationary Operational Environmental Satellite (GOES-East) is used by the NHC to infer storm intensity and is used here to chart the progress of the storms. Imagery from the AVHRR aboard a polar-orbiting satellite was available during the landfall of Tropical Storm Karen.

The MSC, in partnership with the National Research Council (NRC) of Canada, conducted research flights into the three storms introduced earlier. The Convair-580 aircraft (used to carry out the measurements) was first flown into Hurricane Michael in October 2000 (Wolde et al. 2001, Abraham et al. 2004), and in subsequent seasons into Tropical Storm Karen and Hurricane Juan. The primary source of data collected during these storm flights was from GPS dropsondes, launched from a flight level of ~6000 m or ~450 hPa. The dropsondes measured profiles of temperature, humidity, and wind below the aircraft down to the ocean surface. The vertical resolution of the data is ~6 m (i.e. data transmission every 0.5 seconds). Several dropsondes were launched along transects through the storms. The data were mapped to common vertical planes to generate cross sections of standard and derived meteorological fields, such as equivalent potential

temperature. These cross sections were then compared with similar cross sections from the model to identify and compare meteorological features. A 38-GHz, vertically-pointing, Ka-band radar measured reflectivity during the flights, providing unique vertical cross sections of precipitation within the storms.

2.2 Model Description

a. Synthetic Storm Vortex

The model initial conditions are modified by inserting an observationally-consistent, TC-like vortex constructed prior to running the model. The weakly-analyzed hurricane low in the original analysis (or GEM zero-hour) fields is very near the location of the inserted synthetic vortex in these cases, so the original low is completely replaced. The vortex is constructed using key observational data from the NHC best track and operational message archives as described above. Control parameters for the vortex include: (a) the minimum central sea level pressure, (b) storm center position, (c) size (radius of 15 m s^{-1} surface winds, R_{15}) and (d) the percent of the environmental (background) flow used for the initial wind field asymmetry. The sea level pressure profile follows that of Fujita (1952) and is defined as a function of radius (r):

$$p(r) = p_e - dp\left[1+\left(\frac{r}{R_o}\right)^2\right]^{-1/2} \qquad (1)$$

where $dp = p_e - p_c$ (p_e is the ambient sea level pressure and p_c is the MSLP of the storm). R_o is the *characteristic* radius (smaller R_o yields a larger radial pressure gradient). For example, for a given dp, if R_{15} is decreased to give a compact storm, then R_o will also decrease. The temperature and moisture structure of the vortex is cylindrically symmetric about the storm center and defined by a moist adiabat that extends from 1000 hPa (with corresponding environmental temperature for that level) to a level where that moist adiabat intersects the environmental temperature sounding, which defines the cloud top. The relative humidity throughout the storm core is near 90% (following Davidson et al. 1993) and gradually decreases as a function of radius from the storm center. The environmental parameters (including temperature) are obtained from an annular region with inner radius of R_{15} and outer radius of $2R_{15}$. This annulus is essentially the same annulus used as the blending zone for which the vortex is inserted into the environmental fields (i.e. the large scale analysis). This approach has also been used for numerical studies of Hurricane Juan in 2003 by McTaggart-Cowan et al. (2005a).

The raw hurricane vortex built by the program is in gradient wind balance with an axisymmetric wind field. A more realistic three dimensional wind field is obtained by adding a "background" flow to all levels of the vortex, giving an asymmetric wind field. The background flow is found by "filtering out" the original weak cyclone from the analysis fields, leaving a smoothed wind field. The smoothed wind field is then added to the axisymmetric hurricane vortex and merged with the large-scale fields as described above. The result is a more realistic *asymmetric* wind distribution around the storm. Normally a certain (user-specified) percentage (less than 100%, see Tables 2 to 4) of the

background flow is used to give a representative surface wind field since the storm does not follow simple solid body rotation. For a more detailed description of the synthetic vortex, see Davidson et al. (1993).

b. Mesoscale Compressible Community Model

The Mesoscale Compressible Community (MC2) model (version 4.9.6) is used to conduct all experiments using the synthetic TC vortex insertion in the initial conditions described above. This non-hydrostatic, fully compressible limited area model employs three-dimensional semi-Lagrangian advection and semi-implicit time discretization to solve the primitive Euler equations on terrain-following height coordinates (Gal-Chen and Somerville 1975). Version 4.0 of the CMC Physics Library is used for the parameterization of physical processes. A kinetic energy closure scheme described by Benoit et al. (1989) is employed in the boundary layer (BL) to parameterize turbulent transports. Monin-Obukhov similarity theory (Monin and Obukhov 1954) is used in the atmospheric surface layer to determine the vertical profile of the wind field and sea surface fluxes. Standard bulk formulations are used to represent turbulent fluxes of momentum, sensible heat and latent heat. Wind, temperature and humidity used to compute these fluxes are taken from the lowest computational level in the model. The force-restore surface scheme (Benoit et al. 1989) is used in all simulations to predict the surface temperature and moisture budget over land. Deep convective processes are handled with Kain and Fritsch (1990) convective parameterization in the control

simulations on the coarser (12 km) grid, but solved explicitly on the fine (3 km) grid, described below. Shallow convective processes are solved explicitly in all the experiments. Stratiform condensation (cloud microphysical) schemes are given by Tremblay et al. (1996) for the 12 km simulations and Kong and Yau (1997) for the 3 km runs. For a general overview of the model see Benoit et al. (1997).

The model is piloted by regional analyses or GEM forecast fields every six hours, mapped to a 0.25° latitude-longitude (~28 km) grid covering eastern North America and the Western Atlantic Ocean (20.0°N to 70.0°N and 100.0°W to 30.0°W). The model is run on two grids, one is a 12 km (0.108°) latitude-longitude grid appropriately centered on the area of interest for the particular case study, with 25 computational levels (7 in the atmospheric BL), and another on a finer 3 km (0.027°) grid with 40 computational levels (12 in the BL). The lowest computational level (for momentum) in the 3 km version is 40 m. A time step of 120 seconds is used in the 12 km simulations and 30 seconds for the 3 km simulations.

2.3 Description of Various Procedures and Computations

a. Preparation of SST Fields

The primary source of high-resolution SST data for this study is taken from the CLASS website at http://www.class.noaa.gov/nsaa/products/ (see section 2.1 - Data sources). The pre-storm data are extracted from the website over the entire area of available coverage (eastern North Pacific Ocean to western North Atlantic Ocean) and saved to a

file in tabular text format. Only the raw SST data are contained in the text (ASCII) file (textual information is stripped-out). Grid points over land are flagged as "999.9". The MC2 model, however, reads a continuous field of SST even over land, although the over-land values are not explicitly used in the calculations. To populate the missing data points from the CLASS data over land, a modified Cressman interpolation scheme (Cressman 1959) is applied. The procedure eliminates artificial temperature gradients along the coast which would otherwise generate spurious behavior in the model computations. The Cressman procedure creates an updated ASCII file, which is then converted to a special format (Recherche en Prévision Numérique or RPN format) that is used by the model. The next step is to map the new RPN SST file to the 0.25° latitude/longitude model-piloting domain. The high-resolution SST from CLASS does not cover the entire domain, so it is necessary to fill the SST-void region with the existing SST from the CMC archive. It is important to point out that the high-resolution SST exists over the region where the storms in this study occur (see Fig. 4). The final step is to replace the old SST field (from the CMC archive) with the new field in the master file containing all the initial conditions for the model. The SST remains fixed throughout the experiments.

A similar procedure is applied to prepare the SST fields from the Geshelin et al. (1999) monthly climatology. This climatology is used because it contains a much better representation of the SST gradient associated with the Gulf Stream than the CMC climatology. To generate the climatology for a specific date, a weighted average of SST from two months is calculated. For example, to obtain the climatology SST for 28

September, September and October data are used with a slightly larger weighting for September (e.g. $0.6SST_{sept} + 0.4SST_{oct}$). Like the CLASS data, the Geshelin data do not cover the entire model-piloting domain, but *do* cover the main area over which the storm simulations are carried out.

b. Generation of Model Output Statistics

A large number of storm simulations were run for the case studies in this project. To handle the large volume of model output, a quick and effective way to extract the key information was developed. The key information includes a track of the storm center, intensity in terms of maximum surface winds and MSLP, the SST beneath the storm center (defined by the location of the MSLP), plus some other statistics including location of the maximum surface winds and a flag for the storm status (tropical storm, hurricane, etc.). These statistics are generated for every model output time (hourly or three-hourly, depending on the experiment) and stored in tabular format – one file for each experiment. A sample of the output is shown in Table 1.

The process begins with the extraction of certain fields directly from the RPN-standard model output files. A script is run which extracts the sea level pressure (PN), sea surface temperature (TM), zonal wind (UU) and meridional wind (VV). The wind magnitude (modulus) UV is calculated from UU and VV. Latitudes and longitudes (LA, LO) for each grid point are also generated and stored in one file. Another program reads the information from this file and generates the model output statistics (MOS) table. The

first step is to find the location and value of the MSLP. If the storm is the most intense of any cyclone in the model domain, a simple loop through all grid points is effective; otherwise a refined search may need to be set up initially. Once the location is known, a refined search is made to find the maximum surface winds (MSW). This is set to the maximum value in a 6-degree latitude/longitude box about the storm center. To find the storm center at the next model output time, a search is conducted within a small box centered about the previous storm position. The process then repeats until all output files have been processed. To determine the SST beneath the storm center, the grid point corresponding to the location of the center is stored in memory and used directly to retrieve the SST from the TM field.

The file generated from the MOS algorithm is then used as input into a program called GrADS (Gridded Analysis and Display System) to prepare the storm tracks. The same file is ingested into Microsoft Excel spreadsheets to prepare time series of MSLP, MSW and SST. Multiple files are merged within the Excel environment, facilitating statistical computations of means and standard deviations.

c. Model Output and Diagnostics

Snapshots from the model are generated every hour or every three hours (depending on the experiment) and stored in two files – one containing dynamical fields and the other containing fields output from the physics package. The dynamical fields include sea level pressure, air temperature, specific humidity, zonal and meridional wind components

and vertical motion (PN, TT, HU, UU/VV and WW respectively) for various height or pressure levels. The physical fields include screen-level (5 m above surface) output of TT, HU, UU/VV (10-m level), precipitation rate (RT) and cumulative precipitation (PR). Most of the output fields presented in this work were displayed using two CMC software packages (XREC and MAX), specifically designed to handle files of the RPN standard format.

Equivalent potential temperature (θ_e) is diagnosed from the output of air temperature and specific humidity on pressure levels. This field is one of the main diagnostic fields used throughout the project to study the changing thermodynamic structure of the storms. Its calculation is based on the formulation of Bolton (1980) and is applied to both model output and dropsonde data from the research aircraft. The expression for θ_e is

$$\theta_e = T\left(\frac{1000}{p}\right)^{0.2854(1-0.28\times10^{-3}\alpha)} \times \exp\left[\left(\frac{3.376}{T_c} - 0.00254\right)\times\alpha(1+0.81\times10^{-3}\alpha)\right] \quad (2)$$

where T, p and α are the air temperature (Kelvins), pressure (hPa) and mixing ratio, respectively, at a given level. The temperature that an air parcel will attain if lifted adiabatically to its condensation level is given by T_c (Kelvins):

$$T_c = \frac{1}{\frac{1}{T-55} - \frac{\ln(RH/100)}{2840}} + 55 \quad (3)$$

where RH is relative humidity.

To calculate θ_e from the model output, TT and HU are extracted from all pressure levels and converted to SI units. The saturation mixing ratio corresponding to temperature (TT) is computed and used in the calculation for RH. All mathematical operations are performed on each grid point of the model domain, and at all pressure levels, permitting the display of θ_e in both plan view and vertical cross sections. The display of θ_e using the dropsonde data appears in cross section form only. The values are projected to a vertical plane, bound by the first and last sonde in a series of drops along a leg of the aircraft flight. A representative cross section from the model output is then compared with dropsonde data for analysis.

d. Determination of Vortex Size

Determining the size of the tropical cyclone to be inserted into the model initial conditions is one of the most important steps in the model setup. For the cases in this study, a basic estimate for R_{15} (radius of 15-m s^{-1} winds) is derived from quadrant-mean gale force wind radii (i.e. radii of 17.5 m s^{-1} winds) available in the NHC forecast advisory bulletins. It is obtained by first finding the mean gale radius in kilometres for the entire storm, then multiplying that value by a scaling factor (s) of 1.36. To explain the origin of s, note that the vortex satisfies gradient wind balance, which is expressed by the following (gradient wind) equation:

$$\frac{U_G^2}{r} + fU_G = \frac{1}{\rho}\frac{\partial P(r)}{\partial r} \tag{4}$$

where U_G is the gradient wind speed, f is the Coriolis parameter, r is the radius from the storm center, ρ is the density of air at sea level, and P(r) is the sea level pressure as a function of radius given by Eq. (1). The solution for cyclonic flow ($\partial P/\partial r > 0$) in Eq. (4) is

$$U_G = -\frac{fr}{2} + \sqrt{\frac{f^2 r^2}{4} + \frac{r}{\rho}\frac{\partial P(r)}{\partial r}} \tag{5}$$

A scaling analysis using typical values for the variables in (5) (f at 30°N = $8\times10^{-5}s^{-1}$, ΔP ~ 50 hPa, Δr ~ 250 km, ρ = 1.22 kg m^{-3}) shows that the f terms contribute only ~15% to U_G, therefore (5) simplifies to

$$U^2 = \frac{r}{\rho}\frac{\partial P(r)}{\partial r} \tag{6}$$

The derivative of Eq. (1) with respect to r can be inserted into Eq. (6) which, after some rearrangement, gives

$$U^2 = dp\frac{r^2}{\rho R_o^2}\left[1 + \frac{r^2}{R_o^2}\right]^{-3/2} \tag{7}$$

The next step is to find r for the 15-m s^{-1} isotach, knowing r for the 17.5-m s^{-1} isotach, so dividing one expression by the other gives

$$\frac{17.5^2}{15^2} = \frac{r_{17.5}^2}{r_{15}^2}\left[\frac{\left(1+\frac{r_{17.5}^2}{R_o^2}\right)^{-3/2}}{\left(1+\frac{r_{15}^2}{R_o^2}\right)^{-3/2}}\right] \cong 1.36 \qquad (8)$$

Finally, note that R_o corresponds to the radius of maximum winds which is normally small compared to $r_{17.5}$ or r_{15}, so $r^2/R_o^2 >> 1$ and (8) simplifies to

$$\frac{r_{15}}{r_{17.5}} = 1.36 = s \qquad (9)$$

providing a consistent and effective way to determine R_{15} for direct input into the vortex program.

CHAPTER 3

Case Study: Hurricane Juan

3.1 Introduction

a. Overview

When Hurricane Juan struck Nova Scotia, Canada (~44°N latitude) in September 2003 as a category-two storm on the Saffir-Simpson Hurricane Scale (Simpson and Riehl, 1981), most people were surprised by the intensity of the storm and the damage it caused. Millions of trees were blown down, there were widespread power outages, boats were strewn ashore by surge and waves, roofs were torn off buildings and billboard signs were destroyed. The likes of such damage had not been seen since Hurricane Edna (Malkin and Holzworth 1954) hit the same area in 1954 (also see Nova Scotia Department of Natural Resources website at http://www.gov.ns.ca/natr/juan/).

As Hurricane Juan moved northward, it experienced much warmer than normal SSTs south of Nova Scotia (3 to 5°C above normal) on the Scotian Shelf (see Fig. 3). The primary focus for this case is on the assessment and impact of these warmer SSTs on the weakening rate of Juan leading up to landfall. Most of the hurricanes that move toward Nova Scotia weaken to category-one or tropical storm strength. There have only been three documented cases of category-two hurricanes *directly* landfalling in Nova Scotia (based on data from the HURDAT database at http://www.aoml.noaa.gov/hrd/hurdat/easyhurdat_5102.html) in the 150-year period from

1853 to 2003 (Juan in 2003, Ginny in 1963 and an unnamed storm near Yarmouth (western tip of Nova Scotia) in 1891). However, extreme tropical cyclone-related wind events in Nova Scotia are not limited to these three cases. For example, Hurricane Edna made landfall in eastern Maine as a strong category-one hurricane, yet was responsible for an intense wind jet well east of the storm center over Nova Scotia, delivering winds that inflicted damage similar to Hurricane Juan.

b. Background

Numerical weather predictions for Hurricane Juan were quite poor during the event. The most common source of these poor predictions was insufficient representation of the hurricane in the model initial conditions. In the case of the Canadian GEM model, Juan only appeared as a weak ~1008 hPa low south of Nova Scotia that moved in the wrong direction toward the north-northwest, crossing the western end of the province. Operational forecasts[1] of the event were generally good. The CHC warned that Halifax should expect hurricane conditions with anticipated landfall intensity near 65 kts (33 m s^{-1}) that would likely result in the toppling of trees. Notice was taken of the anomalously warm SSTs south of Nova Scotia, which lent confidence to a landfalling hurricane scenario, but forecasters could not necessarily quantify the role of these elevated water temperatures. A quote from the forecast bulletin issued at 18 UTC 28 September (~33 hours before landfall) summarizes the thoughts at the time:

[1] Hereafter meaning a blend of model guidance and human interpretation/experience

"...HURRICANE JUAN HEADING TOWARD NOVA SCOTIA..EXPECTED LANDFALL OVER OR JUST WEST OF HALIFAX SUNDAY EVENING. ... SINCE WATER TEMPERATURES BETWEEN THE GULF STREAM AND THE NOVA SCOTIA COAST ARE RUNNING ABOVE 18C..THE WEAKENING TREND MAY BE SLOWED SOMEWHAT. ...THE HIGH WINDS WILL LIKELY RESULT IN THE TOPPLING OF SOME TREES AND LARGE LIMBS RESULTING IN POWER OUTAGES."

3.2 Synoptic History of Hurricane Juan

The original cyclone that eventually became Hurricane Juan formed approximately 600 km southeast of Bermuda on 23 September 2003. This cyclone formed in a slightly baroclinic environment as an upper-level trough approached a low-level potential vorticity anomaly that had originally formed off the African coast many days earlier. A detailed analysis of the vorticity anomaly associated with the origins of Hurricane Juan is described by McTaggart-Cowan et al. (2005b). A series of satellite images documenting the lifecycle of Juan are shown in Fig. 5 and the storm track with SSTs is shown in Fig. 6. On 24 September, deep convection consolidated near the cyclone center and the system was declared a tropical depression. The cyclone reached tropical storm status by 00 UTC 25 September. The cloud pattern continued to organize and the cyclone developed an eye, becoming a hurricane by 12 UTC 26 September (Fig. 5c).

Juan gradually intensified and reached its peak intensity with MSW of 46 m s^{-1} (90 knots), and a minimum pressure of 969 hPa, at 18 UTC 27 September (between the times shown in Fig. 5e and Fig. 5f). Juan moved northward, embedded in a large tropical airmass over the western Atlantic Ocean. The hurricane gradually accelerated and made landfall west of Halifax, Nova Scotia near the community of Prospect at 0310 UTC 29

September 2003, with estimated MSW of 44 m s^{-1} (85 knots) and a minimum pressure of 973 hPa. Juan moved quickly across Nova Scotia and struck Prince Edward Island as a marginal category-one hurricane, then moved into the Gulf of St. Lawrence as a strong tropical storm. The remnants of Juan moved into Labrador during the afternoon of 29 September and dissipated as an extratropical depression. A map indicating various points of reference in the text appears in Fig. 7.

3.3 Control Simulations

Grid configurations and model integration periods are shown in Fig. 8. The 12 km (0.108°) latitude-longitude grid is centered on the area of interest (Nova Scotia) from 30.4°N to 59.6°N and from 78.2°W to 45.8°W and the 3 km (0.027°) grid is oriented along the storm track from 35.2°N to 47.4°N and from 67.0°W to 61.0°W. Primary attention is spent on the 3 km results here, since Juan was a very compact storm, and high resolution is necessary to adequately resolve the storm core.

The vortex is constructed using key observational data from the NHC best track (Avila 2003) and from NHC forecast advisory archives (available online at: http://www.nhc.noaa.gov/archive/2003/JUAN.shtml).

The first run of the model begins at 00 UTC 28 September on the 12 km grid, piloted by large scale analyses described in chapter 2. This initial time was chosen for two reasons. Firstly, Juan was at its most developed stage (Fig. 5f) - a desirable condition for

effectively applying the synthetic vortex, and secondly, the spin-down (weakening) period of the storm over the cooler SSTs is of primary interest in this work. After the 12 km simulation is completed, the second integration on the 3 km grid (using output from the 12 km grid valid at 06 UTC 28 September) is run for 24 hours. Six hours of "vortex adjustment" are required before beginning the 3 km run (see Fig. 8b). This is the period during which any imbalance between the vortex and the large-scale environment can be corrected in the model. The boundary conditions for the inner domain are updated every 30 minutes with output from the 12 km domain, but transfer is only from the outer domain to the inner domain (i.e. one-way nesting). Note that in order to reduce the possibility of "shocking" the model; the synthetic vortex is implanted into the 12 km grid instead of the 3 km grid.

Two control simulations of Hurricane Juan are conducted, one with analysed SSTs of 28 September 2003, and the other using the monthly climatology of SSTs from Geshelin et al. (1999). The analysed SSTs are from the unsmoothed 1/3° CMC A/ATSR dataset provided by Bruce Brasnet (personal communication). The GEM model began using these data as of July 2005. Both analysed and climatology SST fields are interpolated to the 28 km "piloting" domain for the model (see Fig. 8). The two control runs differ only in their SST surface boundary conditions but the SSTs are fixed in each run, i.e. the model is not coupled with an ocean circulation model. A map showing the observed minus climatology SST (anomaly) over the 3 km computational domain together with the storm track is shown in Fig. 9. The pre-existing SSTs were anomalously warm virtually

everywhere along the storm track, with the largest anomaly of 3-5°C, north of 41°N on the Scotian Shelf (hereafter, simply "shelf").

For fast-moving hurricanes, the storm-induced SST cooling beneath the storm center is usually small (Price 1981) so there will be little negative feedback on the storm (Emanuel et al. 2004). In a pair of test simulations on Hurricane Juan conducted by Emanuel (personal correspondence) using the Coupled Hurricane Intensity Prediction System, it was found that the storm, when coupled with the ocean, was only slightly weaker (by ~1 m s^{-1} in maximum winds) than the uncoupled storm.

Figure 10 shows the tracks for the simulated hurricane in each 3 km *control* run where "JUAN" denotes the run with observed SST and "CLIM" the run with climatology SST. The simulation times marked in the figure correspond to the beginning of the 3-km runs. Table 2 includes the vortex and model specifications for this pair of simulations. The remaining contents of the table refer to the ensemble runs to be discussed in section 3.4. Also plotted is the best track (BT) (Avila 2003) at one hour increments covering the 24-hour period from 06 UTC 28 September to 06 UTC 29 September (hereafter UTC time and date are denoted by HH/DD – e.g. 06/29). The simulated storm tracks follow the course of the real storm rather well with two notable exceptions: 1) the simulated storms are a bit faster than reality, and 2) there is a westward jog in their tracks during the early part of the simulations. The source of these errors is yet unclear, but is consistent among the ensemble experiments to be discussed in the next section. Much of the excess forward speed in the simulations occurs during the six-hour adjustment period, and the

time which the storm spends over the cooler waters north of the Gulf Stream is not much different from reality. Some form of assimilation cycle (using aircraft data at that time, if available, which is not often the case) would be necessary to achieve optimal initial intensity and positions for the early part of the simulation. However, for the purposes of this work and as discussed by McTaggart-Cowan et al. (2005a), it is felt that direct vortex insertion with a suitable (six-hour) adjustment period is sufficient.

Figure 11 displays time traces of MSLP, maximum surface wind (MSW) speed and SST beneath the storm center for the control simulations on the 12 km and 3 km grids, including the BT. Note that the BT is not exact, i.e., it is an estimate with inherent uncertainties on the order of ~±2.5 m s^{-1} for MSW and ~±4 hPa for MSLP throughout the lifecycle of the storm. The CLIM storm is clearly weaker (higher MSLP) than the JUAN storm throughout the simulations. There is some difference in intensity at the start of the 3 km runs (6HR total simulation) because of the spread that develops between 12 km runs during the 6-hour adjustment period. The difference in MSLP between the two 3 km runs mostly develops during the first 3 hours of the simulations (e.g. between 6HR and 9HR). There are two weakening trends later in the integrations: 1) as the storm moves over cooler shelf waters, and 2) as the storm moves over land as indicated by two different slopes in the 3 km MSLP trend curves. Note that the modeled storms make landfall sooner than the real storm as indicated by the earlier onset of rapid weakening compared to the BT. As the storm moves over the shelf waters, the MSW does not change significantly in the JUAN run but decreases steadily in the CLIM run. This behavior suggests that the wind field is becoming more decoupled from the cool marine

BL in the CLIM simulation. Winds from the JUAN run (Fig. 11b) more closely resemble those in the BT although this is not exactly the case with respect to MSLP (Fig. 11a) indicating that the wind/pressure relationship in the model may not be representing reality perfectly. One final point to note here is that the increasing trend in MSW at the very end of the 3 km time series plots is artificial, for the storm is near the northern boundary ("buffer" zone) of the model domain. The primary interest here is with the behavior of the storm much further south in the center of the domain.

A more complete comparison between the surface wind fields from the JUAN and CLIM control experiments is displayed in Fig. 12. These analyses show the maximum surface (40 m) wind speed for each grid point in the model domain over the 24-hour integration. The analyses are produced from one-hourly model output, which explains some of the ribbed features in the fields. As shown in Fig. 11b, the surface winds are generally stronger in JUAN than CLIM, particularly along the axis of highest winds. Strong winds in the center of the swath can be seen in the JUAN run extending to the shore of Nova Scotia with little change in strength. On the other hand, it is quite clear that the maximum winds in the CLIM run taper-off within ~300 km of the coast. The difference is not as evident in the outer part of the wind field. Within the maximum wind region over land, the JUAN winds are between 2 and 6 m s^{-1} (~5-10 knots) stronger than the CLIM winds.

A fictitious control run is also conducted where all SST values below 26°C are made equal to 26°C. In this scenario, the hurricane has no opportunity to weaken while

approaching Nova Scotia, and in fact intensifies to a category-3 hurricane (MSW of 54 m s^{-1} or 105 knots) at landfall (see Fig. 13). This indicates that the situation for Nova Scotia would have been *much worse in the absence of the storm-tempering effect of cooler shelf waters.* The translational speed of the storm increases from ~10 m s^{-1} well before landfall to near 18 m s^{-1} at landfall. It is likely that most of the increase in storm intensity (in terms of maximum (earth-relative) surface winds) near landfall is owing to this translational component.

Before proceeding, it should be clarified that when referring to the BT, MSW is defined as the maximum one-minute mean (sustained) winds anywhere in the storm at 10 m above the surface as described in chapter 2. When referring to output from the model, MSW is the maximum instantaneous (e.g. snapshot) surface wind anywhere in the storm, where "surface" is defined at the 40 m (lowest computational) level. It was found that the 40 m winds from the model are a more reasonable representation of reality than the 10 m "diagnostic" winds from the model. More information regarding this will appear in section 3.3b.

a. Comparison with Aircraft Data

The Canadian NRC's Convair 580 aircraft conducted a mission into Hurricane Juan immediately prior to landfall. Meteorological data from 25 GPS dropsondes were collected, and used here to compare with output from the model. A photograph of the Convair aircraft is shown in Fig. 14a, and the sequence of dropsondes deployed during

the Juan flight is shown in Fig. 14b. Southwest to northeast cross sections of wind speed and equivalent potential temperature parallel to the Atlantic coastline of Nova Scotia are shown in Fig. 15, along with corresponding views from the model. A more detailed description of the aircraft and equipment is given by Abraham et al. (2004).

The wind field in Hurricane Juan was very asymmetric with much stronger winds occurring over a deep layer of the troposphere on the east side of the storm, most likely owing to the rapid forward translation speed. This structure is apparent in Fig. 15a and Fig. 15b. The center of the storm in these images is near dropsondes 16 and 17 where the gradient in wind speed drops off dramatically. No wind data were collected in certain parts of the storm since there were problems with GPS receiver reception (see blank areas in Fig. 15b). The model helps us to fill in these holes in the observational data. Aside from the missing data, the structure of the wind fields compare rather well, especially with regard to the thickness of the layer of strong winds and the wind shear in the BL.

The warm core of Juan immediately prior to landfall is depicted in Fig. 15c and Fig. 15d with cross sections of equivalent potential temperature (Θ_e) calculated using the formulation of Bolton (1980) as described in chapter 2. Overall, the airmass in the model is warmer/moister than the observations indicate, yet the model captures the main features. In particular, there is a narrow strip of high Θ_e in the storm core with values of 345K and higher. There is also a region of lower Θ_e air that is collocated with the region of strongest winds, which suggests that the storm was mixing with cooler/drier environmental air and from contact with the cooler ocean surface. A slight tilt in the

warm core is also observed with height, which is detected in the model as well. The warmer/moister core at landfall in the simulations could be an indication that the initial moisture prescription was too moist.

A cross section of Θ_e taken from the CLIM simulation is shown in Fig. 15e. This is the same view as the panels discussed above. There is a remarkable difference in low-level Θ_e beneath the storm core when comparing JUAN (Fig. 15c) and CLIM (Fig. 15e). It appears that a cold Θ_e dome has formed below ~850 hPa at the circulation center of the CLIM storm, suggesting *thermodynamic decoupling* of the warm core from the sea surface. This dome does not appear to be present in the JUAN simulation. It is interesting - but not surprising - that the CLIM storm was rapidly weakening (with respect to MSW) at this time, while the intensity of JUAN was almost steady (see 3 km curves in Fig. 11b).

b. Comparison with Surface Data

Figure 16 shows contours of sea level pressure and isotachs of 40-m winds from the JUAN and CLIM simulations, plus an analysis of sea level pressure obtained from various surface observations. The central pressure of 973 hPa in Fig. 16a was estimated from dropsonde surface data immediately prior to landfall, and inferred from coastal weather stations. The valid times for the model output are 01/29 (19 hours into the simulation) and 03/29 for the analysis. These staggered times are chosen for spatial comparison because the modeled storm makes landfall ~1.5 hours earlier than reality.

This corresponds to a track error of 110 km. As a matter of comparison, the NHC operational track forecast error (based on several numerical models) for the 24-hour period ending 00/29 was 170 km (too far north), while the simulated track error for JUAN is 100 km for the same period. Many of the operational numerical models had a fast bias with this storm, including the official forecasts. As noted earlier in this section, most of the positional error in the simulations occurs during the 6-hour adjustment period (first 6 hours of the 12-km simulations). The storm speed after that period is modeled very well. Aside from the early arrival time, the storm structure at landfall in the JUAN run (Fig. 16b) compares well with the analysis (Fig. 16a). The model quite accurately pinpoints the landfall location, intensity (44.8 m s^{-1} versus BT of 43.8 m s^{-1}) and the radius of maximum winds (~45 km versus observed ~35 km) approaching the metro Halifax area of Nova Scotia. The CLIM run generates a weaker storm immediately prior to landfall (Fig. 16c) with maximum surface winds 7.3 m s^{-1} weaker (37.5 m s^{-1}) than the JUAN run (i.e. category-one versus category-two hurricane). The track is virtually unaffected by the difference in SST in this pair of control runs, and the same is true of the ensemble experiments to be discussed in section 3.4.

An investigation of the surface winds as a function of time for various weather stations is presented next, and compared with the model results. Four points are chosen for analysis, they are: Halifax International Airport (an inland station), Shearwater (a coastal station), McNab's Island (an exposed island station) and Buoy 44142 (well away from the coast). Locations of these sites are shown in Fig. 7. The data and model results are

plotted in Fig. 17. Note that (instantaneous) model surface winds are defined at 40 m (lowest computational level) and stations are at 10 m.

There is a clear temporal separation between peak winds from the model compared to the observations at these sites owing to the faster simulated storm. Putting this difference aside, attention is focussed on comparing the peak winds from the model with data. At Halifax International Airport (Fig. 17a) the maximum surface winds from the model were ~24 m s^{-1}, which is an underestimate compared to the observed winds (~28 m s^{-1}). The difference between JUAN and CLIM winds is greatest at the airport site. In fact, working out the maximum wind power per unit area which is given by $\frac{1}{2}\rho U^3$ (cf. Emanuel 2005), where U is the 10-m sustained wind speed and ρ the density of air, it is seen that the winds in the JUAN run are approximately two times more powerful (i.e. more destructive) than the CLIM run. At the Shearwater site (Fig. 17a) the model overestimates the winds. At the exposed McNab's Island station (Fig. 17c) the model underestimates the winds by a small amount (3.1 m s^{-1}). This site reported the highest wind speeds of any station at landfall and was important in rendering Juan as a category-two hurricane at landfall. At this site, the maximum winds from the CLIM simulation work out to be ~70% as destructive as the winds in the JUAN run.

Juan moved almost directly over buoy 44142, yet the maximum winds observed at the buoy were only around 30 m s^{-1} (Fig. 17d). This is likely due to the coarse sampling period of one hour (missing the peak winds), and the fact that the anemometer is only 5 m above the water and may have been sheltered in the high seas. It should be noted that the

observed winds shown in Fig. 17d are corrected to standard 10-m winds using a logarithmic profile described in Shearman (1989) and given by

$$U(z) = \frac{u_*}{k} \ln \frac{z}{z_o} \tag{10}$$

where U(z) is the wind speed at height z, u_* is the friction velocity, k is the von Karman constant (k=0.4) and z_o is the roughness length in meters (z_o=0.0016 is a typical value over water).

These results indicate that there is considerable point-to-point variability in the model's representation of wind speed. However, the 40-m model winds are generally more representative of observed winds than are the 10-m diagnostic winds from the model (not shown), especially over land. A microscale model of the BL would likely be necessary to capture the details of the wind field at the 10-m level.

Unlike most hurricanes, Juan did not produce a significant amount of precipitation, owing to its rapid forward speed of motion and the loss of convection on the south side of the storm. It is suspected that the convection was suppressed because of shear-induced subsidence in the upshear (south) side of the storm as discussed by Zhang and Kieu (2005). A similar asymmetry in the vertical motion fields (at 500 hPa) is observed, and the model does a very good job reproducing the northward-skewed rainfall pattern and the aerial distribution of rainfall. Rainfall amounts are slightly overestimated as shown in Fig. 18 when compared with rain gauge data (Fig. 18a). For example, only a small area

of near 50-mm amounts is depicted in the data while the model generates a larger area of 50-mm amounts. The model appears to have a decent handle on the pattern of topographically-enhanced rainfall over Nova Scotia (i.e. greater amounts over elevated terrain and in onshore/upslope easterly wind flow). On the other hand, the model has been known to overestimate rainfall in onshore/upslope flow in other cases (Hurricanes Michael and Karen) which will be shown in the following chapters.

The moisture content in the simulated storm seems to be overestimated as indicted by the high values of equivalent potential temperature in Fig. 15 compared with observations. It is therefore reasonable to expect such an airmass would generate greater rainfall. Model-simulated rainfall from the CLIM run (Fig. 18c) is somewhat less than the JUAN run. The difference is approximately 10 mm near the maximum rainfall region.

c. Vertical Wind Profiles

Snapshots of vertical profiles of wind speed from the model simulations are shown in Fig. 19 for two selected locations, one over the ocean within the high wind region and the other over land. The over-water profiles (Fig. 19a) were chosen at the location of the strongest surface winds in each storm (JUAN and CLIM) not long before landfall. The height and strength of the low level jet over the ocean in the CLIM run clearly differs from the JUAN run. The CLIM jet is ~150 m lower (~350 m versus ~500 m) and the magnitude is ~12 m s^{-1} weaker based on these model output levels. The lower jet height suggests a shallower atmospheric BL over the cooler ocean in CLIM, consistent with

greater BL stability (Stull 1988). This difference was observed at other times before landfall as well, but the wind minimum at ~1000 m in the CLIM profile (Fig. 19a) was a temporary feature. Well away from the high wind region, it is observed that the jet heights in both cases are on the order of 1000 m (not shown), which is much higher than in the storm core region. This is typical in hurricanes and is described by Franklin et al. (2003). The over-land profiles (Fig. 19b) were extracted at Halifax International Airport at the time when model winds were strongest there. The jet height is much higher (~1000 m) than in the vicinity of the maximum wind over water.

Unfortunately, there were problems collecting wind speed data from the dropsondes in the highest wind region of the storm (recall Fig. 15b). However, on the southbound leg of the Convair flight (sondes 1 through 11 in Fig. 14), there were some successful drops near the storm center. There was a great degree of variability in the height of the low-level jet. In fact, there were two low-level jets on the north side of the center at 500 m and 1400 m from sonde number 3 (Fig. 19c). There were also two maxima on the south side (Fig. 19c); one at 200 m and the other at 600 m. There is no evidence of these double-jet features in the model output, although it may be necessary to use finer vertical resolution to resolve them.

A spatial presentation of wind shear in the 50- to 300-m layer (above ground level) from the JUAN control simulation is shown in Fig. 20a. The 50-m level is relatively close to the lowest computational level in the model, while 300 m is the elevation of the highest terrain on mainland Nova Scotia. Over the ocean, it is clear that greater wind shear

magnitudes are present east of the storm center in the high wind region, compared with areas well away from the center. This pattern agrees with the mean vertical wind profiles by Franklin et al. (2003) when comparing vertical wind shear in the BL within the eyewall and the "outer vortex" of Atlantic hurricanes. Based on the results shown in Table 10 of Franklin et al. (2003), the 300-m winds are typically 18% greater than the 50-m winds within the eyewall (strong wind) region. A cursory analysis of winds in the high wind region of the JUAN simulation reveals that there is more wind shear in this layer than the findings of Franklin et al. (2003) indicate. This is not surprising because the boundary layer (BL) beneath Juan was likely more stable than the typical BL in hurricanes studied by Franklin et al. (2003) where SSTs are generally 26°C or more. In particular, the 300-m winds are ~20-25% stronger than the 50-m winds in the JUAN simulation. This is consistent with one of the dropsondes on the southbound leg of the Convair flight in the high wind region north of the storm center that indicated 300-m winds 23% greater than the 50-m winds. However, there is considerable sonde-to-sonde variability in low-level wind patterns.

There is a region of enhanced vertical wind shear in the 50- to 300-m layer in the coastal zone along southern Nova Scotia, which is on the order of 15 m s^{-1}. This corresponds to ~40% increase in winds between 50 m and 300 m and could help to explain the pattern of heavy forest blowdown that was concentrated to ocean-facing hillsides not far inland from the coastline. The elevation of terrain in this high shear zone rises to ~150 m. Figure 20b shows a photograph of a forest blow-down over elevated terrain near

Beaverbank, Nova Scotia (north of Halifax). Similar blow-downs also occurred at lower elevations - particularly downwind of open terrain and in areas with full marine exposure.

3.4 Model Ensemble

a. Description of Ensemble Experiments

To provide a stronger argument for the role of anomalously warm SSTs on the weakening rate of Hurricane Juan, 15 additional simulations were conducted for each of the two SST configurations (JUAN and CLIM), giving a total of 30 additional experiments. Most of the ensemble members involve perturbation of the vortex parameters (initial conditions) such as storm position, size, and intensity (central pressure) within their observational error bounds. This serves as an effective way to gauge the sensitivity of the simulations to the initial conditions as well as other factors associated with the model itself, in particular, convective schemes and vertical resolution of computational levels. A summary of the ensemble experiments is shown in Table 2.

One of the vortex parameters that can be tuned is the percentage of the background flow used as a proxy for the wind field asymmetry and maximum surface winds in the initial specified vortex for a given MSLP (see section 2.2a). The default value for the JUAN control is 75%, but two ensemble members are created by changing the value to 50% and 100%. The corresponding initial maximum surface wind speeds for 50, 75 and 100% are 44, 47 and 51 m s^{-1} respectively. These values are similar to the range of error for winds

in the BT, namely ±2.5 m s^{-1}. Choosing 75% yields a value closest to the BT (46 m s^{-1}) valid at 00/28.

The second set of ensemble members involves adjustment of the initial vortex size. The storm track and intensity are far more sensitive to this than to any of the other parameters. The size is defined by the radius of the 15 m s^{-1} isotach (R_{15}). In the control experiments 250 km is used, which is determined by scaling the mean gale radius included in the NHC bulletin archive (http://www.nhc.noaa.gov/archive/2003/JUAN.shtml) by a factor of ~1.4 as discussed in chapter 2.

An additional pair of members consists of adjusting the initial storm intensity, which is done via perturbation of the MSLP. At 00/28 (the start time of the model) the MSLP of Juan was estimated to be 970 hPa, but the error in that value is approximately ±4 hPa, so that is used as a basis for the ensemble pair (966 hPa and 974 hPa). Four more members are generated by perturbing the initial storm location by 37 km (approximately three grid points) in each cardinal direction. The advertised positional error for Juan at 00/28 was 20 nm (37 km) based on information from the NHC bulletin archive.

Four additional members are created by adjusting the convective scheme of the 12 km run of the model (2 members) and by changing the number of vertical computational levels on the 3 km grid (2 more members). The convective scheme in most runs is given by Kain and Fritsch (1990) while two of the members use the Fritsch and Chappel (1980) and Kuo (1974) parameterizations. For the vertical resolution pair, there are 32 (9) levels

in one member and 48 (15) in the other member, where the number of BL levels is in parentheses. The default number of computational levels is 40 (top one at 35000 m), with 12 levels in the BL (below 1500 m).

The main objective for running an ensemble of experiments is to determine whether the difference in intensities between the control simulations (JUAN and CLIM) is statistically significant. Before presenting the collective results from the ensembles, a brief summary of the highlights from some of the ensemble sets is presented. Please refer to Table 2 for the list of experiments.

b. Overview of Model Sensitivities

By increasing the storm's initial wind field asymmetry, the storm drifts further to the west during the first 12 hours of the simulation (experiment EM2) while the storm whose initial wind field asymmetry is weakest (EM1), moves more slowly during this period and does not drift to the west. It is possible that there is something in the storm environment that is causing the storm to track further to the west, and that the more asymmetric and faster-moving storm (EM2) is encountering the feature sooner.

The simulated storm intensity appears to be most sensitive to initial storm size. The smallest storm (R_{15} = 225 km) weakens prematurely while the largest storm (R_{15} = 350 km) does not weaken fast enough with central pressure remaining slightly above 970 hPa after landfall. The control storm size (R_{15} = 250 km) yields the best landfall intensity

with respect to central pressure. It is no surprise that the larger storms weaken at a slower rate because it takes longer to spin down a large vortex versus a smaller one. It is also observed that the larger storms take a more easterly track across Nova Scotia after landfall. The smallest storm stays farthest to the west of any ensemble member. It is likely that the larger storm interacts differently with the (steering) environment than the smaller storm.

Investigation of the impact of initial storm intensity on the simulation shows that the simulation starting with central pressure of 974 hPa yielded a more realistic trend in SLP and MSW compared to the BT and even compared to the control runs with initial pressure of 970 hPa. When starting with a central pressure of 966 hPa, the model deepens the storm too much initially and then weakens it too rapidly. The SSTs are likely not warm enough to support this intense storm and the consequence is an unrealistic weakening trend.

The greatest impact of adjusting the initial storm position is on the storm track. The run with initial position furthest to the north yielded the greatest westward deviation in track and earliest landfall time (by just over two hours). A noticeable westward deviation was also observed in the initially more asymmetric and faster-moving member (EM2), which supports the claim that there was likely something in the environment ahead of Juan that may have induced the westward jog in the track in those simulations.

Although convection is explicitly computed on the 3 km grid, influences are detected on the storm track and intensity when using different convective schemes in the 12 km "driving" grid (refer to Fig. 8b for model integration layout). These 12 km simulations provide the initial and boundary conditions for the corresponding 3 km runs, which ultimately lead to somewhat different solutions. One key observation using the Fritsch-Chappel (FCP) and Kuo (KUO) schemes is that the MSLP slowly rises during the early part (first six hours - adjustment period) of the 12 km simulations while in the Kain-Fritsch (KFC) (control) simulations the MSLP slowly falls during this period. The trend in MSLP during the first six hours of the 3 km simulations driven by the 12 km simulations that use FCP and KUO convection is much steadier than for KFC convection. The KUO member actually yields a better result than the control run (JUAN). The track is very good (aside from the speed), and the MSLP and MSW are close to the BT curve (not shown). When run with the observed SST, this member shows that the MSW speeds are actually increasing slightly as the storm makes landfall (possibly the storm acceleration affect), while the climatology SST run of that member shows decreasing winds during the pre-landfall hours.

The final set of ensemble members are generated by altering the vertical resolution of the model. By increasing the number of levels throughout the troposphere and in the BL, the intensity of the storm is closer to the BT, especially while the storm is approaching land. The runs with coarser vertical resolution seem to lead to an overestimation of storm intensity. With fewer levels in the BL, the estimation of surface winds tends to be biased

on the high side because winds are computed at a slightly higher level (with stronger winds) than in the member with finer vertical resolution.

Although not part of the main ensemble of experiments here, a test simulation was run on the 12 km grid using GEM regional forecast model output every 6 hours, for comparison with analysis-piloted results. The forward speed of motion was similar to the analyses-piloted control run; however, the storm was ~100 km farther west near landfall. This would not have been a great forecast. The intensity of the storm at that point was somewhat weaker (MSW ~39 m s^{-1} or 75 knots) which is likely related to the longer track over cooler water. This simulation highlights the sensitivity of the track to the driving boundary fields (steering environment) which can, in turn, have an impact on the storm's intensity.

c. Analysis of Ensemble Means

A composite map showing the tracks of all 15 ensemble members from the observed SST (JUAN group) including the control run and the BT is shown in Fig. 21. The members are rather well clustered with no extreme outliers. The along-coast spread in landfall positions is ~100 km. The westward drift in the tracks during the early part of the simulations is apparent in the composite. The maximum positional error at the end of the 24 hour simulations was ~160 km which compares to the mean 24-hr operational NHC forecast error of ~150 km for this event (see Avila 2003).

Figure 22 shows time series of ensemble means of MSLP and MSW for each group of members (JUAN and CLIM) including the control runs (16 runs comprise each curve). These are all based on the 24-hour, 3-km runs. There is a consistent difference between the intensity of the JUAN members compared with the CLIM members. In terms of MSW, the difference is smallest near the beginning of the simulations and is greatest at 19 hours, which represents the landfall time of most members. The actual difference in landfall intensity works out to 4.9 m s^{-1} with a standard deviation of 1.6 m s^{-1}. This difference is statistically significant at least at the 99% confidence level using a paired t-test. Even the difference at hour zero is significant at the 99% confidence level. An important observation here is that the mean rate of pre-landfall weakening (in terms of MSW) in the CLIM members is greater than the JUAN members during the hour leading up to landfall. Also, it is noted that there is a period of strengthening in the winds between 7HR and 13HR in both cases corresponding to a period when the storm is already moving over cooler water. It is likely that this is related to acceleration of the storm during that time.

It is clear from the results that a sizable fraction of the difference (3.1 m s^{-1}) between simulated storm intensities for each ensemble group (JUAN group and CLIM group) occurs by 4 hours into the model run. In fact, the difference between the groups begins during the 6-hour, 12 km adjustment period, since at 0HR there is already a difference in intensities (1.4 m s^{-1}) (see Fig. 8b for time reference). Between 4HR and 18HR there is little change in the spread between the groups, and it is not until the one- to two-hour period prior to landfall that the spread increases to 4.9 m s^{-1} (e.g. intensity of the JUAN

group levels off while the CLIM group continues to rapidly weaken). In other words, ~65% of the difference in intensities between the two ensemble groups occurs during the early part of the simulation when the storm was over a weak warm anomaly of 1-1.5°C south of ~38°N (see Fig. 9). This may lead one to suspect that a significant contribution to storm intensity at landfall is owing to this weak warm anomaly, and that the shelf anomaly (between ~41°N and the Nova Scotia coast) has a secondary contribution. In the next subsection the influences of these SST anomalies on landfall intensity are examined.

d. Role of Specific SST Anomalies

There appear to be two zones of anomalously warm SST influencing the intensity of the Hurricane Juan simulations. Referring to Fig. 9, there is a 1-1.5°C warm anomaly south of 38°N over which the storm tracked. Between 38°N and 39.5°N the SST is near normal, while it is well above normal north of 41°N.

To diagnose the roles of these anomalies individually, groups of simulations are run for two SST configurations, one with the SST anomaly south of 38°N removed (group S38) and the other with only the northern (shelf) anomaly removed (group N38). The anomalies are simply computed by subtracting the climatology SST from the observed SST. The anomaly field is then edited in such a way to remove one anomaly while retaining the other. In Juan's case, the anomaly field is set to zero everywhere north or south of 38°N. A one-degree latitude linear transition zone is calculated along 38°N to remove the sharp gradients that result from the anomaly removal. The modified anomaly

field is then added to the climatology field, giving a new SST field used to run the sensitivity experiments. The groups of reruns for these experiments are based on a subset of the 15-member ensemble discussed earlier. Specifically, they include one member from each of the following experiments (see Table 2): EM1, ES2, EI2, EP2, EC2 and ER2. This selection of experiments is based on members demonstrating the greatest overall sensitivity (in terms of maximum surface wind speeds at landfall) to SST from the original set of simulations. This increases the likelihood of being able to distinguish the role of the individual anomalies.

The results from these experiments are plotted in Fig. 23 together with a subset of ensemble means (see section 3.4c) corresponding to the experiments listed above. It is clear that the near-landfall intensity is primarily dependent on the SST anomaly on the shelf. For example, by removing the shelf anomaly (N38), the near-landfall intensity is the same as climatology (Fig. 23b). To test the hypothesis that the near-landfall intensity of the N38 ensemble subset *differs* from climatology, a paired t-test is used on the 18-hour MSWs and a computed t-value of 0.5 with 6 degrees of freedom is found. With this very small t-value, one can certainly reject the alternative hypothesis that the means are different and conclude they are equal. Conversely, when the southern anomaly (S38) is removed and a t-test is conducted to determine whether this ensemble *differs* from the JUAN ensemble, a t-value of 0.4 is found, and a similar conclusion is drawn. It is observed that by removing the shelf anomaly, the storm responds rather quickly to the ocean beneath it and the intensity (as measured by MSLP and MSW) switches from an

"anomalous" state to a "climatological" state over a 6- to 8-hour period. The converse is also true.

At first it may seem that this result contradicts the observation made in section 3.4c that 65% of the difference between landfalling intensities of JUAN and CLIM occurred well before landfall. However, from the analysis of individual SST anomalies, one can see that the storm intensity is not strictly a direct function of how strong it was much earlier in its lifetime. A similar conclusion is drawn from the study of Hurricane Karen in chapter 5.

e. Extended Integration Experiments

Results discussed so far are based on numerical experiments beginning at a time when the hurricane was halfway through the weak southern SST anomaly around 00/28, and near maximum intensity. Although the main objective has been to study the spin-down period of the storm, it is instructive to obtain information on the role of SST over a longer period of the storm's lifecycle by conducting a set of additional experiments starting at 00/27, when Juan was still developing further to the south. The set consists of three simulations, one with observed SST for 00/27 (JUAN), the second with climatology SST (CLIM) and the third with the SST anomaly south of 38°N removed (S38) as in the earlier experiments starting at 00/28. The results from all 12- and 3- km runs of these experiments are shown in Fig. 24.

The near-landfall intensity of the JUAN and CLIM (3 km) simulations is 44.2 m s^{-1} and 35.4 m s^{-1}, compared to 44.8 m s^{-1} and 37.5 m s^{-1} from the previous control runs, respectively. However, the location of landfall is 70-100 km east of the actual landfall and approximately two to three hours *slow*. This is in contrast with earlier simulations where mean landfall time was approximately two hours too *fast*. The reasons for the differences are numerous and certainly related to the earlier start-up and overall longer integration (48 hours versus 24 hours for 3 km runs). The near-landfall intensity of the 3 km S38 simulation here is 40.2 m s^{-1}, which is approximately midway between JUAN and CLIM intensities. As a matter of comparison, recall the ensemble mean of near-landfall intensities for the of S38 experiments in Fig. 19 was very similar to the JUAN mean.

The 12 km MSLP and MSW traces in Fig. 24a and Fig. 24b highlight the necessity to allow at least 6 hours of "vortex adjustment" at the beginning of the runs. During the first hour of integration, the MSLP and MSW suddenly change in an unrealistic fashion, and then recover to a more realistic state after ~6 hours. The recovered intensity is weaker than the observed intensity, but experiments can still be compared in a relative sense, permitting fundamental conclusions to be drawn.

Based on these test experiments, which involve a much longer integration period incorporating part of the storm's developmental stage, it is seen that the storm begins to transition from the "climatological" state to an "anomalous" state in the S38 simulation. The transition is not completed prior to landfall, as was the case in the S38 simulations

initiated at 00/28. This difference is a consequence of the greater intensity spread between JUAN and CLIM prior to entering shelf waters, which occurs around 40HR.

3.5 Summary and Conclusions

Insertion and merging of the synthetic hurricane vortex into the initial large-scale analysis drastically improves the model's simulation of Hurricane Juan, compared to operational weather models that did not employ vortex insertion.

The primary result of the numerical simulations of Hurricane Juan revealed that there was a statistically significant impact of the anomalously warm SST south of Nova Scotia on the simulated intensity of the hurricane. The mean landfall intensity of the simulations using observed SST (JUAN), as measured from the maximum surface winds, was 42.5 m s^{-1} compared to 37.6 m s^{-1} for the simulations with climatology SSTs (CLIM). The difference was 4.9 m s^{-1} with a standard deviation of ±1.6 m s^{-1}, and is significantly different from zero at the 99% confidence level. Since the destructiveness of wind is proportional to the power of the wind (which is proportional to wind speed cubed – Emanuel (2005)), the CLIM storm was only ~70% as destructive as the JUAN storm at landfall.

Simulations proved very sensitive to a number of vortex and model configurations. They were most sensitive to the vortex size specified in the initial conditions. The larger storm weakened too slowly when moving over land and cool water, and tracked too far to the

east over Nova Scotia. Since larger vortices take longer to spin down, the intensity behavior is not surprising. The smaller storm weakened too quickly and tracked too far to the west. Storms of different size would also interact differently with the environment which could explain the difference in tracks. It was discovered that simulations employing the Kuo convective parameterization on the 12 km grid yielded better intensity and track results than Fritsch-Chappel and Kain-Fritsch schemes. Increasing the vertical resolution in the model lead to improvements in the surface wind field, since the lowest computational level in atmospheric BL was closer to the surface.

The vertical structure of the wind field in the BL was analyzed over the cool waters on the Scotian Shelf. The wind shear was strong below the low-level jet in the high wind region of the storm, comparing well with observations. The height of the low-level wind jet was lower (300-400 m) in the high wind region of the CLIM (cooler water) storm than the JUAN storm (500 m) with observed SSTs. However, the magnitude of BL wind shear in the CLIM storm was not significantly different from that of the JUAN storm. The reason being that — along with the weaker surface winds — the low-level jet itself was weaker, since the winds also weakened *above* the surface after encountering the cooler water.

Model output was compared with surface weather data and GPS dropsonde data taken from a research aircraft that flew into the storm immediately prior to landfall. The model effectively reproduced the deep layer of high winds on the right side of the rapidly-moving storm with low-level winds in excess of 60 m s^{-1}. It also simulated

thermodynamic structures (as denoted by θ_e) in the storm rather well, but overestimated the θ_e overall. The horizontal structure of the wind field at landfall was reproduced quite accurately with the area of maximum winds striking Halifax and areas to the east. The radius of maximum winds in the control simulation was near 45 km compared with an estimate of 35 km based on wind damage patterns.

Two distinct warm SST anomalies (a southern one and a northern one) played a role on the intensity of Juan. The role of each anomaly was investigated separately by removing one from the analysis while retaining the other. Ensembles were run for initial time at 00 UTC 28 September while single control runs were run for initial time at 00 UTC 27 September (not shown). It was found that as the storm moved over the continental shelf waters, it began to transition from a "climatological" state to an "anomalous" state when only the northern warm SST anomaly was retained. For the simulations starting on 28 September, the storm was as intense as the JUAN control simulation at landfall, implying that the southern SST anomaly made little difference in landfall intensity. *However*, when starting the model on 27 September, the landfall intensity was midway between that of the CLIM and JUAN experiments, implying that the SST anomalies made an equal contribution to the landfall intensity. The latter conclusion is more realistic, for the influence of SST over a greater period of the storm's lifecycle was diagnosed.

CHAPTER 4

Case Study: Hurricane Michael

4.1 Introduction

On 17 October 2000 meteorologists at the MSC and the CHC were monitoring the development of Hurricane Michael some 500 km west-southwest of Bermuda. The large-scale atmospheric flow suggested that the hurricane would move northeastward toward eastern Nova Scotia or Newfoundland and would require the issuance of forecast bulletins and warnings by the CHC.

While the CHC began issuing warnings on the storm, the weather research group at the MSC was considering Michael as a candidate storm for a research aircraft mission using the Convair 580 aircraft. Plans to conduct such a flight had been in the works prior to the formation of Michael to gather data and gain insight into the structural changes taking place in storms undergoing ET. On 18 October a mission was arranged by the MSC in partnership with the NRC to fly the Convair 580 (owned and operated by the NRC) into Hurricane Michael southeast of Nova Scotia. A summary of the research mission and the meteorological data that was collected is discussed by Abraham et al. (2004).

Almost five years after the storm, this case is revisited here from a numerical modeling standpoint. The primary focus for this case is to simulate the evolution of Hurricane Michael with the MC2 model (Benoit et al. 1997), and to demonstrate how simple

insertion of the synthetic, observationally-consistent TC vortex into the model initial conditions (Davidson et al. 1993) prior to the onset of ET, leads to a greatly-improved hindcast of the event. Following the same approach as for Hurricane Juan, the model is initiated using only observational data (~24 hours prior to landfall) that would have been available in real time, as if being run in forecast mode. Furthermore, the model is used to diagnose structural changes in the storm during ET and compare with aircraft data and surface meteorological observations.

The specific operational forecast challenge with extratropically-transitioning Hurricane Michael was determining whether the hurricane or a new baroclinic (i.e. frontal) cyclone north of the hurricane would become the dominant storm center. Unfortunately, operational weather forecasters at the CHC did not have much information in terms of high-resolution numerical guidance at the time. The Canadian GEM forecast model (the primary weather forecast model in Canada) incorrectly developed the new baroclinic cyclone, since the hurricane (which in reality became the dominant circulation) was poorly represented in the initial conditions. Furthermore, at the time, the GEM model only had a horizontal resolution of 24 km in its high-resolution window, which is insufficient for modeling hurricanes.

The situation is summarized below in a quote from the forecast bulletin issued at 12 UTC 19 October 2000 by the CHC:

"THE NEW BAROCLINIC LOW HAS APPEARED AROUND 05Z AND IS INTENSIFYING RAPIDLY. AT 09Z IT WAS LOCATED BETWEEN BUOY 44142 AND THE NOVA SCOTIA COAST. THE TWO SYSTEMS WILL EVENTUALLY MERGE INTO AN INTENSE MID-LATITUDE LOW. THE PROBLEM REMAINS WHERE THE MERGER WILL TAKE PLACE AND WHICH SYSTEM WILL BECOME DOMINANT."

Late in the morning of 19 October it became apparent to forecasters that the hurricane would remain the dominant circulation center, but there was still considerable uncertainty about how the storm was going to evolve during its approach to Newfoundland. These issues resulted in only a short forecast lead-time for severe conditions in southern Newfoundland. It will become apparent in this chapter how the mesoscale modeling approach with synthetic vortex insertion would provide valuable guidance if run in a forecast setting for this event.

4.2 Synoptic History of Hurricane Michael

Hurricane Michael originally formed from an extratropical low pressure system to the southwest of Bermuda from 12 to 15 October 2000 (see Fig. 25). Davis and Bosart (2003) give a detailed description of this formation period. At 12/15 the large cyclonic system had developed organized convection about its center and was declared as a subtropical depression by the NHC. A day and a half later at 00/17 it was designated as Tropical Storm Michael and by 18/17 Michael had reached hurricane strength with MSW near 33 m s^{-1} (65 kts).

On 18 October Michael began to accelerate toward the northeast as it moved into the region of stronger environmental winds north of 30°N. These winds caused a spreading-out of high clouds to the north of Michael as shown in Fig. 26. Michael reached its maximum pre-ET intensity with maximum sustained surface winds of 39 m s^{-1} (75kts) at

00/19 (Fig. 26b). After some weakening between 00/19 and 06/19, ET began to take place[2] (Fig. 26e) followed by significant intensification between 06/19 and 18/19 (Fig. 26d to Fig. 26i) while interacting with a sharpening mid-tropospheric trough (Fig. 26c and Fig. 26f) and a strong surface baroclinic zone. Michael was also accelerating very rapidly during this period with maximum forward translational speeds near 30 m s^{-1} over decreasing SSTs (see Fig. 25). The "hybrid" storm made landfall at 2230/19 on the south coast of Newfoundland with MSW near 39 m s^{-1} (75 kts). At that time the storm was rapidly loosing tropical characteristics. For a more detailed description of this event the reader is referred to Abraham et al. (2004).

The lifecycle of the baroclinic low introduced in the previous section began around 06/19 approximately 200 km south of Cape Sable, Nova Scotia. A subjective (i.e. manually drawn) sea level pressure analysis of the hurricane and this baroclinic low at 12/19 is shown in Fig. 27. The key to identifying a circulation in that region came from weather buoy 44142 which showed light southwest winds not far south of the estimated center of the low in Fig. 27. The low tracked toward the northeast initially, then toward the east after 12/19 (Fig. 28). By 18/19 the low had become incorporated into the circulation of the rapidly expanding sea level pressure field of the hurricane. A discussion of the evolution of this low will be presented in more detail in section 4.3.

4.3 Control Simulations

[2] The onset of ET here is determined subjectively by observing satellite imagery and noting that dry air was being advected into the storm early on 19 October 2000.

Grid configurations and model integration periods are shown in Fig. 29. The 12 km (0.108°) latitude-longitude grid is centered on the area of interest from 25.4°N to 54.6°N and from 78.2°W to 45.8°W and the 3 km (0.027°) grid includes Nova Scotia and Newfoundland from 36.2°N to 49.7°N and from 65.7°W to 52.2°W.

The vortex is constructed using key observational data from the NHC best track (Stewart 2000) and from NHC operational message archives (available online at: http://www.nhc.noaa.gov/archive/2000/MICHAEL.html).

The experiments are initiated at 00/19 on the 12 km grid and are piloted by large scale analyses as described in chapter 2. This initial time was chosen when Michael was at its most developed *pre-transition* stage (Fig. 26b). It is important to apply the insertion before the onset of ET since the technique is most appropriate for TCs with a generally symmetric moisture structure. After the 12 km simulation is completed, the second integration on the 3 km grid is run for 18 hours. The initial time of the 3 km simulations is 12 hours after the vortex insertion, which is believed to be enough time for the model to "adjust" to the hurricane in this case.

a. No-vortex Simulation

A no-vortex simulation of this event is first conducted (hereafter called NOVOR) on the 12 km grid beginning at 00/19 with a 42-hour integration length ending 18/20. The results of this simulation are compared with output from the regional GEM model

forecasts for the same period. The GEM had a horizontal resolution of 24 km at the time of this event and was one of the primary sources of numerical guidance for weather forecasters during the storm. This will be referred to hereafter as GEM24.

With its relatively coarse resolution and scarcity of hurricane observations in the initial conditions, the GEM24 simply forecast a trough of low pressure at the location of Hurricane Michael. The model developed a baroclinic low south of Nova Scotia (the same low introduced earlier) and tracked it toward southwestern Newfoundland as shown by the track in Fig. 28. The NOVOR simulation yielded a similar solution (see Fig. 28) with the baroclinic low being the dominant cyclone; however the model did generate a weaker low in the location of Hurricane Michael (not shown). This low was much too weak to be considered an adequate representation of the hurricane and tracked too far to the east over the Avalon Peninsula in eastern Newfoundland. Also in Fig. 28, the subjectively-analysed track of the baroclinic low is shown for comparison (taken from Abraham et al. 2004).

The important difference between the observed track of the baroclinic low compared to the model results is that the observed low moves eastward between 12/19 and 18/19 while the GEM24 and NOVOR model runs show a motion toward the northeast close to the coast of Cape Breton (see Fig. 28). This eastward motion occurs when the low becomes incorporated into the circulation of the hurricane – this was not captured by the models, but would have been the key to a decent numerical forecast of the event. Surface weather data described by Abraham et al. (2004) suggest that the low may not have

completely merged with the center of the hurricane (indicated by the northward turn in the track in Fig. 28); however it was clear that the hurricane became the dominant cyclone.

b. Vortex-initiated Control Simulations

The 12 km control simulation (MICH12) for this event is initiated in the same fashion as for Hurricane Juan using the vortex insertion technique described in section 2.2a. The fine-scale 3 km control simulation for this event will be referred to hereafter as MICH3. For these runs, SST data from the CLASS archive valid at 00/19 is used for the model ocean surface boundary condition.

Simulated storm tracks are shown in Fig. 30a for MICH12 and in Fig. 30b for MICH3 including results from the climatology SST (CLIM) runs, which will be discussed in section 4.4. Table 3 includes the vortex and model specifications for the 12 km control run. The remaining contents of the table refer to the ensemble system to be discussed in section 4.4. Also plotted is the BT from Stewart (2000) with some refinements made during the pre-landfall period from the study of Abraham et al. (2004). The overall track prediction is very good. The location of landfall is within 50 km of the actual landfall for both the 12 and 3 km runs. The timing of landfall is only 1 to 1.5 hours later than reality. The model reproduces the deceleration of the storm after landfall with an eastward motion during the day on 20 October indicating that it was "captured" by the upper level

low shown in Fig. 26l. The general track of the baroclinic low in the MICH12 run (not shown) compares with the observed track shown in Fig. 28.

Figure 31 displays time traces of MSLP, MSW and SST beneath the storm center for MICH12 and MICH3 simulations including the BT. Simulation hour zero in Fig. 31a-c corresponds to the time of vortex insertion. Focusing first on the MICH12 results, it is apparent that the model tends to deepen the storm from the start when in reality it weakened before undergoing rapid intensification after 6 hours (06/19). Given that the model requires approximately 6 hours adjusting to the new initial condition, little faith is put in the early part of the simulation. Most of the mismatch between observed MSLP and modeled MSLP occurs in the first 6 hours of the simulation. The greatest difference in the MSW values occurs at the 9-hour mark. It appears that the model is still "accommodating" the prescribed vortex at 9 hours, so starting the 3-km simulation after 12 hours seems reasonable. The model does not capture the rapid intensification, but it does deepen the storm over the cooler waters and accurately represents the storm-central sea level pressure immediately prior to landfall. The modeled storm continues deepening to below 960 hPa after landfall (~5 hPa deeper than reality) however the MSW is quite close to the observed winds during that period.

Results from the MICH3 control are also shown in Fig. 31a-c. One noticeable difference from MICH12 is that the MSW reaches 52 m s^{-1} (100 kts) in MICH3 compared to 47 m s^{-1} (91 kts) in MICH12. Both are overestimates of the observed MSW, which was near 44 m s^{-1} (85 kts). Regardless, this is much better than the NOVOR run which generated

maximum winds of only 28 m s^{-1} (55 kts) at that time (not shown). Before proceeding, it should be once again clarified that when referring to output from the model, MSW is the maximum instantaneous (e.g. snapshot) surface wind anywhere in the storm, where "surface" is defined at the 60-m (40-m) (e.g. lowest computational) level in the 12 km (3 km) simulations. Given that low-level wind shear magnitudes were very strong in Hurricane Michael (see Abraham et al. 2004) it is not a surprise to see differences between 10 m, 40 m and 60 m.

c. Impact of Vortex Insertion

The impact of employing the vortex insertion method in the model initial conditions will now be examined, and compared to the no-vortex simulation discussed in section 4.3a. Fields of sea level pressure at 00/20 (24-hour prediction) are shown in Fig. 32 for GEM24, NOVOR, MICH12 and are compared with a manually drawn sea level pressure analysis (Fig. 32a). The NOVOR and GEM24 solutions clearly fail to capture the storm structure. The NOVOR run produces the baroclinic cyclone (discussed in section 4.3a) of 980 hPa not far east of Cape Breton and a weak (985 hPa) cyclone moving toward the Avalon Peninsula of Newfoundland (see Fig. 3). The eastern low is the model's poor interpretation of the hurricane. The experiment with the vortex inserted into the initial conditions (MICH12) leads to a much different solution at 00/20 (Fig. 32d) with a 964-hPa storm immediately south of Newfoundland and an area of high winds on the east side of the low. This matches well with the analysis in Fig. 32a and with wind damage reports

within about 200 km east of landfall. The no-vortex runs fail to produce this tight wind and pressure pattern.

Operationally, forecasters at the CHC did not have numerical guidance of the form in Fig. 32d. A conceptual blending of the GEM24 solution (Fig. 32b) and real time observations (buoys, ships, satellite imagery, etc.) was made to produce amended forecasts for the Newfoundland area as Michael raced toward the coast. Hypothetically speaking, had the hurricane configuration of the MC2 model existed in October 2000 with results available in real time, forecasters would have had a much better idea of the storm evolution well before landfall and thus a more accurate forecast (with less uncertainty) would have been likely, with an improved forecast lead-time. As presented in section 4.4, even when the uncertainties in the initial vortex prescription are accounted for, the simulation remains superior to GEM24 and NOVOR.

All simulations on the 12km grid in the present study are "piloted" by analyses from the CMC Data Assimilation System archive (Chouinard et al. 1994) as described in chapter 2. A test run on the 12 km grid using GEM regional forecast model output every 6 hours was conducted for comparison. The result of that experiment (not shown) was similar to the analyses-piloted solution (in terms of storm structure); however the location of landfall was approximately 100 km further east. This emphasizes that the simulation or forecast of the storm track is also sensitive to the large scale environment (i.e. grid boundary conditions), as was discovered from a similar experiment of Hurricane Juan in chapter 3.

d. Structural Evolution During ET

A manually drawn sea level pressure analysis[3] of Hurricane Michael at maximum intensity is shown in Fig. 33a. Model-simulated sea level pressure and surface (40 m) wind speeds from the MICH3 simulation are shown in Fig. 33b for comparison. Simulated surface temperatures (40 m) are shown in Fig. 33c. Generally there is good agreement on the central pressure and overall storm circulation as depicted by the isobars - keeping in mind that the model time is one hour later to account for the ~1-hour delay of the simulated storm. Although the baroclinic low (which formed south of Nova Scotia) is represented in the model, it is not as close to the center of Michael as indicated in the analysis in Fig. 33a. It should be noted, however, that there is not enough data to confirm the actual location of the baroclinic low in Fig. 33a. Based on the work of Abraham et al. (2004) it was speculated that the low was not far to the southwest of Michael as shown by "L?" in Fig. 33a. The trough in SLP associated with the baroclinic low extends west of Michael in the model, while it is southwest of Michael in the analysis. Despite these differences, the hurricane is the dominant cyclone in the model.

The wind field around the center of Michael in Fig. 33b seems very realistic although there are not enough surface wind observations to construct a 2D wind field for Fig. 33a. The MSW (at 40 m) at this time is 41 m s^{-1} (80 kts) 85 km to the south-southeast of the center. The magnitude is consistent with a ship report of 41 m s^{-1} measured 30 m above

[3] The analysis was originally constructed at the Newfoundland Weather Centre in October 2000 and modified by Abraham et al. (2004) prior to the numerical simulations.

sea level approximately 20 km east of the storm center at 17/19 (keeping in mind the error in storm position is on the order of 25 km based on the analysis on page 1330 of Abraham et al. (2004)). This also suggests that the wind field was extremely "tight", which is replicated in the simulation.

The presence of a significant background temperature gradient (i.e. baroclinic zone) shown in Fig. 33c highlights the extratropical nature of the environment. The warm front in the analysis in Fig. 33a is reflected well in Fig. 33c as denoted by the tight gradient in temperature. The storm would be considered as purely extratropical if the tight temperature gradient (front) extended into the center, but that is not seen here because the storm is still a hurricane with a warm core. A similar pattern in temperature is present above the BL (not shown) indicating that this pattern is not confined to the surface.

Rainfall from Hurricane Michael and the baroclinic cyclone was spread over a large portion of Atlantic Canada as shown in Fig. 34a. Much of the rainfall over the Maritime Provinces (New Brunswick, Nova Scotia and Prince Edward Island – see Fig. 3) was related to the baroclinic system that moved south of Nova Scotia. Heaviest rainfalls occurred over the Cape Breton Highlands with amounts of 80 mm or more as indicated in the figure. Over Newfoundland, the heaviest rainfalls occurred over the western part of the island. Amounts over 70 mm were reported along the Northern Peninsula. By the time the remnants of Michael had exited Newfoundland, the storm was moving much more slowly than when it arrived. This slow forward motion likely contributed to the higher rainfalls over the Northern Peninsula. Accumulations were less over eastern

Newfoundland to the right of the storm track, which is typical of a storm undergoing ET (Klein et al. 2000).

Simulated rainfall accumulations from the MICH12 control run are displayed in Fig. 34b. The overall pattern and amounts of rainfall are consistent with the analysis. There are greater rainfall amounts over eastern Nova Scotia with a maximum over the Cape Breton Highlands similar to what was observed. The model indicates large amounts of rainfall over the Northern Peninsula and along the west coast of Newfoundland, although the amounts along the immediate coastline appear to be overdone. Also overestimated are the amounts over eastern Newfoundland in the regions of onshore flow. The model has a tendency to inflate precipitation amounts in onshore/upslope flow regardless of deep convective parameterization scheme or cloud microphysical scheme. This was observed in the rainfall output for Tropical Storm Karen, which will be noted in the next chapter. The operational GEM forecast model (which employs the same physics package as the MC2 model) also has a tendency to over-predict precipitation amounts in onshore/upslope flow (personal experience).

In the following discussion, vertical cross sections through Michael's high wind region sampled by dropsondes from the Convair 580 (Fig. 35a) over a distance of ~500 km valid near 17/19, will be analyzed. The cross sections of horizontal wind speed and equivalent potential temperature from both dropsondes and the 3 km control run of the model are shown in Fig. 36. The cross sections from the model are taken from a similar cut through the high wind region of the storm, but at 18/19, to account for the slightly slower storm

motion in the model. Displays of the magnitude of the horizontal winds are shown in Fig. 36a and Fig. 36b. The model generally does a good job replicating the deep layer of high winds on the right side of the storm (storm is moving into page and located near the center of the cross sections). On the other hand, the model failed to capture the extreme wind values in the 950 to 750 hPa layer observed in the dropsonde data. The bottom of the wind jet appears close to 925 hPa in both. Cross sections of equivalent potential temperature (θ_e), as calculated in chapter 2, are shown in Fig. 36c and Fig. 36d. The warm core of the tropical cyclone is evident in both model and data, but the shape and orientation of the feature differs. The model contains lower θ_e air intruding on the east (right) side around 600 hPa. Both show an area of low θ_e air (~328 K) in the lower and eastern side of the storm near the high wind region. It is believed that this is related to cooler/drier air being entrained into the storm as discussed by Abraham et al. 2004.

Time series of vertical cross sections of θ_e and horizontal wind speeds from the MICH3 control experiment provide a summary of the thermodynamic and dynamic changes in the storm structure during ET in Fig. 37. The cross sections run from west to east through the center of the storm along a distance of 500 km. Panel (a) shows the structure of the initial idealized storm vortex. By 12/19 (Fig. 37b), ET has already begun as seen by the jet of low θ_e air on the west side of the storm. Drier air also intrudes into the mid levels of the storm (~500 hPa). As ET continues, the warm core tilts toward the west and the strong wind jet encircling the storm contains increasingly drier air, in effect "secluding" the warm core from the cooler airmass to the north. This pattern is observed to a certain extent from the dropsonde analysis in Fig. 36d. The jet on the east side of the storm

becomes elevated to near the 700 hPa level by 19/19 (Fig. 37d) and the warm core becomes thermodynamically decoupled from the cooler SSTs (~14°C) as shown by the cool θ_e air in the lower BL. In the hours leading up to landfall, drier air intrudes into the midlevels of the storm imparting an eastward tilt to the warm core and then destroying the upper part of it (Fig. 37e). Immediately prior to landfall (Fig. 37f) very low θ_e air (< 310 K) floods in from the west and the storm becomes frontal, although an elevated warm core remains.

4.4 Sensitivity Experiments

a. Summary of the Ensemble System

An ensemble of 15 experiments is run on the 12 km grid for Hurricane Michael to provide a measure of storm sensitivity to various initial conditions and model parameters. Many of the members are based on perturbations to the synthetic vortex in the initial conditions (same as for the Juan experiments) within the bounds of observational uncertainties upon which the vortex is constructed. One of the ensemble members for Michael employs a different cloud microphysical scheme, to be discussed below. A summary of the members is displayed in Table 3.

The default (control) value for percentage of the background flow used as a proxy for the wind field asymmetry and maximum surface winds in the initial specified vortex is 50%, but two additional ensemble members are created by changing the value to 25% and 75%. The corresponding initial maximum surface wind speeds for 25, 50 and 75% are

34, 38 and 41 m s^{-1} respectively. These values represent a realistic range in the observed storm intensity (typically ±5-10 knots in MSW, or ±2.5-5 m s^{-1}). Choosing 50% yields a value closest to the observed (BT) intensity of 39 m s^{-1} at 00/19.

The initial vortex size (R_{15}) for the control run is 320 km. Three additional members of the ensemble are created by perturbing R_{15} to 290, 380, and 430 km. The control radius was determined by scaling the mean gale radius included in the NHC forecast advisory archive (http://www.nhc.noaa.gov/archive/2000/MICHAEL.html) by a factor of ~1.4 as described in chapter 2.

An additional pair of members is generated by adjusting the initial storm intensity, which is done through perturbation of the MSLP. At 00/19 (the start time of the model) the MSLP of Michael was estimated to be 983 hPa, but the error in that value is approximately ±4 hPa, so that is used as a basis for the pair (979 hPa and 987 hPa). Four more members are generated by perturbing the initial storm location by 74 km (~six grid points) in each cardinal direction. The advertised positional error for Michael at 00/19 was 40 nm (74 km) based on information from the NHC forecast advisory archive.

The convective scheme is switched from Kain and Fritsch (1990) in the control run to Fritsch and Chappel (1980) for one member and to Kuo (1974) for another to examine the sensitivity of the storm simulations to the choice of convective parameterization. Vertical resolution was increased from 25(7) levels in the control run to 35(10) comprising another member of the ensemble suite (number of BL levels below 1500 m is

shown in parentheses). The final member in the suite employs the cloud microphysical scheme of Kong and Yau (1997). The default (control) microphysical scheme in the simulations follows that of Tremblay et al. (1996).

A composite of simulated storm tracks from the 15-member ensemble plus the control run is shown in Fig. 38. The tracks are clustered fairly closely together with no significant outliers. The degree of spread in tracks with time is also quite small. This is likely owing to the fact that the atmospheric steering flow is very strong and there is not a lot of time for the storm to deviate from the control solution. The mean 24-hour error in storm position (valid time 00/20 near landfall) for the ensemble was 161 km. The 24-hour CHC operational forecast position for Michael (valid at 00/20) was 47°N, 60°W with maximum surface winds near 28 m s^{-1} (55 kts) and central pressure of 994 hPa. This corresponds to an error in the track forecast of 400 km and intensity error of 11 m s^{-1} (20 kts) and 28 hPa too high in terms of central pressure. This highlights the difficulty in the forecasting of this event. Incidentally, subsequent forecasts (closer to the time of landfall) did improve once it became clear what was happening.

The ensemble means for MSLP and MSW are shown in Fig. 39 compared with the BT. The ensemble means do not differ significantly from the control run (Figs. 31a and 31b), but the degree of variability among ensemble members can be seen, as indicated by the one-standard deviation range bars in the plots in Fig. 39. There is a significant amount of variability in MSLP that grows with time during the first 15 hours of the experiments. In terms of MSW, the degree of variability is greatest between simulation hours 9 and 18.

Incidentally this corresponds very closely to the period when Michael was undergoing ET. The variability then drops after 18 hours and is relatively small after 24 hours, which corresponds to the extratropical phase of the storm. The landfall intensity in terms of wind speed at simulation hour 24 does not appear to be highly sensitive to the perturbed initial conditions and model parameters. Much of the variability during the ET period occurs among members employing different convective and cloud microphysical schemes. This suggests that cloud processes are important in governing the intensity during the ET re-intensification period of Hurricane Michael.

b. Influence of SST

To diagnose the influence of SSTs on the intensity evolution of Hurricane Michael, simulations identical to MICH12 and MICH3 are conducted, but the climatological SST field from Geshelin et al. (1999) is used instead. A map showing the observed minus climatology SST (anomaly) with the storm track is shown in Fig. 40. The SSTs were near normal south of ~40°N and anomalously warm north of that along the storm track, with the largest anomaly of 3-4°C near 43°N.

Results from the climatology SST runs (CLIM12 and CLIM3) are shown in Fig. 30 and Fig. 31. The impact on storm track is negligible, especially when compared with the variability in tracks from the ensemble system. There appears to be some impact on storm intensity, but the signal is not as clear as it was for similar experiments with Hurricane Juan in chapter 3. For instance, there is not a great difference in MSLP and

MSW between the MICH3 and CLIM3 at the time of landfall (see Fig. 31a and Fig. 31b). The only difference in MSW that appears significant occurs during the high resolution runs (MICH3 and CLIM3) between total simulation hours 14 and 18. This corresponds to the period when the simulated storm travelled between 40 and 43°N over the warm SST anomalies shown in Fig. 40. Although a CLIM ensemble was not conducted, the same behavior was observed when comparing the same SST experiments for two other members (EC1 and EP2, not shown) run at 3 km resolution.

4.5 Summary and Conclusions

During the ET of Hurricane Michael south of Newfoundland, a baroclinic cyclone formed to its north and became absorbed into the hurricane circulation. The model successfully simulated this evolution when inserting a synthetic hurricane vortex into the model initial conditions. On the other hand, when a hurricane vortex was not used in the initial conditions, the baroclinic cyclone became the dominant circulation. During the actual event, forecasters did not have access to a hurricane-resolving model, and therefore were unsure which scenario would materialize until approximately six hours before landfall. A "pseudo-forecast" (piloted by synoptic-scale numerical weather forecasts from the GEM model) conducted as a test for Hurricane Michael, lead to a significantly improved depiction of the storm lifecycle as in the simulations piloted by analyses.

Michael intensified over water less than 26°C while interacting with a strong baroclinic zone. This intensification was captured by the model; however, the intensification was

not as rapid as that observed during the event. The model (run at 3 km resolution) produced realistic storm intensity at landfall with central pressure of 967 hPa (compared to observed pressure of 966 hPa) and maximum surface winds of ~36 m s^{-1} (compared to observed winds of ~39 m s^{-1}). The location of strongest surface winds correlates very well with the area that experienced the most wind damage and highest wind reports over the Burin and Connaigre Peninsulas of Newfoundland (see Fig. 3).

Aircraft measurements of Hurricane Michael showed the presence of a deep layer of strong winds on the southeastern side of the storm. The model also simulated this structure, but the model winds were not as intense as the observations. Aircraft, satellite and radar data indicated that Michael was tilted toward the east or northeast prior to landfall. The model showed storm tilt toward the northwest originally then toward the east and northeast during its approach to southern Newfoundland, which is consistent with the observed tilt during that time.

A suite of sensitivity experiments was conducted to diagnose the sensitivity of the simulations to various initial conditions and model parameters. Variability in storm intensity (in terms of maximum wind speeds) among the experiments was greatest during the ET phase of the storm while it was much less during the extratropical phase. When testing the role of warm sea surface temperature (SST) anomalies along the track of Michael by conducting a climatological SST simulation, the intensity appears to be sensitive to the local SST anomaly between 40° and 43°N (~2.5-5 m s^{-1} weaker winds

than in the control run) yet there was no significant impact on storm intensity at or following landfall.

CHAPTER 5

Case Study: Hurricane Karen

5.1 Introduction

During mid-October, 2001, Hurricane Karen formed in the western North Atlantic Ocean, near Bermuda, and moved northward making landfall in Nova Scotia, Canada as an extratropically-transitioning tropical storm. Although Karen's impact in Nova Scotia was not significant, there was considerable uncertainty as to how quickly the storm was going to weaken, and undergo extratropical transition, while traversing cooler ocean surface temperatures prior to landfall. In particular, there was a much greater degree of uncertainty in the storm track predictions than is normally the case for tropical cyclones in the middle latitudes.

The focus for this case is on the weakening and subsequent ET of Hurricane Karen in October 2001 over Nova Scotia. The MC2 model is used to run a suite of sensitivity experiments of the event to diagnose sensitivity to 1) initial specifications of the vortex, 2) boundary conditions, and 3) model physics parameterizations in much the same way as done for Hurricanes Juan and Michael. Some of the operational and numerical forecasting challenges are also presented, and the model results are used as a framework for analysis and discussion.

5.2 Synoptic History of Hurricane Karen

Hurricane Karen formed from a large baroclinic cyclone southeast of Bermuda on 11 October, 2001. The cyclone eventually acquired tropical characteristics and became a subtropical storm by 00/12 as classified by the NHC. The storm continued to develop tropical characteristics on 12 October and completed "tropical transition" by 06/13 when it was declared as Tropical Storm (TS) Karen. Figure 41 shows the complete track of Karen from incipient extratropical low to hurricane, then back to an extratropical low via ET over Nova Scotia. Both subtropical and tropical storm periods are denoted by the conventional TS symbol in the figure. The track is constructed from the BT from Stewart (2001) and is extended beyond 18/15 using objective sea level pressure analyses archived at the CMC. This extended best track will continue to be referred to as 'BT' throughout this chapter.

Karen had become a 65-knot (33-m s^{-1}) hurricane at 18/13 and attained maximum intensity of 70 knots (36 m s^{-1}) by 06/14. The storm quickly weakened back to TS status by 12/14 and steadily weakened during its approach to Nova Scotia where it made landfall as a 40-knot (21-m s^{-1}) TS at 12/15 near Liverpool, approximately 150 km west-southwest of Halifax. By that time, Karen had already begun to exhibit signs of undergoing ET since much of the heavy rain had shifted to the western half of the storm – a telltale sign of ET (Klein et al. 2000). An infrared satellite image (courtesy of the Johns Hopkins University Applied Physics Laboratory) from the AVHRR prior to landfall (0941 UTC) is displayed in Fig. 42. Karen was declared extratropical by NHC at 18/15.

The remnant low continued to race northward into Labrador where it had become absorbed into a larger extratropical system near 06/16.

5.3 Control Simulations

Grid configurations and model integration periods are shown in Fig. 43. The 12 km (0.108°) latitude-longitude grid is centered on the area of interest from 25.4°N to 54.6°N and from 78.2°W to 45.8°W and the 3 km (0.027°) grid includes Nova Scotia from 36.7°N to 48.9°N and from 67.0°W to 61.0°W.

The vortex is constructed using key observational data from the NHC best track (Stewart 2001) and from NHC operational message archives (available online at: http://www.nhc.noaa.gov/archive/2001/KAREN.html) as well as surface wind information from the "QuikSCAT" scatterometer storm archive available online at http://manati.orbit.nesdis.noaa.gov/cgi-bin/qscat_storm.pl.

The first run of the model begins at 06/14 on the 12 km grid. This initial time was chosen when Karen was at its maximum intensity and well before ET. After the 12 km simulation is completed, the second integration on the 3 km grid is run for 30 hours beginning at 12/14 – 6 hours after the initial time for the 12-km run.

Two control simulations are run for Hurricane Karen, beginning with the 12 km domain (KAR12 run) which runs for 48 hours ending 06/16, and is piloted by large scale analyses

as described in chapter 2. The 3 km control simulation ends at 18/15 which will be referred to as the KAR3 run. Specifications for the KAR12 run are shown in Table 4. The initial size of the hurricane (R_{15}) was determined by "eyeballing" the mean radius of 15-m s^{-1} (~30-knot) winds around the storm circulation using QuikSCAT satellite overpasses near the initial time. As for the Hurricane Michael experiments, analysed SSTs from the CLASS website (http://www.class.noaa.gov/nsaa/products/) valid at 00/14 are used for the model ocean surface boundary condition.

Tracks of the simulated storm including the BT are displayed in Fig. 44. The overall speed of motion of the storm while approaching Nova Scotia is close to reality, but there is a clear departure of the track toward the east, leading to landfall at Halifax as opposed to near Liverpool (~150 km to the west-southwest). The same behavior is apparent in the KAR3 run (Fig. 44b). Incidentally, most of the operational and numerical track guidance during this event had an eastward bias, which is likely related to incorrect steering currents in the large-scale circulation (piloting fields). This will be discussed in section 5.5. The modeled storm lags behind the observed one toward the end of the integration. Simulations using climatology SST (also shown) will be discussed in section 5.4.

Time evolutions of MSLP and maximum surface winds (MSW) from KAR12 and KAR3 are shown in Fig. 45 (the CLIM (climatology SST) cases shown in the figure are discussed in section 5.4c). There is a trend toward intensification (with respect to MSWs) during the first 12 hours of KAR12 (first 6 hours of KAR3). This behavior is to be expected during the early period as the model becomes accustomed to the imposed

vortex. After ~12 hours into the KAR12 run, the storm behaves more like the real storm with a steady weakening trend. The model replicates the modest deepening period with regard to MSLP after 36HR. Maximum winds generally level-off during that period as shown in the BT and in the model.

Tropical Storm Karen was weakening and undergoing ET during the period of integrations in this study. The characteristic leftward shift in rainfall (typical during ET) is shown by surface weather observations over Nova Scotia in Fig. 46a. The shaded region denoting rainfall at 12/15 (inferred from radar, surface and aircraft observations) was primarily west (left) of the storm center as it tracked to the north. Also shown is a subjective sea level pressure analysis with the center of Karen not far inland with a MSLP of 998 hPa. Sea level pressure and rain rate from the KAR12 simulation valid at 30HR (12/15) is shown in Fig. 46b (KAR3 results are very similar, but KAR12 are shown here so as to cover an area similar to panel (a)). The position of the low is ~100 km southeast of the actual position and the central pressure is slightly higher. Rainfall is heaviest to the northwest of the storm center at this time.

A subjective analysis of rainfall amounts from Karen is shown in Fig. 47a. They clearly reflect the leftward shift in rainfall mentioned above. Heaviest amounts occurred over westernmost Nova Scotia and southern New Brunswick. Very little rain fell to the east (right) of the storm track.

The simulated rainfall amounts from the KAR12 control run appear in Fig. 47b. A band of heavy rainfall extends through western Nova Scotia and southeast New Brunswick with maximum amounts in the 40 to 50 mm range. This is very similar to the observed amounts. The simulated axis of heaviest rainfall is further east than what was observed, but is reasonable considering the modeled track was also farther east over central Nova Scotia (see Fig. 44a). Strips of greater rainfalls are noted along the Atlantic coast of Nova Scotia and Cape Breton. This pattern was not observed by the rain gauge network. As mentioned in chapter 4 on Hurricane Michael, the model has a known tendency to inflate amounts in onshore/upslope wind flow, regardless of physical parameterizations.

The Convair 580 aircraft was flown into Karen prior to landfall. Several dropsondes were deployed along a transect paralleling the Atlantic coastline of Nova Scotia from northeast to southwest (Fig. 35b). Vertical cross sections of horizontal wind speed and equivalent potential temperature from the dropsonde data and the 3 km control run (KAR3) of the model are shown in Fig. 48. The cross sections of dropsonde data represent a northeast-to-southwest slice through the storm center over a distance of ~250-km near 11/15. The cross sections from the model are taken from a similar cut through the storm center, but at 12/15, to account for the slightly slower storm motion in the model. Cross sections of the magnitude of horizontal winds are shown in Fig. 48a and Fig. 48b. The light wind region associated with the storm center (moving out of the page) is evident in both observations and model. The modeled version seems to be tilted or decoupled because there are stronger winds above ~700 hPa while the dropsondes show a deep layer of light winds extending to flight level. Wind speeds in the model are

generally lighter, and not as tightly concentrated near the storm center as they are in the dropsonde data. This is consistent with the weaker modeled storm noted in the previous discussion. There is consistency, however, in the height of the low-level wind jet on the left side of the storm motion which is ~850 hPa in both. Furthermore, the model appropriately depicts the much deeper layer of winds on the right side of the storm motion which are closer to the surface than on the left side. Cross sections of equivalent potential temperature, whose calculation is described in chapter 2, are shown in Fig. 48c and Fig. 48d. There is a large discrepancy in the magnitude and girth of the warm/moist core between observations and model. The model appears to be preserving much of its initial warm core properties. Both analyses are at least clear in the fact that the warm/moist core is decoupled from the surface, designated by low Θ_e air in the boundary layer.

5.4 Sensitivity Experiments

The primary focus for this case is to study the sensitivity of numerical simulations of Karen to various factors, particularly initial and boundary conditions. The main set of experiments is summarized in Table 4. All simulations are run on the 12 km domain. Given the small difference between KAR12 and KAR3, it is felt that running at 12 km is a reasonable decision and will not compromise the results. This ensemble is very similar to the ensemble used for Hurricane Michael.

A composite of simulated tracks from the ensemble (including KAR12 control run) is shown in Fig. 49. Tracks are tightly clustered and there is little divergence of the tracks with time. Note that the northern boundary of the grid is near 54°N. Despite the tight clustering of members, most are to the east of the BT, suggesting that an error in the large scale forcing fields is responsible for the eastward bias. All runs showed the remnant low pressure center of Karen becoming absorbed by a large extratropical low by 48 hours. The ensemble mean of MSLP and MSW compares with the BT is shown in Fig. 50. The mean storm intensity compared reasonably well with reality, with some notable biases during the early and latter part of the period. For instance, there is a high bias in wind speed after the storm becomes extratropical. This can be explained by locally enhanced surface winds within the storm circulation, but that are removed from the storm center in the Cabot Strait between Nova Scotia and Newfoundland, and in the Strait of Belle Isle between Newfoundland and Labrador (see Fig. 3 for strait locations). This is not reflected in the BT.

a. Sensitivity to Initial Conditions

Since the vortex is prescribed in the initial conditions, the user has control over its size, intensity, position and wind field asymmetry as outlined in chapter 2. These parameters are perturbed about the control (observed) values by amounts that are representative of the observational errors as was done for Hurricanes Juan and Michael. The advertised positional error for Karen from the NHC forecast advisory archive was 30 nm or 55 km (http://www.nhc.noaa.gov/archive/2001/KAREN.html) near the time of initiation (06/14).

Storm radius (R_{15}) was estimated to be 360 km at 06/14 and perturbed to reflect smaller and larger circulations (see Table 4 for specific radii).

The control value for the percentage of environmental flow is 0.25 (25%). The corresponding MSW for the control run at 00HR (06/14) is 36.6 m s^{-1} (71 knots) which is essentially the same as the BT value of 36.1 m s^{-1} (70 knots). The ensemble members are EM1 (50%, 39.2 m s^{-1}) and EM2 (75%, 41.7 m s^{-1}) where the second value in the parentheses is the corresponding initial MSW. The impact of these configurations on the simulated storm evolution is most apparent in the track. Member EM2 has the westernmost track of any members in the ensemble. The MSLP is also lower than the control run after landfall. This may simply be a consequence of the storm being further to the west, where environmental pressures were lower.

The initial storm size has a notable bearing on its intensity evolution, as was observed for Hurricane Juan experiments in chapter 3. All storms in the "size" set (ES1, ES2 and ES3) begin with the same intensity (MSLP = 982 hPa and MSW = 36.6 m s^{-1}) but the larger storm weakens at a much slower rate than the smallest storm (see Table 4 for reference). This is not particularly surprising knowing that larger vortices typically take longer to "spin down" than smaller ones.

The initial MSLP was perturbed by 4 hPa to 978 hPa and 986 hPa for members EI1 and EI2, respectively. Changing the central pressure effectively changes the wind field for a fixed storm radius through the gradient wind balance (Eq. 4). The solution for cyclonic

flow is given by Eq. 5. As $\partial P/\partial r$ increases in Eq. 5, so will U_G and MSW. Since Karen was a large storm, the difference in MSW between the control and members EI1 and EI2 is small, approximately ± 1.5 m s^{-1}. After a period of 15 to 18 hours into the simulations, the MSLPs and MSWs of these members are virtually identical to the control simulation, KAR12. There was virtually no impact on storm track by perturbing the initial intensity by this amount.

Additional simulations are also run with the initial hurricane intensities corresponding to hurricanes of categories two and three (CAT2, CAT3) strength. In reality, Karen only reached category-one status. The initial intensity (MSW / MSLP) of the CAT2 storm is 46 m s^{-1} (90 knots) / 960 hPa and the CAT3 storm is 55 m s^{-1} (107 knots) / 935 hPa. The results of these experiments are shown in Fig. 51. The initially more intense storms decay more quickly than the control, with the most rapid weakening observed in the CAT3 storm. Interestingly, after ~18 hours there is little difference in their intensities compared with the control. The CAT3 storm is faster and farther west than the CAT2 storm, which in turn is faster and further west than the control KAR12 (not shown). The landfall times are indicated in Fig. 51a. The CAT3 case makes landfall approximately 200 km farther west along the coast compared with the control.

The intensity change *after* the initial vortex adjustment period (after 06HR) appears proportional to the initial intensity. Although there are only a few runs to compare with here, it is suggested that the intensity can be generalized as having a negative exponential-type dependence in time consistent with Kaplan and DeMaria (2001), with a

decay rate that scales as the difference between the intensity at time-zero (to be defined) and some background intensity:

$$\frac{dV}{dt} = -\alpha(V - V_b) \tag{11}$$

where V is the intensity (i.e. MSW), α is a proportionality constant determining the decay rate and V_b is a "background" or "final" intensity (to be defined). Let $V(t = 0) = V_o$, then the general solution will be

$$V(t) = V_b + (V_o - V_b)e^{-\alpha t} \tag{12}$$

At large t, the exponential term in Eq. 12 approaches zero and the intensity approaches the "final" state. In the Karen cases in Fig. 51b, the value can be estimated as ~23 m s^{-1} (~45 knots). An appropriate choice for $t=0$ in the current framework would be at 6HR. Generally speaking, it is reasonable to presume that the proportionality constant (α) would be dependent on SST along the storm track. In the Karen scenarios, a very approximate estimate can be obtained by rearranging Eq. 12 in terms of α and finding a mean value for the three curves in Fig. 51b. An estimate for α here is 0.127 hr^{-1}, corresponding to an e-folding time of ~8 hours. This value represents a weaker decay rate than for landfalling TCs in this part of the world (Kaplan and DeMaria 2001). This is not surprising since the primary weakening factors over land are due to friction and the shut-down of surface heat fluxes that fuel the storm. For cold-water cases, the frictional

effects generally do not increase – if anything, frictional effects may be reduced as the storm becomes thermodynamically decoupled from the cold ocean.

These assumptions and arguments would certainly be complicated for storms undergoing baroclinic intensification or rapid acceleration, but Karen is a good test case because the synoptic environment near the storm was not particularly conducive to baroclinic development. Also, the e-folding time estimated above would vary depending on the storm size prior to weakening. The primary purpose of this analysis is to postulate that intensity change for TCs encountering cold water follows a negative exponential law in a fashion similar to that described by Kaplan and DeMaria (2001).

For the final set of initial conditions experiments, the storm's initial position is perturbed. Uncertainty in the initial storm position for Hurricane Karen at 06/14 was 30 nm (55 km). This information is used as a basis for the EP set of experiments (see Table 4) by perturbing the initial storm position by 55 km (5 grid points) in each cardinal direction. The most apparent impact was on the storm track. When the storm was nudged west or north initially, it tracked farther west than the control run while it tracked farther east when nudged east or south. The results (not shown) indicate that the westward-tracking storm was weaker (by ~ 2.5 m s^{-1}) at landfall and vice versa for the eastward-tracking storm. Although far from conclusive, this is not surprising given that the SSTs were warmest to the east and cooler toward the west.

b. Sensitivity to Parameterizations of Convection and Cloud Microphysics

It is appropriate to investigate the choice of parameterization of deep convective in the model, given that TCs are convectively active storms by nature. The Fritsch and Chappel (1980) (FCP in Table 4) scheme is used for one member and the Kuo (1974) (KUO in Table 4) scheme is used for another. There was very little impact on storm intensity and precipitation from both schemes compared with the control run (employing Kain and Fritsch (1990) convection). However, based on experiments of Hurricanes Juan and Michael, there was an unmistakable sensitivity of storm intensity to deep convective parameterizations. Those storms were much more intense than Karen, suggesting (not surprisingly) that more intense storms are sensitive to this parameterization.

A significant portion of the precipitation in Karen was stratiform in nature as measured by vertically-pointing airborne radar aboard the Convair 580 flight into the storm near landfall (personal observations). In light of this, additional experiments are run choosing an alternate stratiform condensation (cloud microphysical) scheme given by Kong and Yau (1997) ("excrig" in Table 4). The results from this experiment (not shown) reveal a slightly weaker storm throughout much of the integration, with the main area of simulated rainfall over western Nova Scotia amounting to only ~75% of that in the control run. This is not an improvement since rainfall amounts and intensity from the control run (employing the stratiform condensation scheme of Tremblay et al. (1996) – "exc" in Table 4) were in fact more consistent with observations (see Fig. 47).

c. Sensitivity to Boundary Conditions

The sensitivity of the simulated storm intensity to different boundary conditions will be examined here.

1) SEA SURFACE TEMPERATURE

Tropical Storm Karen tracked over anomalously warm water south of Nova Scotia prior to landfall as shown in Fig. 52a. To determine whether the warm anomaly had any impact on the storm intensity at landfall (as was shown to be the case for Hurricane Juan), the control simulations (KAR12 and KAR3) described in section 5.3 are rerun, using climatological SST from Geshelin et al. (1999). The corresponding simulations are called CLIM12 and CLIM3. The monthly mean SST for October is used since Karen occurred during the middle of the month.

The results of these experiments appear in Fig. 44 and Fig. 45. There is very little influence of SST on the overall storm track (Fig. 44) or intensity (Fig. 45) at landfall. The CLIM12 simulation produces a slightly more intense storm after 12 hours of integration compared to KAR12, most likely because the SST is anomalously negative beneath the storm during that period (Fig. 45c and Fig. 52a). Between 12HR and 24HR (see Fig. 45a) the tendency in the MSLPs is towards equality as the storm moves over anomalously warm water. By 24HR the simulated storms have weakened considerably

and the anomalously warm water of 3°C (16°C versus 13°C) near the storm center does not appear to play a major factor in the landfall intensity. Given the weak SST anomaly influence in the control runs, it was decided that the ensemble of experiments for the climatology SST need not be carried out.

A second (more interesting) test of the sensitivity of storm intensity to SST (during the decay and ET phase) is run for Karen using the observed SSTs during Hurricane Juan in late September, 2003. This experiment is similar to looking at the possible impact Karen would have had if it arrived earlier in the season, when SSTs are normally warmer. The difference between the observed SSTs at 00/28 2003 and 00/14 2001 (i.e. SST_{JUAN}-SST_{KAREN}) is shown in Fig. 52b. Clearly, SSTs over a large area were warmer during Juan than they were during Karen. The track in Fig. 52b represents the control run of Karen for the Juan-SST (J-SST) scenario. The landfall intensity of this run is appreciably different (stronger) than the control run, therefore an ensemble for J-SST using the same suite of experiments in Table 4 is carried out.

Results from the 15-member ensemble plus the control runs are shown in Fig. 53. It is clear that the J-SST ensemble is more intense than the Karen-SST (K-SST) ensemble (MSW of 28.5 m s^{-1} versus 22.5 m s^{-1} near landfall). It is interesting to note that there is much more variability among the J-SST ensemble during the pre-landfall period (i.e. before 31.5HR) and that there is actually an increase in MSW at 27HR. The increase in wind speed results from the formation of a strong low-level wind jet on the south side of the storm. The wind fields from the control runs are shown in Fig. 54, with the location

of the aforementioned low-level wind jet indicated in the figure. The jet forms not as a result of increasing forward storm motion, but as a consequence of destabilization of the BL when cooler/drier air is drawn into the storm circulation. There is considerable downward mixing of air from above the BL, below ~800 hPa and in the vicinity of the low-level jet that is not observed in the K-SST runs. In addition, the thermodynamic core in the J-SST cases is much smaller (tighter) than the K-SST cases. A similar wind jet was observed in simulations of Hurricane Michael and in dropsonde data (Abraham et al. 2004) during that storm.

Explaining the larger degree of variability in intensity (between 15HR and 30HR) is not trivial. It cannot be readily explained through analysis of SST variability since the standard deviation in (storm-centered) SST (Fig. 53c) is actually less than the K-SST ensemble during the period when intensity variability is greatest. The enhanced variability is observed among all members, making it difficult to attribute this to initial conditions or model specifications.

Rainfall amounts generated by the J-SST control simulation were approximately three times greater than those in the K-SST control over the ocean not far south of western Nova Scotia, but the amounts over land within the maximum rainfall region in western Nova Scotia were comparable (not shown). In fact, the rainfall amounts were actually less (by ~50%) in the J-SST case throughout the extratropical phase of the storm's lifecycle compared with the K-SST case. The ingestion of cool/dry environmental air

observed in the J-SST case could explain this rapid reduction in precipitation as the storm approached the coast and during its extratropical phase.

2) PILOTING FIELDS

All of the simulations on the 12 km grid so far in this case study are driven ("piloted") by analyses at the outer boundary of the grid. The analyses, as described in chapter 2, are from the CMC Data Assimilation System (DAS) archive (Chouinard et al. 1994) and can be thought to represent the "best" boundary conditions for running hindcast simulations of the event. It is instructive to also pilot the model with different grid-peripheral boundary conditions to study the influence on the storm compared with analyses. Archived output from the GEM model is chosen for this task. The GEM forecasts consist of two prediction cycles at 00 UTC and 12 UTC. To reflect the "forecast mode" of operation, the MC2 simulations of Karen are initiated at a time corresponding to the prediction cycle, in this case, 00/14 (versus 06/14 in the runs so far) when Karen was still near maximum intensity. The following are the observations for Karen at 00/14 from the BT (Stewart 2001): MSLP: 985 hPa, MSW: 33 m s^{-1} (65 knots), position: 37.9°N / 64.0°W, R_{15}: 360 km, status: hurricane. The same ensemble summarized in Table 4 is employed for the GEM-piloted (GEM-P) and analyses-piloted (ANL-P) cases beginning at 00/14, with the updated initial conditions (above) for the control runs. The grid is the same as shown in Fig. 43a.

Composites of storm tracks for the ANL-P and GEM-P ensembles are shown in Fig. 55. Overall, the tracks from both sets are similar with the exception being a more westward drift in the tracks during the early period of the GEM-P runs. This translates to a mean landfall that is farther to the west (by ~100 km), and is surprisingly more realistic than the ANL-P set. Ensemble means of MSLP and MSW are shown in Fig. 56. In terms of MSLP, the GEM-P simulations are weaker throughout the integration. The mean MSW near landfall in each set is ~18 m s^{-1} (~35 knots) which is slightly less than the estimated landfall intensity of 21 m s^{-1} (40 knots) for Karen.

Rainfall amounts from the GEM-P control simulation differed significantly from the ANL-P control run (not shown). For instance, the band of heavy rainfall over western Nova Scotia generated from the ANL-P simulation was not depicted by the GEM-P case. This shows that in spite of decent intensity (in terms of MSW) and track prediction, the precipitation may not be well predicted.

5.5 Comparison with Operational Predictions

a. Summary of Forecasts and Challenges

Operational predictions for Hurricane Karen were issued at the NHC and CHC where forecasters have access to various numerical weather models with primary output for track and intensity. In general, the intensity of Karen in Nova Scotia was over-predicted and the storm was forecast to make landfall too far east over the eastern mainland of the province and was forecast to arrive at the coast about 6 to 12 hours later than reality

(based on forecasts issued at or near 00/14). As is often the case when TCs approach this region, forecasters were uncertain about how quickly Karen would weaken over the cool water south of Nova Scotia. Storm-force wind warnings were posted for parts of the marine district south of Nova Scotia while heavy rainfall (up to 100 mm) and wind warnings (gusts to 100 km/h (28 m s^{-1})) were posted for inland regions.

The GEM regional model did not successfully forecast Hurricane Karen given the scarcity of observations in the storm region (necessary to adequately initialize the model), and a horizontal resolution of 24 km — not fine enough to properly resolve a hurricane. Although its horizontal resolution has been refined to 15 km, higher resolution and a better representation of initial conditions are still needed to effectively capture TC events such as Karen.

b. Forecast and Model Intercomparison

A summary of forecast tracks beginning at 00/14 is shown in Fig. 57, highlighting the variability in predictions. The official (operational) hurricane center forecast tracks from CHC and NHC are included in this analysis. Numerical forecast tracks are from the Geophysical Fluid Dynamics Laboratory (GFDL) model and the MC2 model used here. The GFDL model (Bender and Ginis 2000) employs a balanced vortex insertion approach similar to that described in chapter 2. The MC2 "forecast" is the control run from the GEM-P ensemble described in the previous section. The MC2 result is very much like a forecast because only observational data are used to initiate the model, and is piloted by

fields from another (GEM) model, as opposed to analyses. The track from the Florida State Superensemble (SENS) contains information from multiple dynamical models to produce a weighted ensemble mean (weighting being proportional to the past performance of model members) as described by Williford et al. (2003).

Predictions for landfall location were spread across the length of Nova Scotia. The westernmost (more accurate) predictions were from the GFDL and MC2 models. This could be related to the fact that these models resolve the vertical structure/depth of the TC, which is important for resolving the steering component and track. The SENS track was, surprisingly, the easternmost of the tracks. The SENS has generally performed very well with storms affecting this region in recent years, including Hurricane Juan in 2003, and is often the best guidance on track and intensity forecasts (personal experience). The official track forecasts from NHC and CHC were a compromise between the SENS and the GFDL, which is one of the more reputable dynamical hurricane models. All predictions underestimated the speed of the storm. The error in 48-hour forecast position from the CHC and NHC was approximately 700 km too far south. In terms of time, this was ~9 hours too slow. This error is much greater than the late 1990s mean NHC 48-hour track error of 280 km (McAdie and Lawrence 2000).

Intensity predictions (see Fig. 58) were scattered between 60 knots (31 m s^{-1}) to near 35 knots (18 m s^{-1}) at 36HR. The GFDL had a decent track prediction, but a poor intensity forecast (60 knots at landfall at 36HR). This is quite surprising given the cold SSTs south of western Nova Scotia. The MC2 solution was the most realistic in terms of both

track and intensity, but did not have a decent handle on precipitation, as discussed in section 5.4. Quantitative precipitation forecasts from the GFDL model are not available for comparison.

5.6 Summary and Conclusions

The MC2 model was able to reproduce the significant weakening of Hurricane Karen over the cool SSTs south of Nova Scotia, and depicted the leftward shift in rainfall, characteristic of ET. On the other hand, the track simulations were consistently too far east, likely owing to errors in the large scale steering flow (piloting analyses). The model was not able to reproduce the tightness of the vertical wind field as seen in dropsonde data, and overestimated the breadth of the remnant warm/moist core near landfall. On the other hand, the model did successfully capture the marked thermodynamic decoupling of the warm core from the cool marine boundary layer.

The primary focus for this event was to test the sensitivity of the decay/ET phase of Karen to various boundary and initial conditions. The landfall intensity was rather insensitive to the storm intensity at time of initiation (before Karen moved over coolest SSTs). For instance, the landfall intensity differed little between runs that were initiated with category-two or category-three hurricanes versus a category-one hurricane (the control). The intensity change (maximum winds) for these simulations appears to follow a negative exponential law with a rate of decay proportional to the initial intensity and an e-folding time of ~8 hours. It was also found that the intensity was sensitive to the size

of the prescribed vortex in much the same way as was seen in the Hurricane Juan experiments. The largest vortex weakened more slowly than the smallest vortex.

Different configurations of SST were used to study the impact on intensity. Sea surface temperatures immediately prior to Karen were anomalously warm (with respect to climatology) on the Scotian Shelf south of Nova Scotia, however, they were anomalously cool well offshore. When comparing with runs with climatological SST as the surface boundary condition, there was some evidence of local sensitivity on storm intensity to the anomalies, but their net influence was negligible at landfall. During mid-October, SSTs in this region are quite cool, so TCs often weaken quickly. A case where this did not occur was Hurricane Juan in September, 2003. An ensemble of simulations was therefore run for Hurricane Karen, using the unseasonably warm SSTs from the Juan event, to study the impact on landfall intensity. Those results suggest that Karen would have likely made landfall as a much stronger tropical storm than was the actual case. A strong low-level wind jet developed in the Juan-SST scenario, very similar to the jet observed in the ET of Hurricane Michael southeast of Nova Scotia in October 2000 (chapter 4). Surprisingly, over-land rainfalls in the Juan-SST scenario were generally equal to or less than the Karen-SST case. This can possibly be attributed to the more pronounced ingestion of cool/dry environmental air into the Juan-SST storm.

Sensitivity to model parameterizations was also examined. The intensity was sensitive to the prescribed vortex size. The intensity evolution was neither very sensitive to the choice of parameterization for deep convection nor to the type of stratiform condensation

scheme. This is contrary to the studies of Hurricanes Michael and Juan. These storms were much more intense than Karen, so these findings suggest it is probable that the sensitivity to model parameterization is greater for more intense hurricanes.

Hurricane Karen was a particularly challenging storm to predict. There was a large degree of spread in numerical guidance of track and intensity. Karen moved more quickly than expected while approaching Nova Scotia yet spent enough time over cool sea surface temperatures (SSTs) to permit significant pre-landfall weakening. Rainfall and wind forecasts over Nova Scotia were over-predicted.

When operated in "forecast mode" the MC2 performed well with respect to track and intensity compared with official and dynamical forecasts. The timing and location of landfall was very good (error of ~70 km or ~1.5 hours slow). However, the simulations piloted with forecast fields from the Canadian GEM model failed to generate realistic rainfalls for the event. Simulations piloted by large scale analyses yielded better precipitation fields and more realistic intensity with respect to storm central pressure and maximum surface winds. Surprisingly, the forecast-piloted cases had a better track forecast than the analyses-piloted runs.

CHAPTER 6

Conclusion

6.1 General Summary

The Meteorological Service of Canada's Mesoscale Compressible Community (MC2) model has been used to conduct numerical simulations of selected cases of hurricanes moving into Eastern Canada. A multitude of experiments (ensembles) was carried out to study the sensitivity of each storm track, intensity and structure to initial conditions, boundary conditions, model resolution and its microphysical parameterizations. Initial conditions consisted of the merging of an observationally-consistent, synthetic hurricane vortex with large scale meteorological fields before the onset of extratropical transition (ET), or near the time of maximum intensity.

The cases chosen for the modeling study were well sampled by the surface meteorological network and the Canadian National Research Council's Convair 580 research aircraft. These data proved very useful for verifying the model's performance. The cases include Hurricane Michael (2000), Hurricane Karen (2001) and Hurricane Juan (2003). Michael was a vigorous case of ET while Juan maintained its tropical hurricane structure when it struck Nova Scotia. Karen weakened while undergoing ET over Nova Scotia. The significantly different structure and behavior of these storms make them ideal for study, and effectively represent a cross section of tropical cyclone (TC) evolutions in the middle latitudes of the North Atlantic Ocean.

Primary results from this work are summarized below:

1. Direct insertion of a synthetic TC bogus in the model's initial conditions greatly improves the representation of the storm structure and intensity as it migrates into the middle latitudes, compared with simulations initiated without the vortex. A summary of the results is shown in Fig. 59.

2. The intensity evolution of the TC is highly sensitive to the prescribed size of the synthetic vortex in the initial conditions.

3. The weakening rate of the TC over cool sea surface temperatures (SSTs) in the relative absence of atmospheric baroclinicity (Juan and Karen cases) appears to be proportional to a) the actual value of SSTs below ~26C, b) the storm's intensity prior to reaching the cool SSTs, and (c) the forward acceleration of the storm vortex.

4. The storm's motion and track are sensitive to its initial position and to the large-scale piloting boundary conditions.

5. The synergy of observations and numerical simulations has improved our knowledge of the intriguing (and often difficult to predict) structural changes occurring as these TCs moved into the middle latitudes.

Through experimentation of various initial and boundary conditions as well as model physics, knowledge of the model's strengths and weaknesses has been acquired. The model has potential to serve as a prognostic tool for TC forecasting using the vortex insertion approach, as learned by running it in "forecast mode", piloted by large scale fields from the Global Environmental Multiscale (GEM) model. Provided care is taken when prescribing the initial vortex using real-time data (weather satellites, aircraft, etc), a decent forecast can be generated as discussed below.

6.2 Model Application During the 2005 Hurricane Season

During the 2005 hurricane season, the same configuration of the MC2 model used to conduct this research was applied to tropical systems in real time. Those cases include Tropical Storms Franklin and Ophelia, which tracked through Canadian waters south of Nova Scotia. Output from the 15-km GEM regional model every three hours was gathered after its forecast cycle was completed, and used to pilot the 12 km MC2 grid. The vertical resolution consisted of 35 computational levels with 12 in the boundary layer and with the lowest wind level near 35 m. The same vortex insertion procedure was employed with these storms prior to their ET south of Nova Scotia using key observational data of intensity, size and center position from the National Hurricane Center forecast bulletins.

The model was initiated when the storms were below hurricane intensity. For example, a run for Tropical Storm (TS) Ophelia was initiated with MSW near 55 knots at 00 UTC on

17 September 2005 with a central pressure of 998 hPa. Traditionally, the vortex insertion approach is best applied to well-developed storms – i.e. hurricanes. In spite of this, it was found that initiating the model with this relatively weak (but moist) vortex lead to a more realistic wind and pressure pattern as the storm moved northeastward when compared with the GEM forecast, at least in the case of TS Franklin. It turns out that the 15-km GEM model resolved TS Ophelia rather well; likely due in part to dropsonde data from an American research aircraft being assimilated into the model, and to the storm's proximity to the coast of North Carolina where buoy observations were plenty. However, it is very often the case where the storm is not being surveyed by aircraft and is well away from the buoy network, in which case, the vortex insertion procedure works best.

It turns out that both GEM and MC2 predictions for TS Ophelia (as well as other numerical models) did not perform very well. Ophelia's circulation had become sheared apart by strong upper-level winds during its approach to Nova Scotia, leaving the low-level circulation exposed and displaced from the convection. The models did not appear to handle this very well, instead, deepening the storm during ET and moving the center too far north across Nova Scotia. This reminds us that challenges remain with regard to the numerical simulation and predictions of these events.

6.3 Future Work

The hurricane configuration of the MC2 model discussed in this work will continue to be run experimentally on real-time storm events as part of its development as an operational

forecast tool. There currently exists a limited area domain of the GEM model (called GEM-LAM) over eastern Canada, with a horizontal resolution of 10 km, which can be employed in the future as an operational framework for numerical tropical cyclone forecasts. There is also a fine resolution grid of 2.5 km, which can be relocated to cover the region of the TC in much the same way as has been done with the 3 km grid in this research. Since the configuration and codes of the GEM-LAM are similar to the MC2, applying the research to GEM-LAM should be relatively straightforward.

In an effort to overcome the start-up and vortex adjustment challenges, successive integrations of the model could potentially be conducted in the future, using output from previous runs – where only the first run would be initiated with the synthetic vortex (when the storm is well developed in the tropics).

Parts of the current model setup and running procedures can be automated in the future to hasten the availability and displays of model output for forecasters. Automating the vortex insertion is possible, but not recommended, since it is important that the modeler/forecaster be satisfied with the storm structure in the initial fields. The most critical step is generating initial conditions that represent reality as closely as possible.

Coupling of the hurricane configuration of the GEM-LAM with a barotropic ocean model will likely be the focus of a future project. The ocean model would be driven by realistic hurricane wind and pressure fields to generate storm surge and wave predictions. Coupling of the atmospheric model with a fully baroclinic ocean circulation model (or

simple mixed layer model) is also a possibility to generate changes in SST induced by the storm. This is of less importance in Eastern Canada because storms are normally moving very quickly. Storm-induced changes in SST typically occur too slowly to feed back into the storm intensity (e.g. results by K. A. Emanuel (2003, personal communication) for Hurricane Juan using a simple axisymmetric hurricane model and a mixed layer model of the ocean).

TABLES

Hurricane	Juan	(12km)	JUAN_12CT					
NODE	LATC °N	LONC °W	STAT	MSLP hPa	SST °C	MSW kts	LATW °N	LONW °W
1	36.36	63.62	3	970.3	26.8	92.5	36.68	63.08
2	36.79	63.73	3	968.8	26.9	77.6	36.90	63.19
3	37.33	63.84	3	968.3	27.0	89.3	37.76	63.62
4	38.09	63.94	3	965.8	26.5	91.4	38.41	63.94
5	38.95	64.16	3	965.2	25.1	89.1	39.28	63.73
6	39.82	64.27	3	968.4	24.9	84.7	39.82	63.73
7	41.00	64.27	3	969.5	22.6	87.5	40.90	63.73
8	42.30	64.27	3	968.9	19.9	87.2	42.19	63.73
9	43.70	64.05	3	970.9	18.2	88.9	43.70	63.51
10	45.32	63.62	3	980.8	17.1	66.7	44.68	62.54
11	47.16	63.51	3	986.2	15.5	69.1	47.05	62.22
12	48.78	62.97	3	991.4	13.9	65.6	48.78	60.92
13	50.51	62.22	2	997.4	10.3	59.2	49.97	59.84

Table 1. Format for the model output statistics. The first row is the experiment identifier, second row includes column headers. The node denotes storm location (given by the location of the minimum sea level pressure - MSLP) every three hours, located at LATC/LONC. The storm status code (hurricane, tropical storm, etc) appears in the STAT column. The location of the maximum winds is shown in LATW/LONW columns. The other columns include other primary statistics as described in the text.

Experiment	MSLP (hPa)	lat (N)	lon (W)	R15 (km)	basicp (frac)	convec	comp_levs (3km) ( ) = # in BL
JUAN & CLIM	970	36.3	63.6	250	0.75	kfc	40 (12)
EM1	970	36.3	63.6	250	***0.50***	kfc	40 (12)
EM2	970	36.3	63.6	250	***1.00***	kfc	40 (12)
ES1	970	36.3	63.6	***225***	0.75	kfc	40 (12)
ES2	970	36.3	63.6	***300***	0.75	kfc	40 (12)
ES3	970	36.3	63.6	***350***	0.75	kfc	40 (12)
EI1	***966***	36.3	63.6	250	0.75	kfc	40 (12)
EI2	***974***	36.3	63.6	250	0.75	kfc	40 (12)
EP1	970	36.3	***64.0***	250	0.75	kfc	40 (12)
EP2	970	***36.6***	63.6	250	0.75	kfc	40 (12)
EP3	970	36.3	***63.2***	250	0.75	kfc	40 (12)
EP4	970	***36.0***	63.6	250	0.75	kfc	40 (12)
EC1	970	36.3	63.6	250	0.75	***fcp***	40 (12)
EC2	970	36.3	63.6	250	0.75	***kuo***	40 (12)
ER1	970	36.3	63.6	250	0.75	kfc	***32 (9)***
ER2	970	36.3	63.6	250	0.75	kfc	***48(15)***

Table 2. List of experiments used in the Hurricane Juan study. JUAN and CLIM are the control runs using observed and climatology SST respectively. Minimum sea level pressure is MSLP, lat/lon indicate the storm center position, R15 is the radius of 15 m s^{-1} winds, "basicp" is the fraction of the background flow used to prescribe the initial wind field asymmetry, "convec" is the convective parameterization scheme (abbreviations are explained in the text), and the final column indicates the number of computational levels in the model. Changed parameters in each experiment are in bold italics.

Experiment	MSLP (hPa)	lat (N)	lon (W)	R15 (km)	basicp (frac)	convec	comp_levs ( ) = # in BL	stcond
MICH12	983	34.2	67.8	320	0.50	kfc	25(7)	exc
EM1	983	34.2	67.8	320	***0.25***	kfc	25(7)	exc
EM2	983	34.2	67.8	320	***0.75***	kfc	25(7)	exc
ES1	983	34.2	67.8	***290***	0.50	kfc	25(7)	exc
ES2	983	34.2	67.8	***380***	0.50	kfc	25(7)	exc
ES3	983	34.2	67.8	***430***	0.50	kfc	25(7)	exc
EI1	***979***	34.2	67.8	320	0.50	kfc	25(7)	exc
EI2	***987***	34.2	67.8	320	0.50	kfc	25(7)	exc
EP1	983	34.2	***68.4***	320	0.50	kfc	25(7)	exc
EP2	983	***34.9***	67.8	320	0.50	kfc	25(7)	exc
EP3	983	34.2	***67.1***	320	0.50	kfc	25(7)	exc
EP4	983	***33.6***	67.8	320	0.50	kfc	25(7)	exc
EC1	983	34.2	67.8	320	0.50	***fcp***	25(7)	exc
EC2	983	34.2	67.8	320	0.50	***kuo***	25(7)	exc
ER1	983	34.2	67.8	320	0.50	kfc	***32 (10)***	exc
EQ1	983	34.2	67.8	320	0.50	kfc	25(7)	***excrig***

Table 3. List of experiments used in the Hurricane Michael study with the 12 km grid. MICH12 is the control run using 19 October observed SST surface boundary condition. Minimum sea level pressure is MSLP, lat/lon indicate the storm center position, R15 is the radius of 15 m s^{-1} winds, "basicp" is the fraction of the background flow used to prescribe the initial wind field asymmetry, "convec" is the convective parameterization scheme, "comp_levs" indicates the number of computational levels in the model, and "stcond" is the stratiform condensation scheme (schemes are explained in the text). Changed parameters in each experiment are in bold italics.

Experiment	SLP (hPa)	lat (N)	lon (W)	R15 (km)	basicp (frac)	convec	comp_levs ( ) = # in BL	stcond
KAR12	982	38.6	63.7	360	0.25	kfc	25(7)	exc
EM1	982	38.6	63.7	360	***0.50***	kfc	25(7)	exc
EM2	982	38.6	63.7	360	***0.75***	kfc	25(7)	exc
ES1	982	38.6	63.7	***300***	0.25	kfc	25(7)	exc
ES2	982	38.6	63.7	***265***	0.25	kfc	25(7)	exc
ES3	982	38.6	63.7	***420***	0.25	kfc	25(7)	exc
EI1	***978***	38.6	63.7	360	0.25	kfc	25(7)	exc
EI2	***986***	38.6	63.7	360	0.25	kfc	25(7)	exc
EP1	982	38.6	***64.3***	360	0.25	kfc	25(7)	exc
EP2	982	***39.1***	63.7	360	0.25	kfc	25(7)	exc
EP3	982	38.6	***63.1***	360	0.25	kfc	25(7)	exc
EP4	982	***38.1***	63.7	360	0.25	kfc	25(7)	exc
EC1	982	38.6	63.7	360	0.25	***fcp***	25(7)	exc
EC2	982	38.6	63.7	360	0.25	***kuo***	25(7)	exc
ER1	982	38.6	63.7	360	0.25	kfc	***32 (10)***	exc
EQ1	982	38.6	63.7	360	0.25	kfc	25(7)	***excrig***

Table 4. List of experiments used in the Hurricane Karen study with the 12 km grid. KAR12 is the control run using 14 October observed SST surface boundary condition. Minimum sea level pressure is MSLP, lat/lon indicate the storm center position, R15 is the radius of 15 m s^{-1} winds, "basicp" is the fraction of the background flow used to prescribe the initial wind field asymmetry, "convec" is the convective parameterization scheme, "comp_levs" indicates the number of computational levels in the model, and "stcond" is the stratiform condensation scheme (schemes are explained in the text). Changed parameters in each experiment are in bold italics.

FIGURES

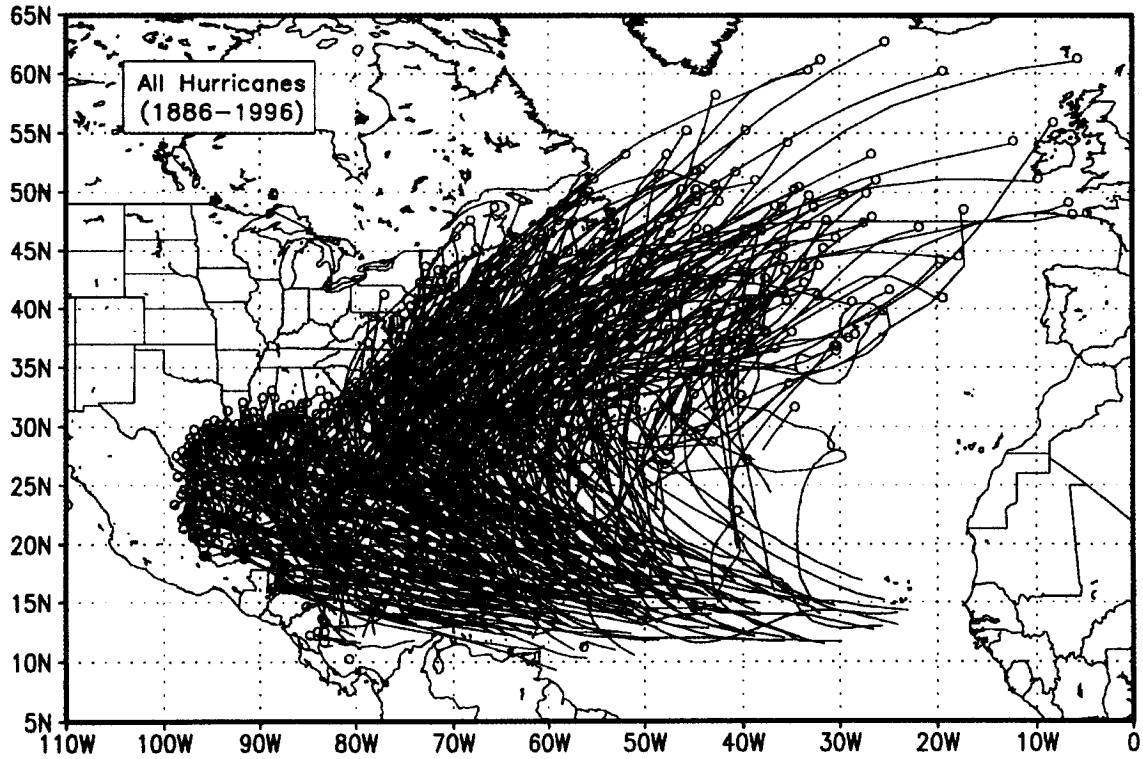

Figure 1. Storm tracks of all hurricanes in the Atlantic Ocean between 1886 and 1996. Tracks are plotted from the location where the tropical cyclone first gained hurricane intensity until the location where the hurricane diminishes to tropical storm intensity. Figure taken from Elsner and Kara (1999).

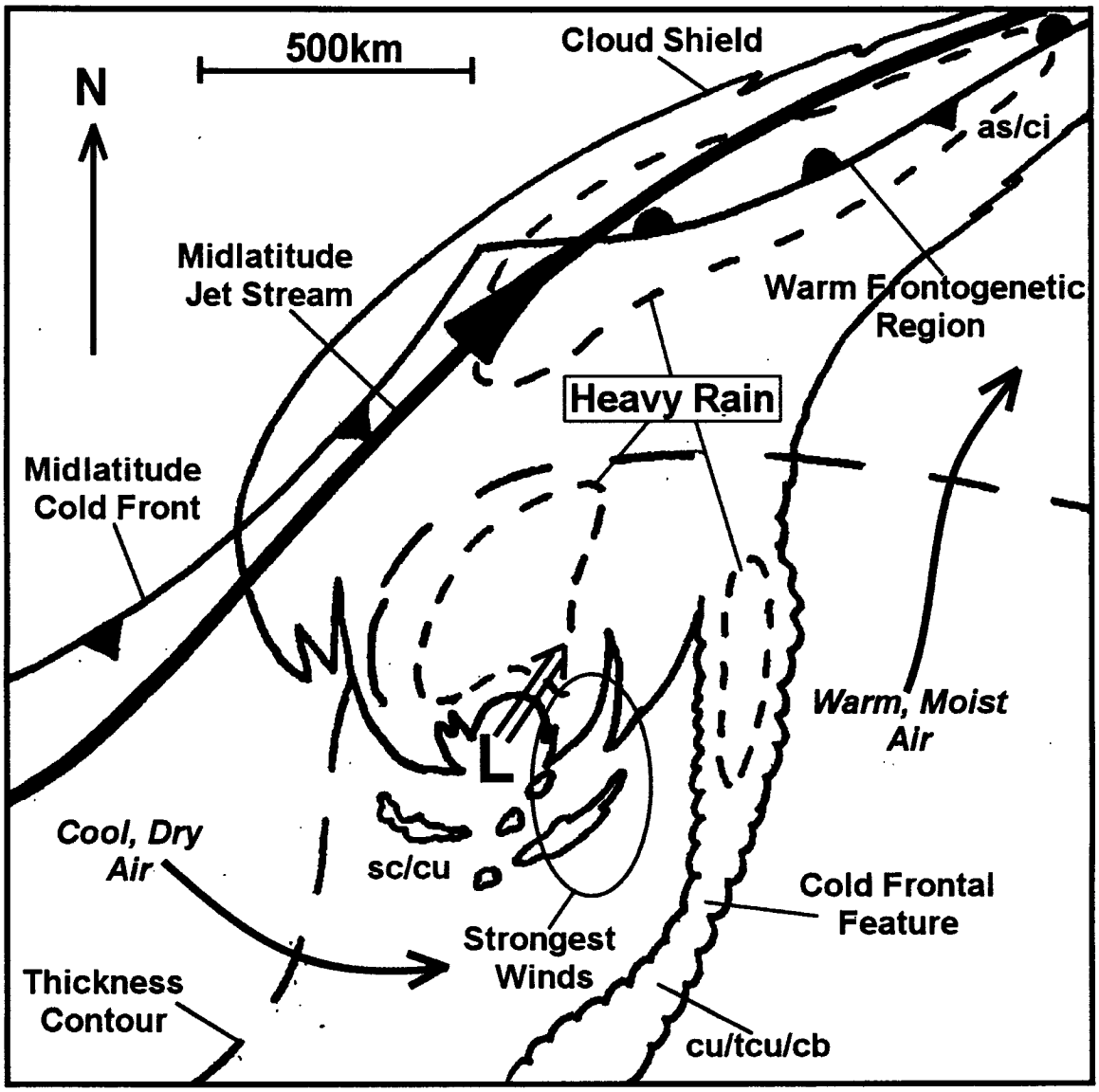

Figure 2. Schematic of a tropical cyclone undergoing extratropical transition. The primary outline denotes the cloud structure. Most common meteorological features are labeled including cloud types: altostratus/cirrus (as/ci), stratocumulus/cumulus (sc/cu) and cumulus/towering-cumulus/cumulonimbus (cu/tcu/cb). The thickness contour shows the pattern of geopotential thickness in the vicinity of the storm. The center of the transitioning storm is shown with an "L".

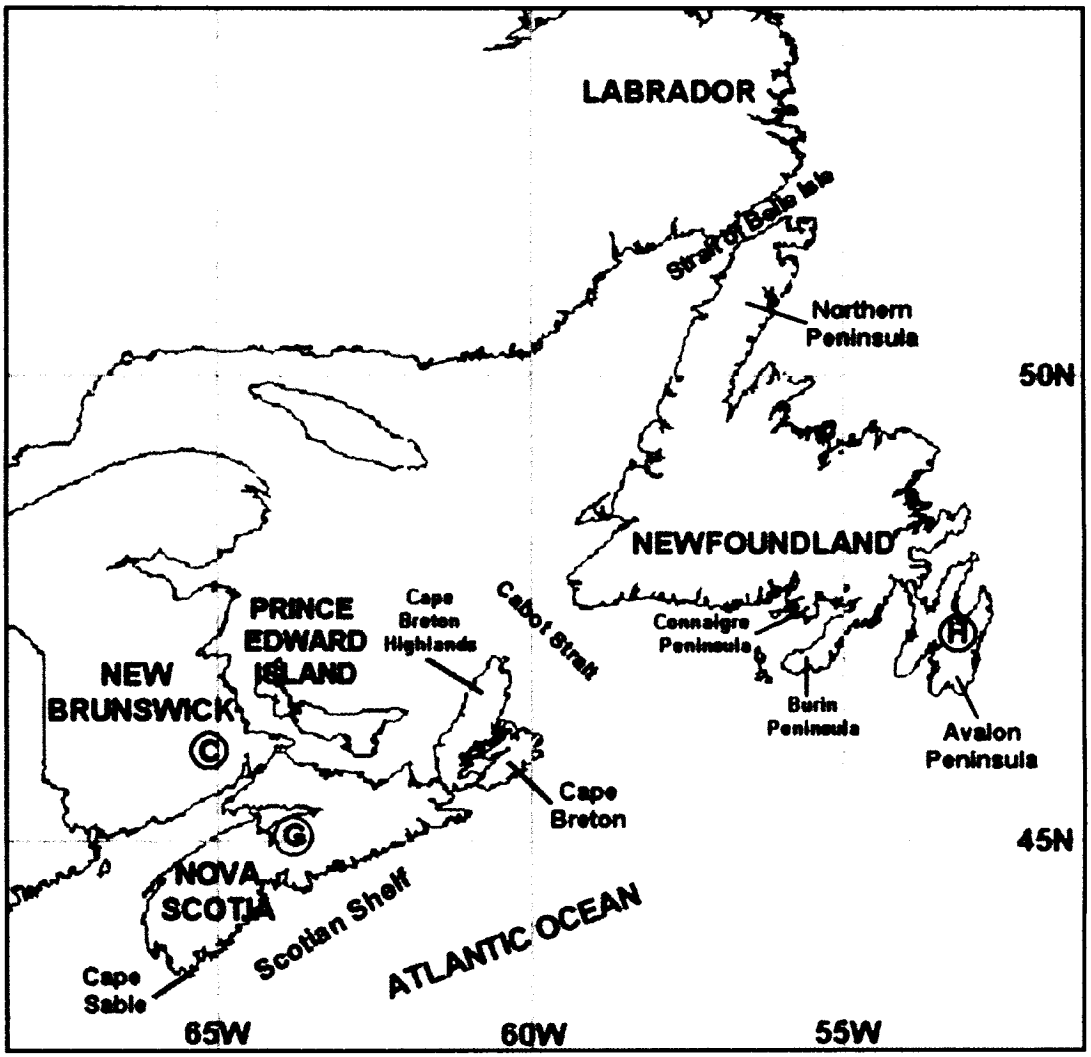

Figure 3. General reference map for locations cited throughout the text. Doppler radar sites are indicated by circled letters. Chipman (C), Gore (G) and Holyrood (H).

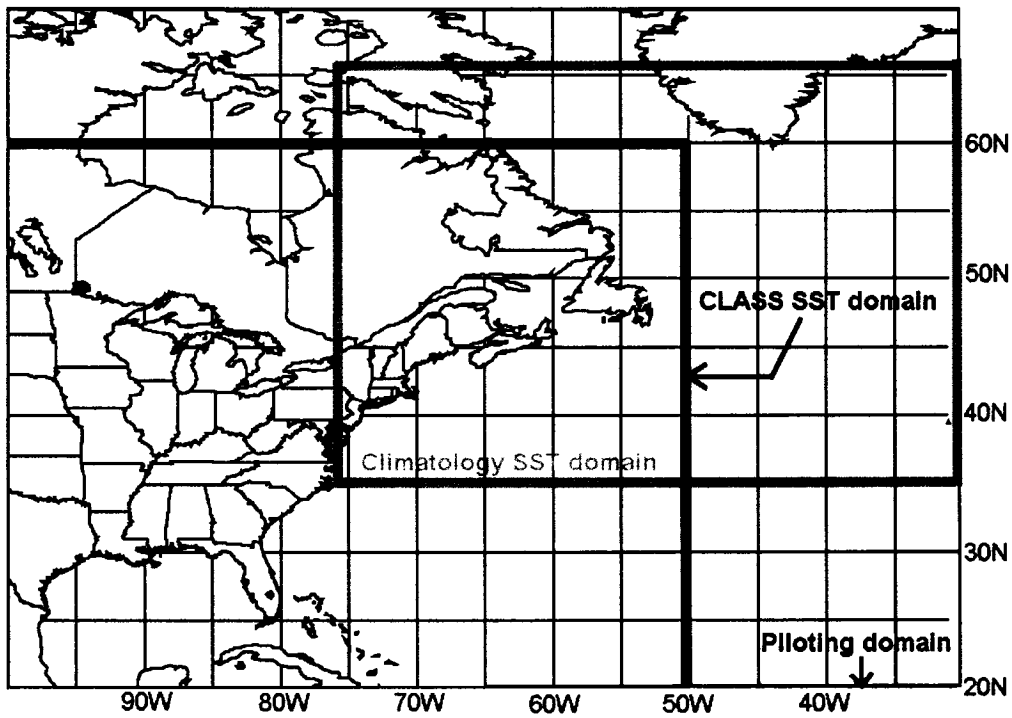

Figure 4. Data coverage for the sea surface temperature (SST) datasets. The large domain contains the model piloting fields, the solid black border marks the region where CLASS SST data are available, and the grey border marks the climatology SST domain (Geshelin et al. 1999).

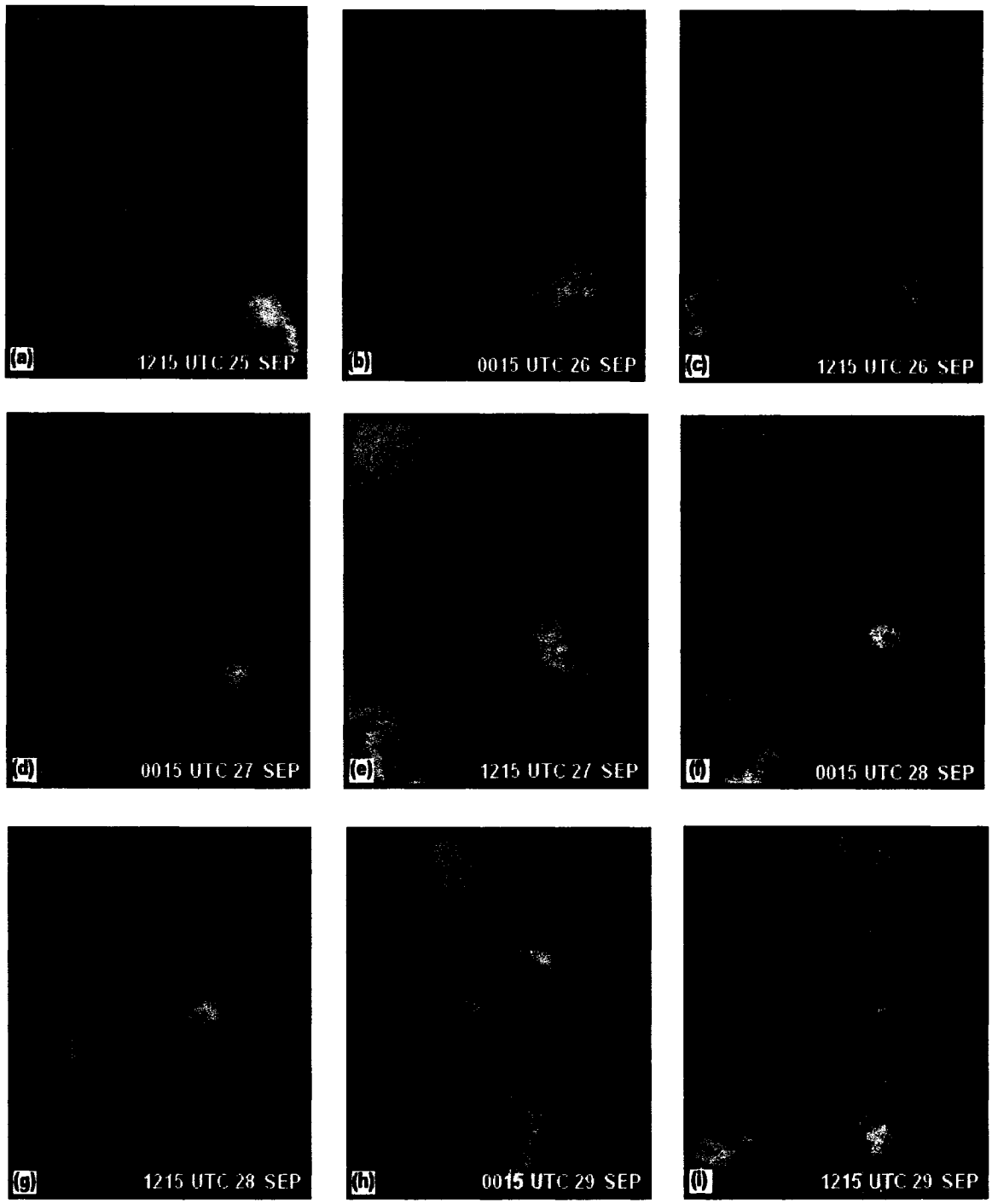

Figure 5. GOES infrared satellite imagery showing the evolution of Hurricane Juan.

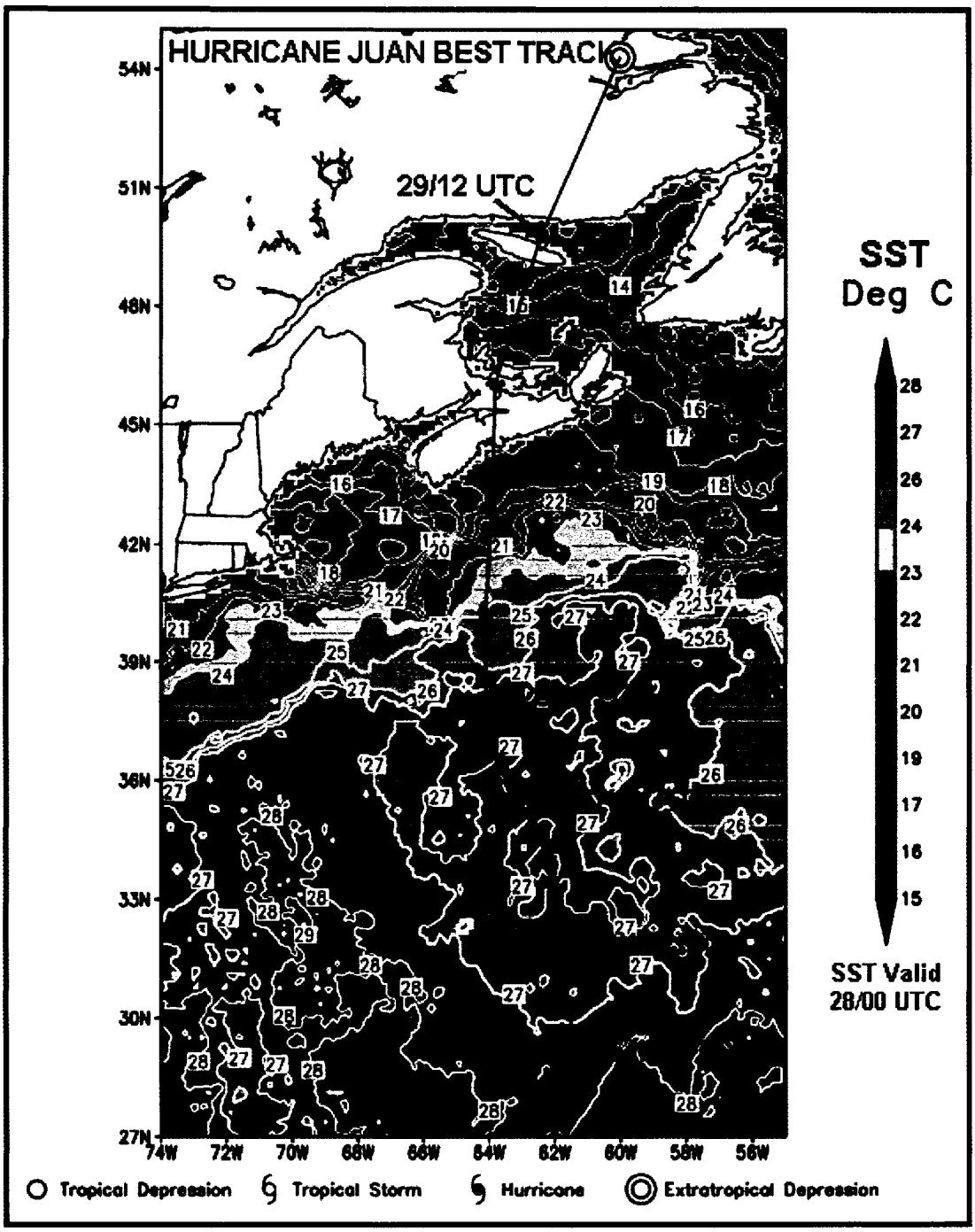

Figure 6. Best track for Hurricane Juan with sea surface temperatures. Sea surface temperatures (contours every 1°C) are valid at 00 UTC 28 September, 2003.

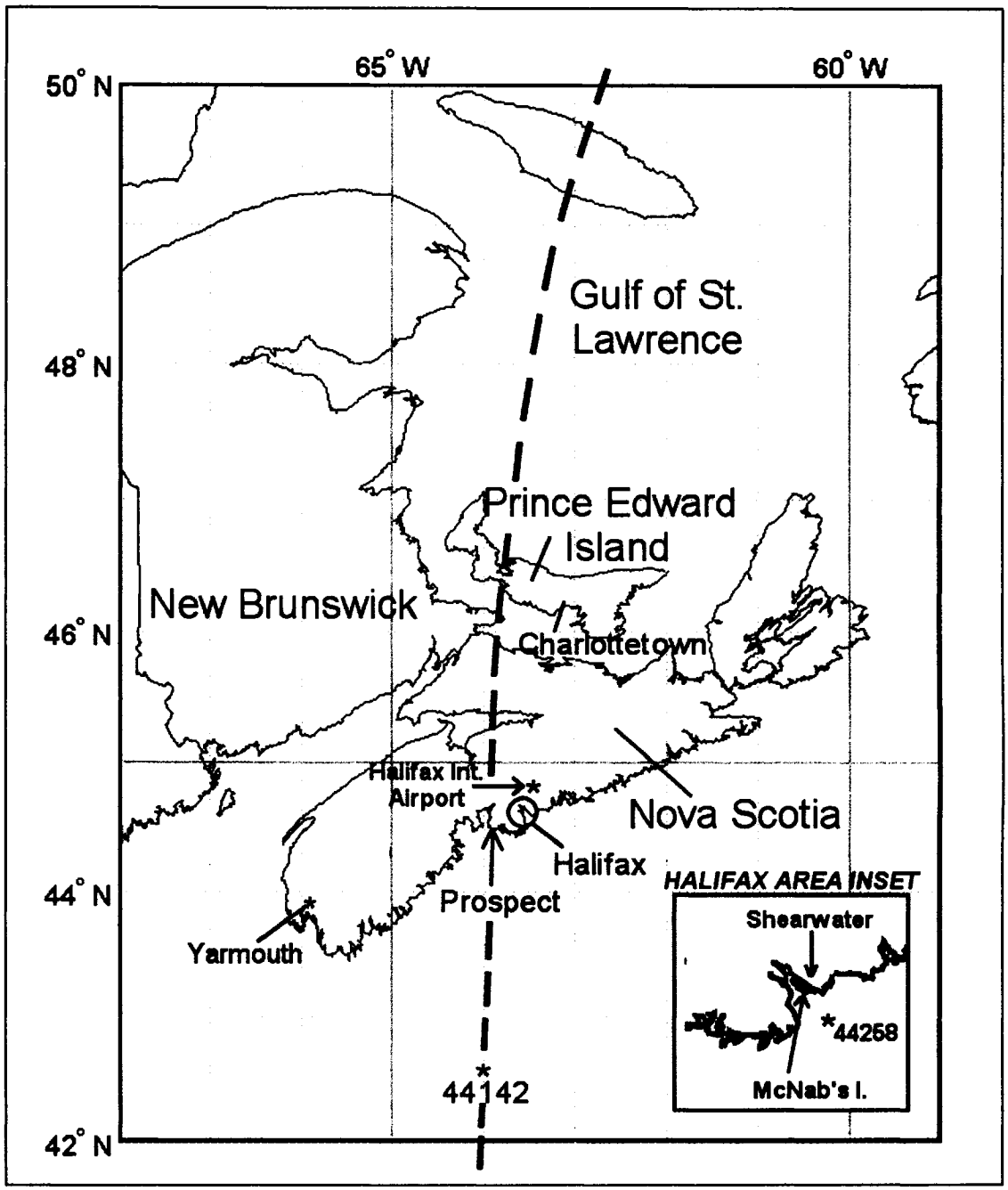

Figure 7. Reference map for locations cited in chapter 3. The storm track for Hurricane Juan is shown as a dashed line.

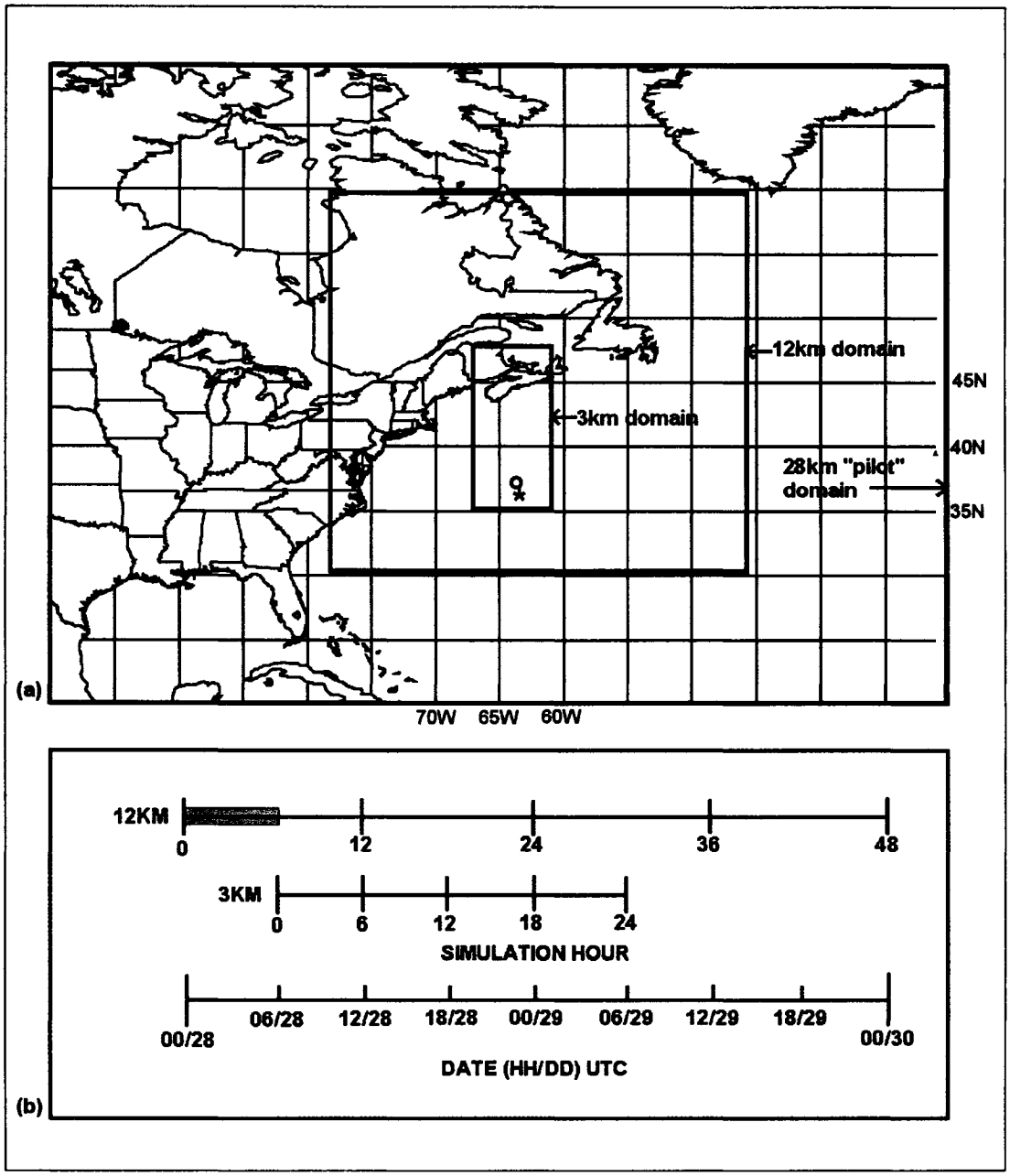

Figure 8. Layout for the Hurricane Juan model simulations: (a) grid configuration and (b) timelines for the model integrations. The asterisk in (a) marks the storm center at time-zero of the 12 km control simulations and the open circle marks the mean position of the storm at time-zero of the 3 km control simulations. The grey region on the 12 km timeline in (b) denotes the six-hour model adjustment period.

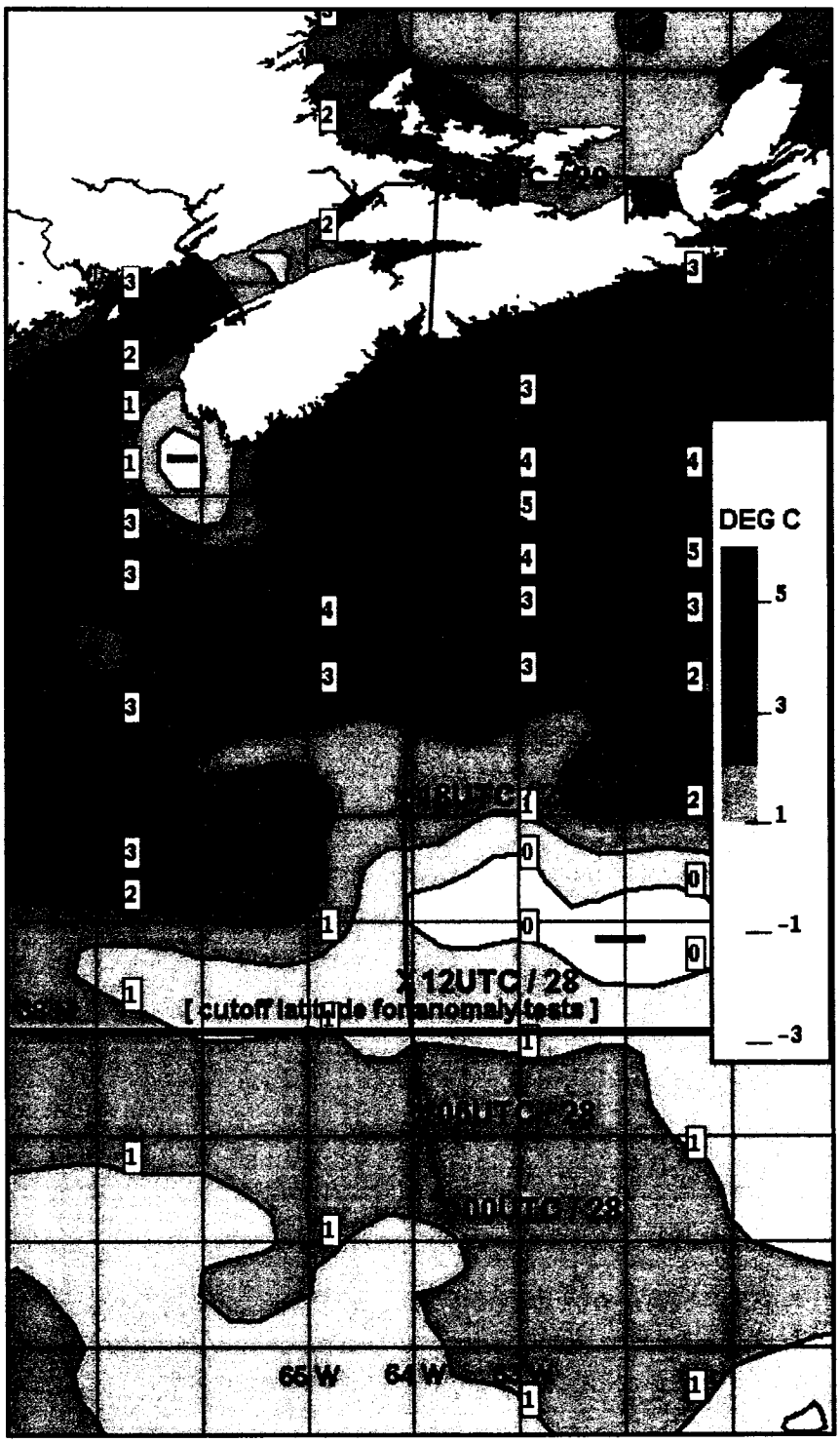

Figure 9. Pre-storm sea surface temperature anomaly (degrees Celsius) for Hurricane Juan. The storm track segment is also indicated by the solid curve with 6-hourly nodes marked with an "X". The bold latitude line marks the cut-off for the anomaly tests. Anomaly centers are marked with + or -.

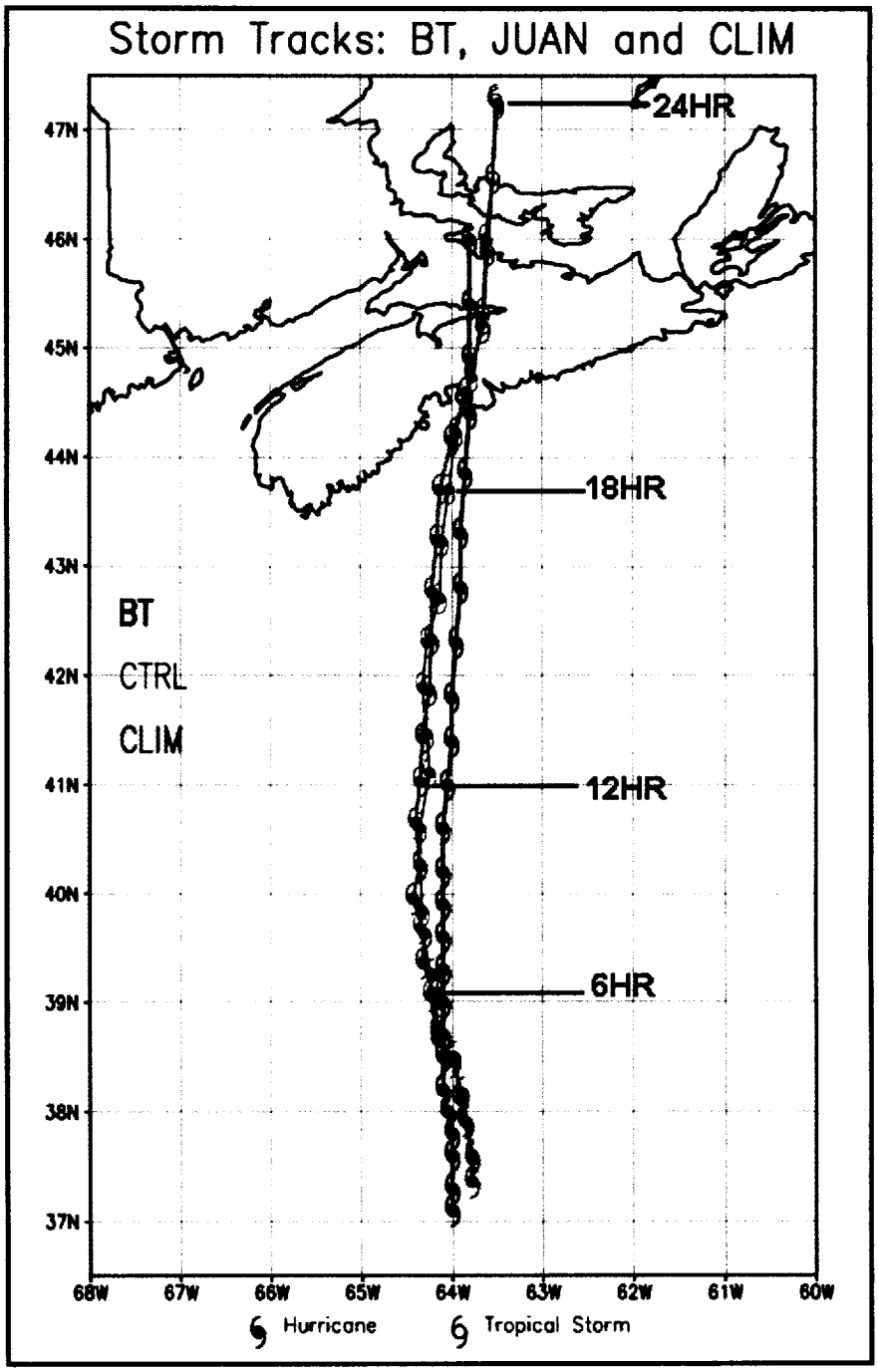

Figure 10. Storm tracks for the Hurricane Juan control simulations. Tracks are shown for the JUAN (red) and CLIM (green) runs and the best track (BT) (black). Positions are marked every hour for the 24-hour period from 06/28 to 06/29 September, 2003. The simulation times shown are from the start of the 3 km runs.

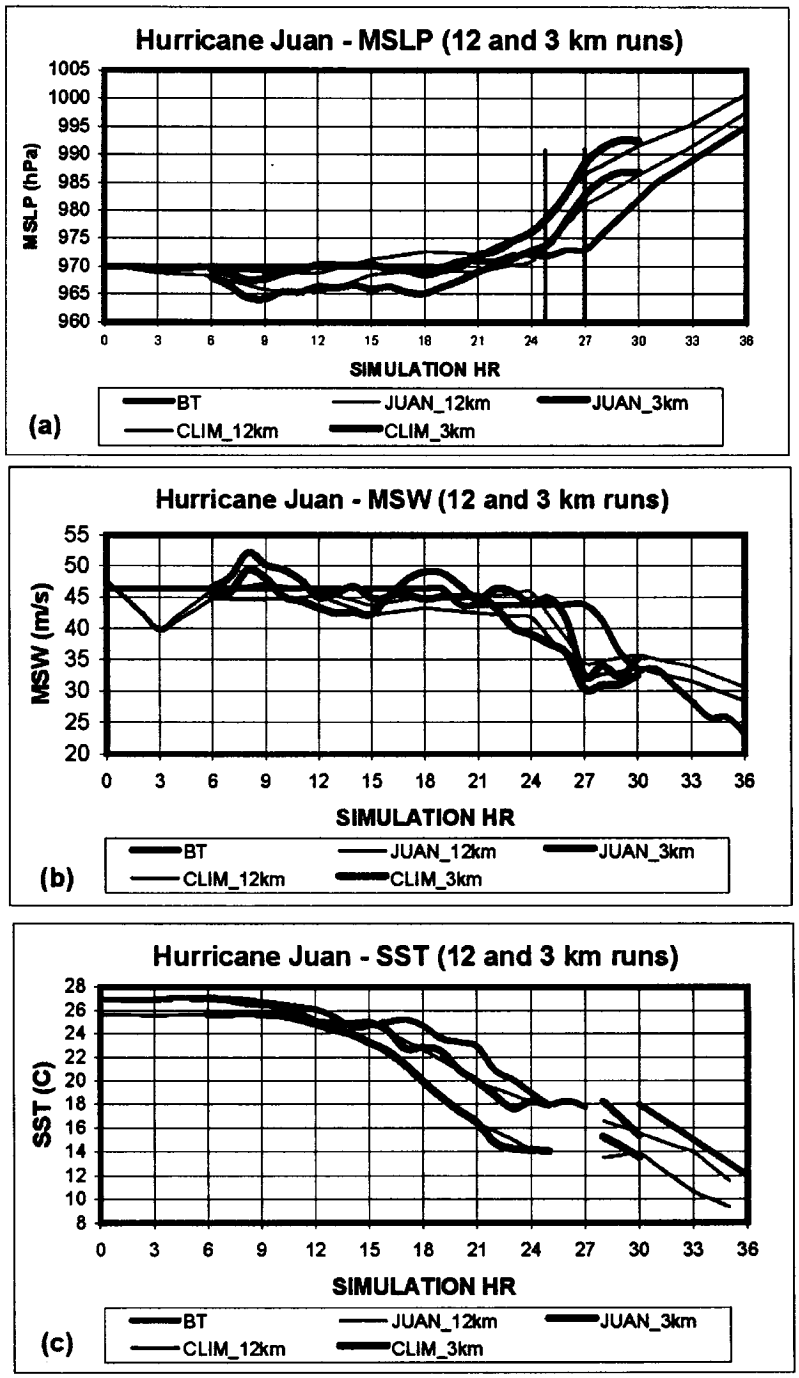

Figure 11. Time traces for the Hurricane Juan control simulations: (a) evolution of minimum sea level pressure (MSLP) for 12 km JUAN (thin red line), 12 km CLIM (thin green line), 3 km JUAN (thick red line), 3 km CLIM (thick green line) and the best track (BT) (black line); (b) maximum surface winds (MSW); and (c) sea surface temperature (SST) beneath the storm center (defined by the location of the MSLP) as a function of model simulation time (hours). The vertical lines in (a) denote the approximate model landfall time (blue) and observed landfall time (black).

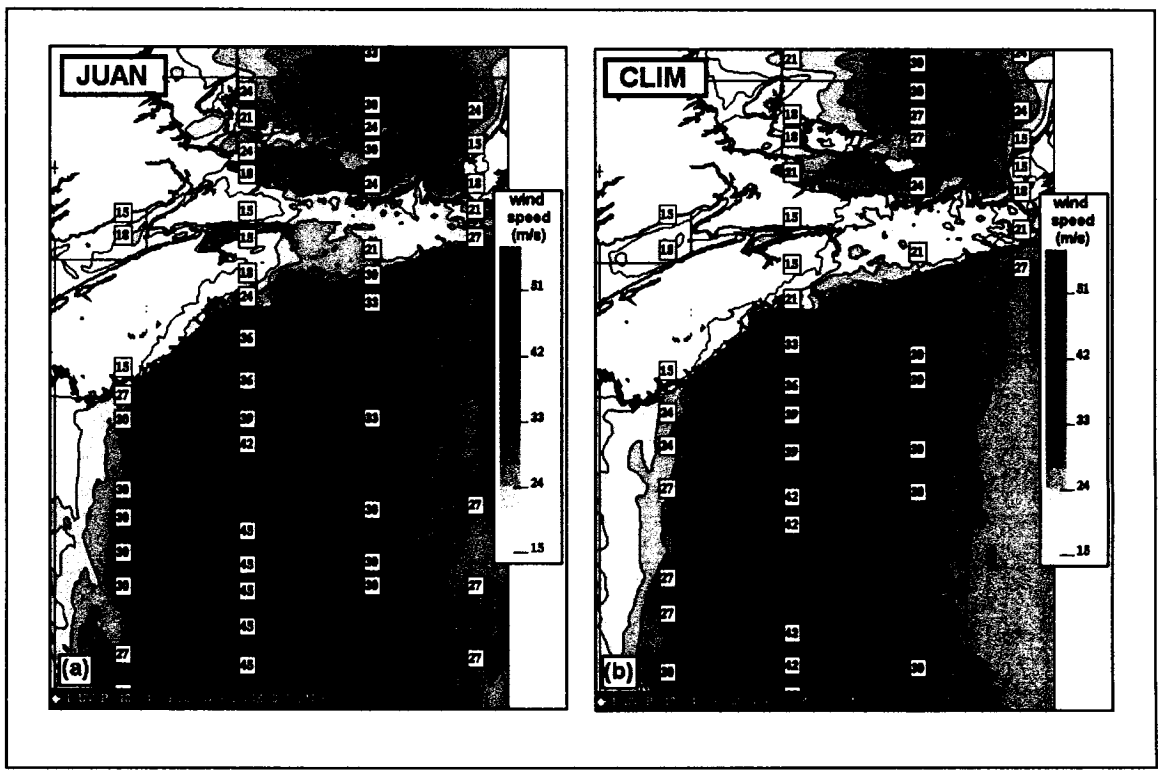

Figure 12. Swaths of maximum surface winds (every 3 m s^{-1}) for each 3 km control simulation of Hurricane Juan: (a) JUAN and (b) CLIM.

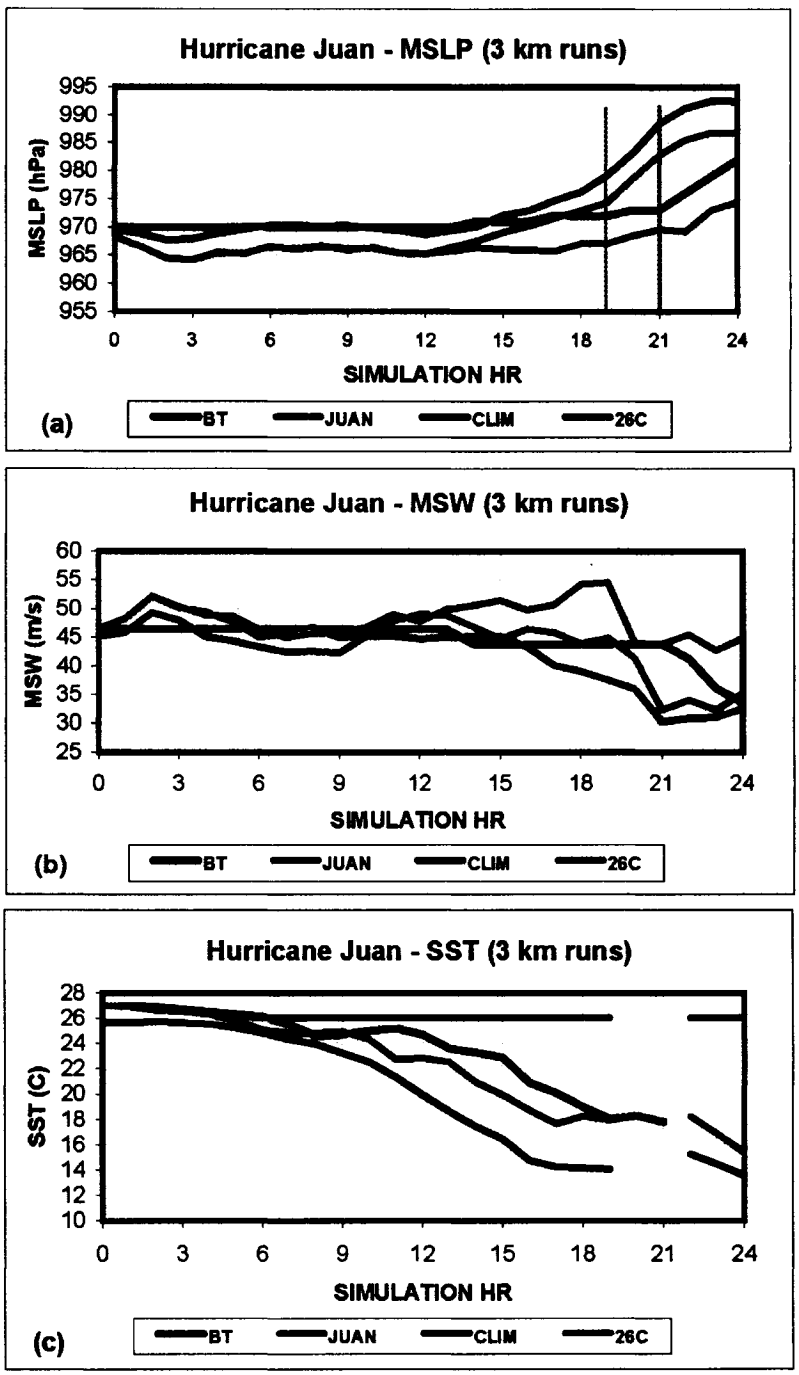

Figure 13. Model results for the 3 km control simulations and the fictitious 26-C SST run for Hurricane Juan: (a) evolution of minimum sea level pressure (MSLP) for JUAN (red), CLIM (green), best track (black) and the 26-C SST (26C) run (blue); (b) maximum surface winds (MSW); and (c) SST beneath the storm center (defined by the location of the MSLP) as a function of model simulation time (hours). Observed landfall time is shown by vertical black line in (a) and model landfall time shown by vertical blue line.

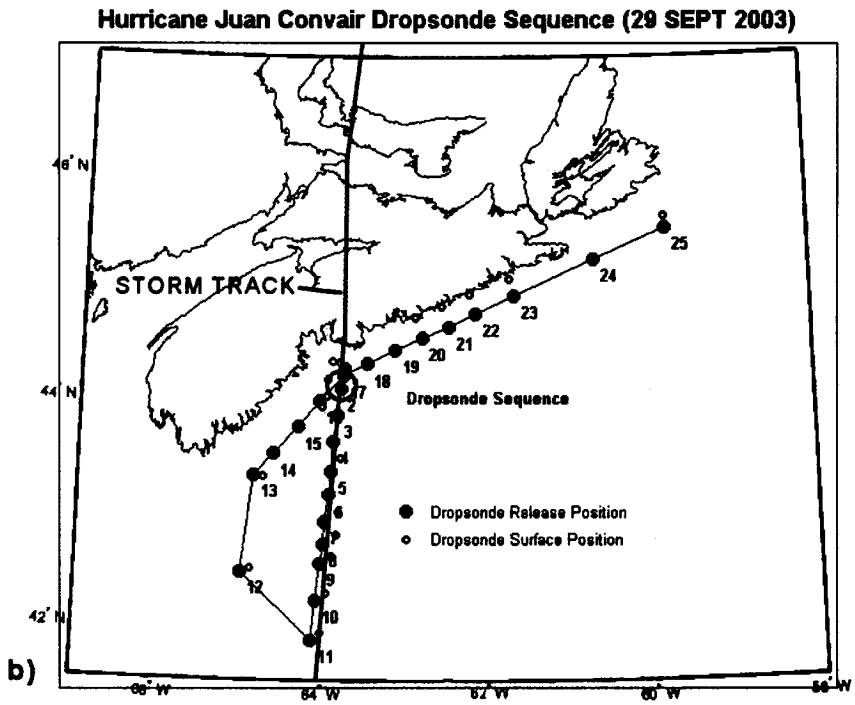

Figure 14. Convair 580 research aircraft and dropsonde deployment configuration in Hurricane Juan: (a) photo of the aircraft and (b) sequence of dropsondes deployed into the storm. The individual sondes are numbered to the lower right of their release position. The approximate storm position corresponding to the cross sections discussed in the text is indicated with a large open circle.

Figure 15. Observed and simulated vertical cross sections of wind speed and equivalent potential temperature near the time of landfall for Hurricane Juan. Panel (a) - output of wind speed from the control run of the model (JUAN) in m s^{-1} (every 5 m s^{-1}) as a function of pressure and distance compared with dropsonde data (b). The horizontal scale in (a) is the same as (b). Panel (c) – output of equivalent potential temperature from the JUAN control run in Kelvin (every 2K) compared with dropsonde data (d). Panel (e) - same as (c) except from the CLIM control run. The location of dropsondes in (b) and (d) are shown by vertical lines and are numbered accordingly.

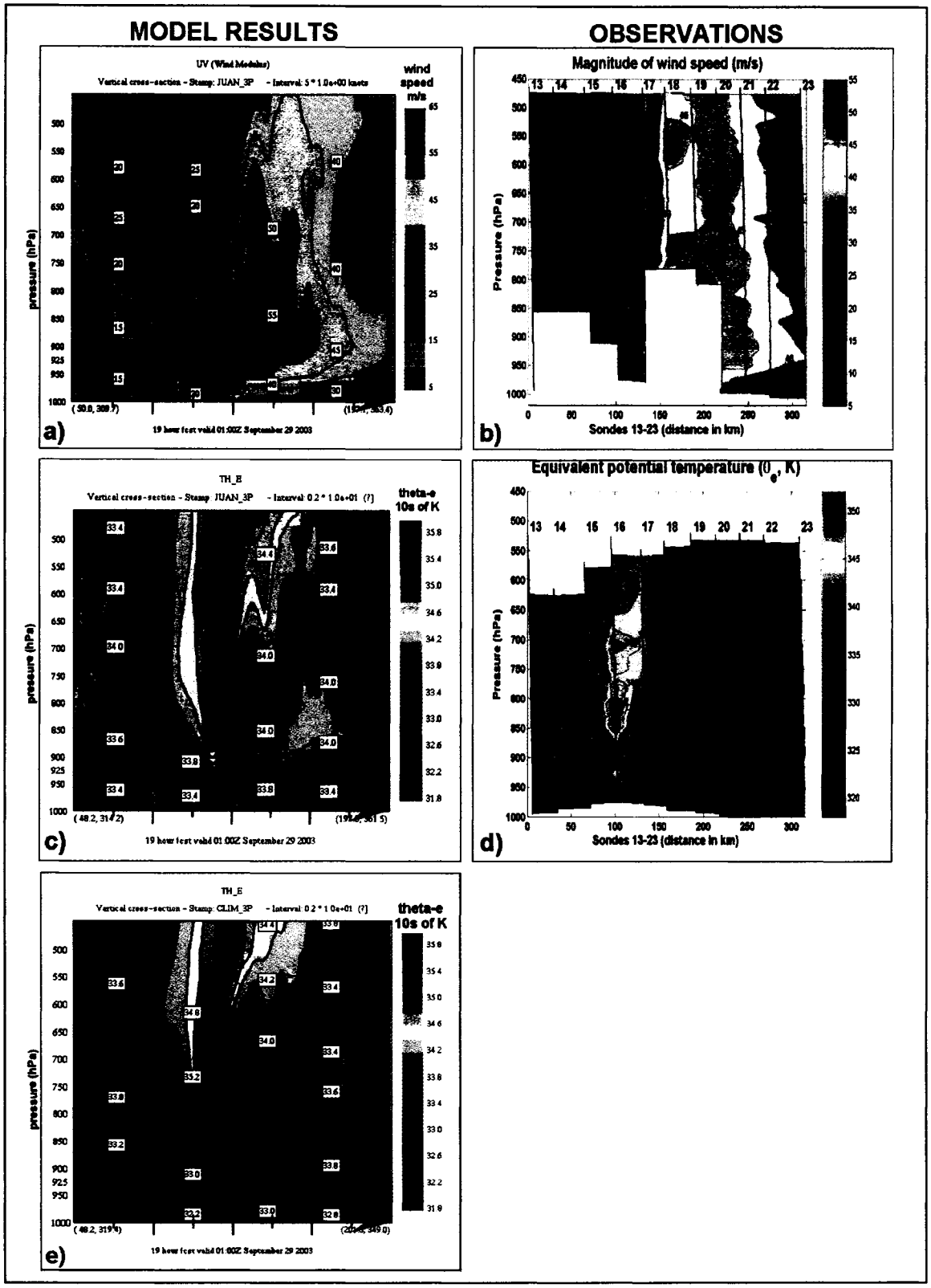
MODEL RESULTS
OBSERVATIONS
UV (Wind Modulus)
Vertical cross-section - Stamp: JUAN_3P - Interval: 5 * 1.0e+00 knots
wind speed m/s
pressure (hPa)
19 hour fcst valid 01:00Z September 29 2003
a)
Magnitude of wind speed (m/s)
Pressure (hPa)
Sondes 13-23 (distance in km)
b)
TH_E
Vertical cross-section - Stamp: JUAN_3P - Interval: 0.2 * 1.0e+01 (?)
theta-e 10s of K
19 hour fcst valid 01:00Z September 29 2003
c)
Equivalent potential temperature (θ_e, K)
Sondes 13-23 (distance in km)
d)
TH_E
Vertical cross-section - Stamp: CLIM_3P - Interval: 0.2 * 1.0e+01 (?)
theta-e 10s of K
19 hour fcst valid 01:00Z September 29 2003
e)

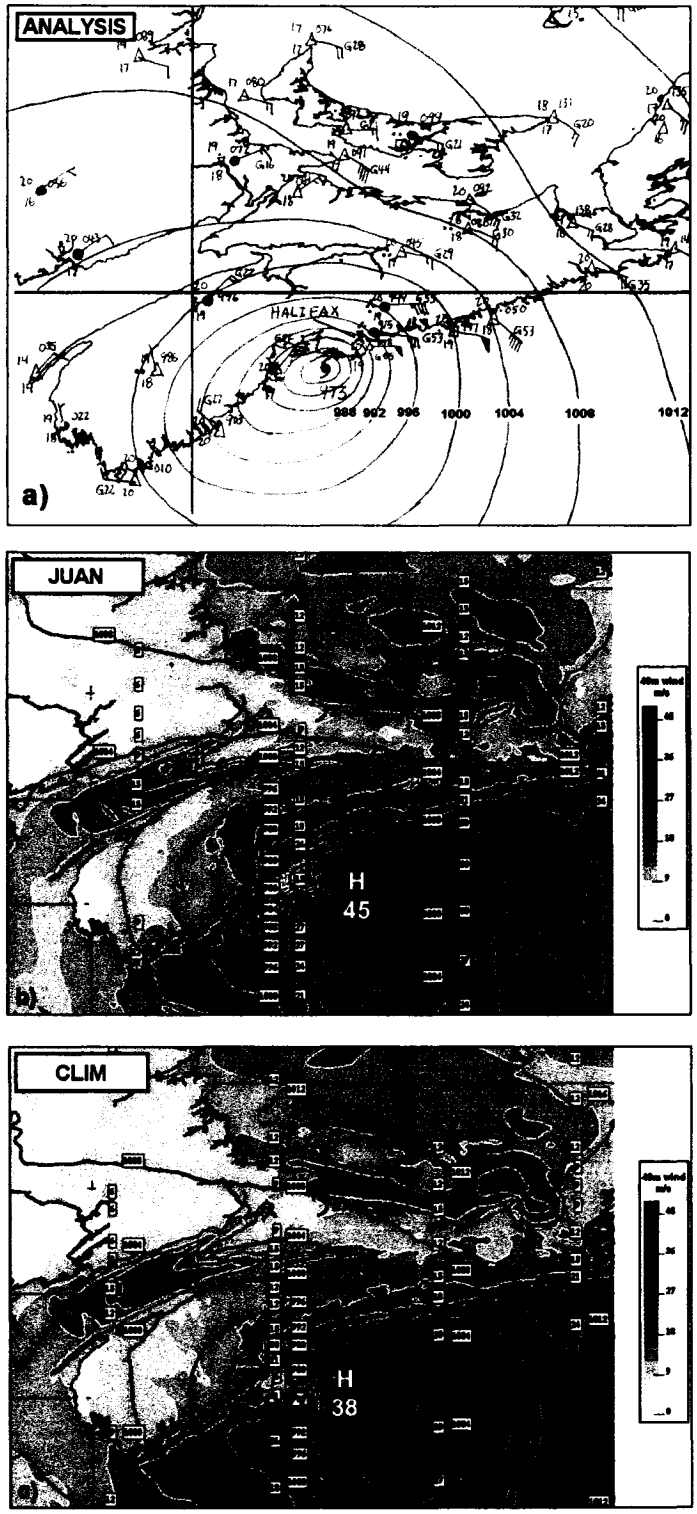

Figure 16. Observed and simulated sea level pressure and wind speed for Hurricane Juan immediately prior to landfall: (a) hand-drawn analysis of sea level pressure (solid contours every 4 hPa) with weather station data plotted using conventional synoptic format; (b) output from the JUAN control simulation showing sea level pressure (black contours) with 40-m wind speed in (shaded field every 3 m s^{-1}); and (c) same as (b) except for output from the CLIM control simulation.

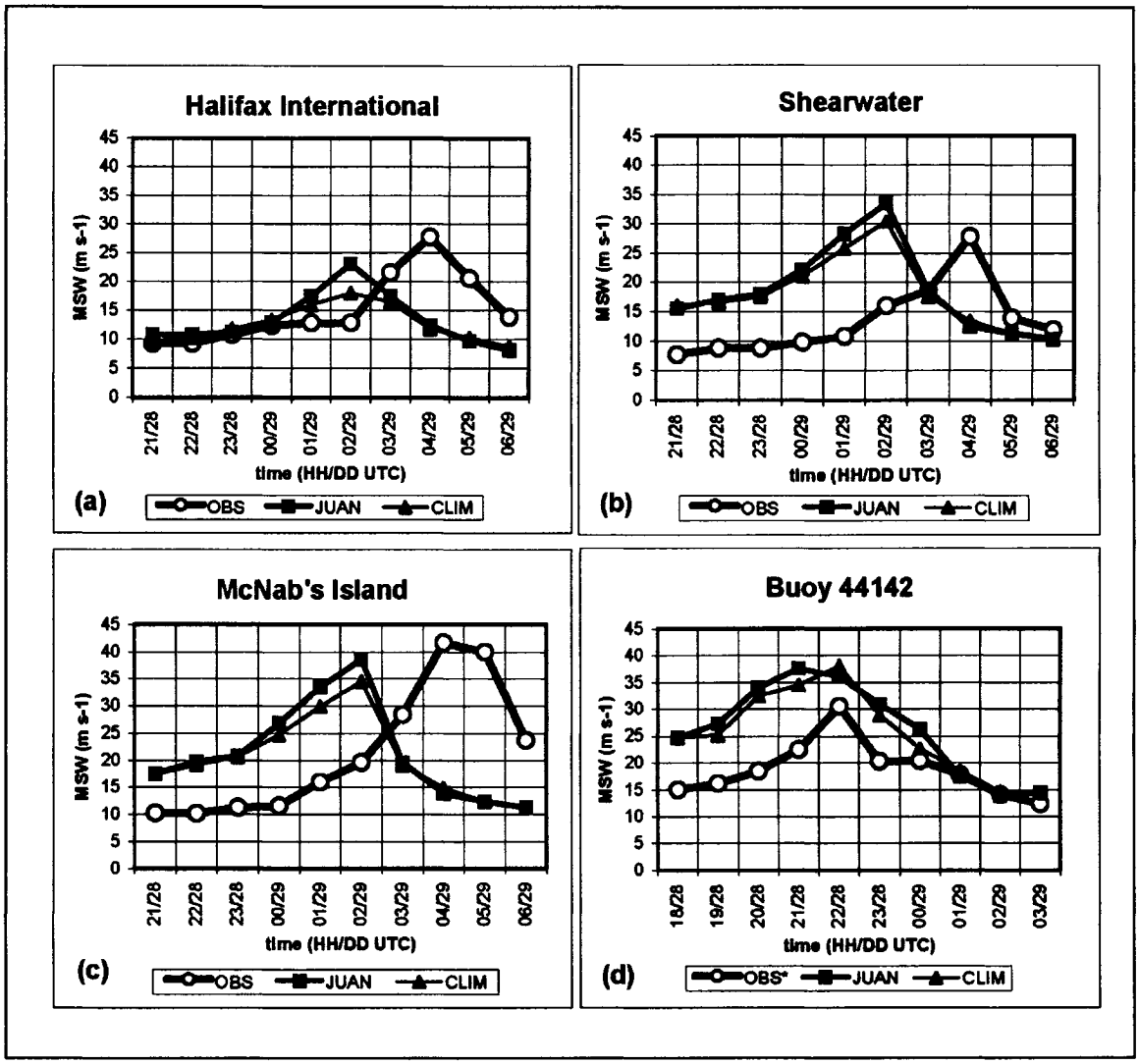

Figure 17. Times series of observed and model-simulated instantaneous surface wind speeds during Hurricane Juan. Model output is at 40 m and weather stations at 10 m for various locations: (a) Halifax International Airport, (b) Shearwater, (c) McNab's Island (Halifax Harbour), and (d) buoy 44142 (~200 km south of storm landfall location).

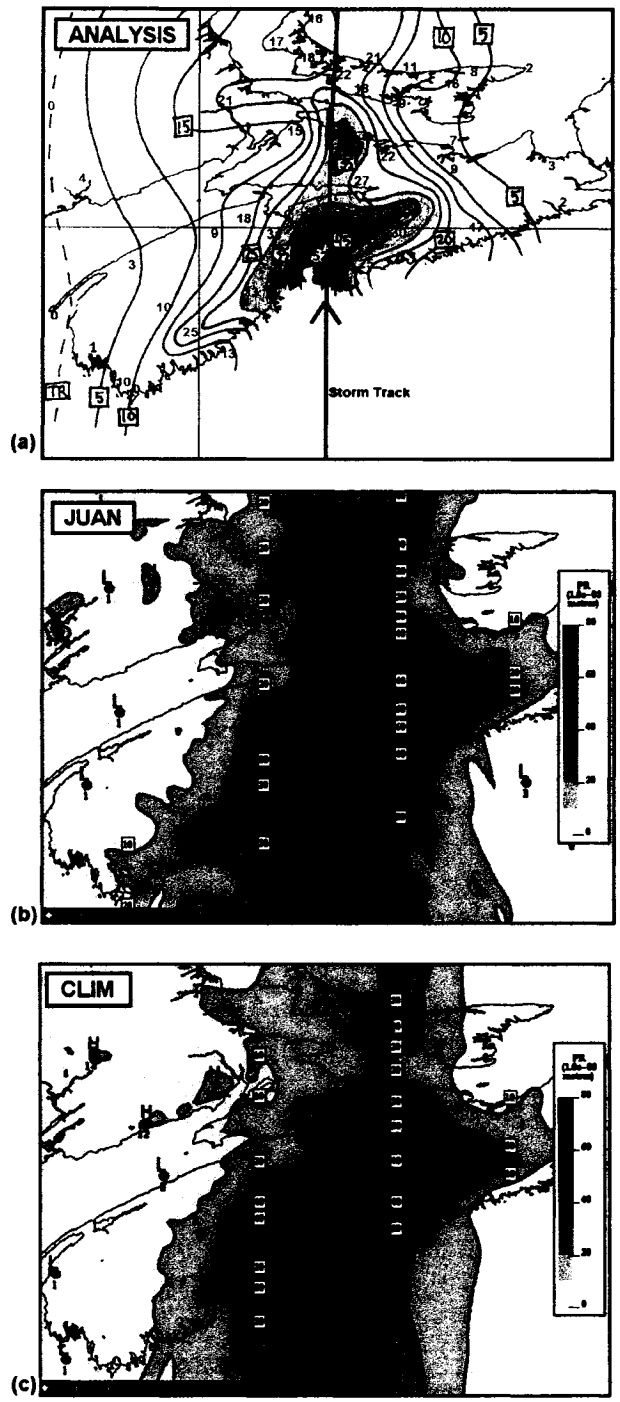

Figure 18. Observed and simulated storm-total rainfall accumulations for Hurricane Juan: (a) subjective analysis (solid contours every 5 mm) with various station amounts plotted on map; (b) model-generated rainfall from the JUAN control simulation (shaded contours every 10 mm), and (c) same as (b) except for the CLIM simulation.

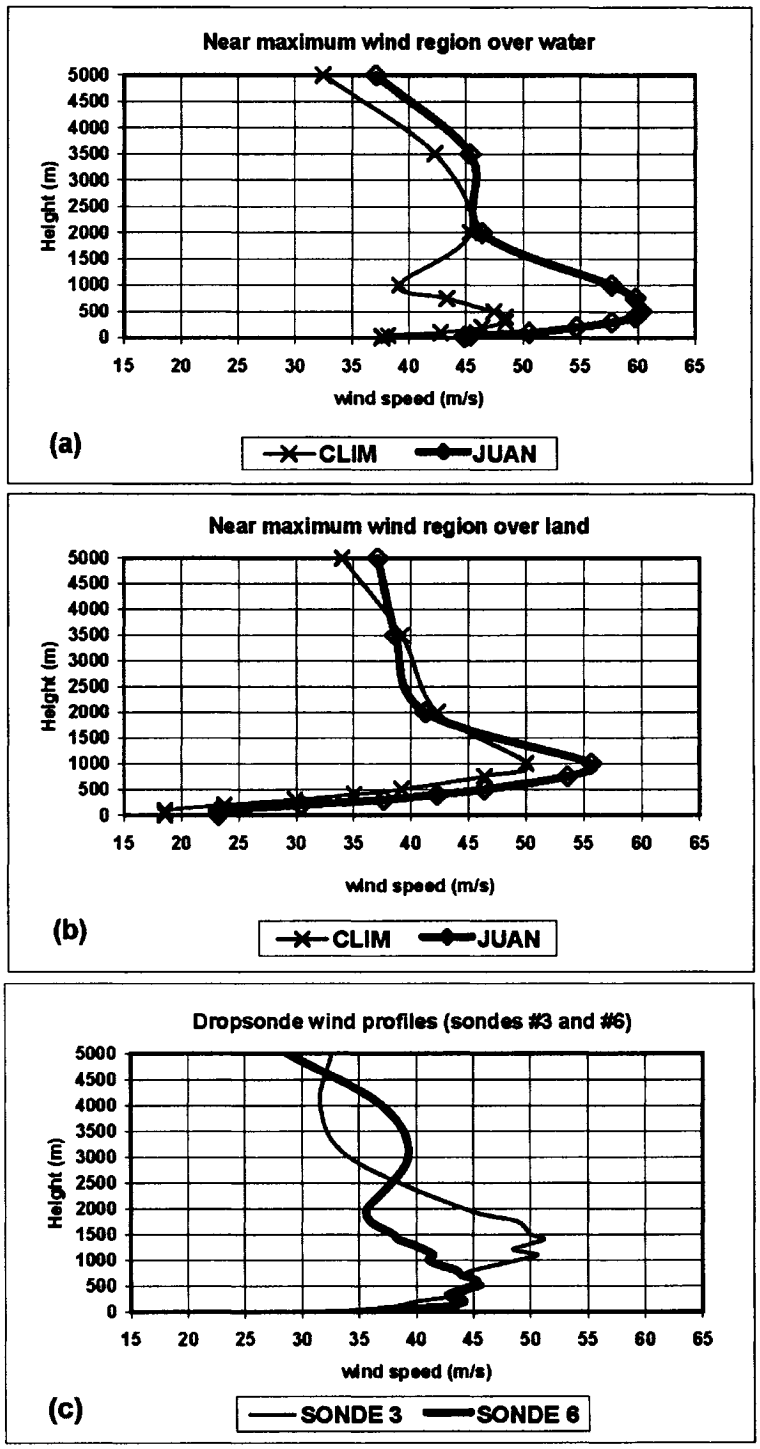

Figure 19. Model output and dropsonde wind speed profiles for Hurricane Juan. Model output is shown for (a) the high wind region in the storm over water immediately prior landfall, and (b) the high wind region at Halifax International Airport (when winds were strongest there) from the JUAN (solid, bold curve) and CLIM (solid, thin curve) simulations. Select over-water dropsonde profiles near the storm center (see sonde locations in Fig. 14) are shown in (c).

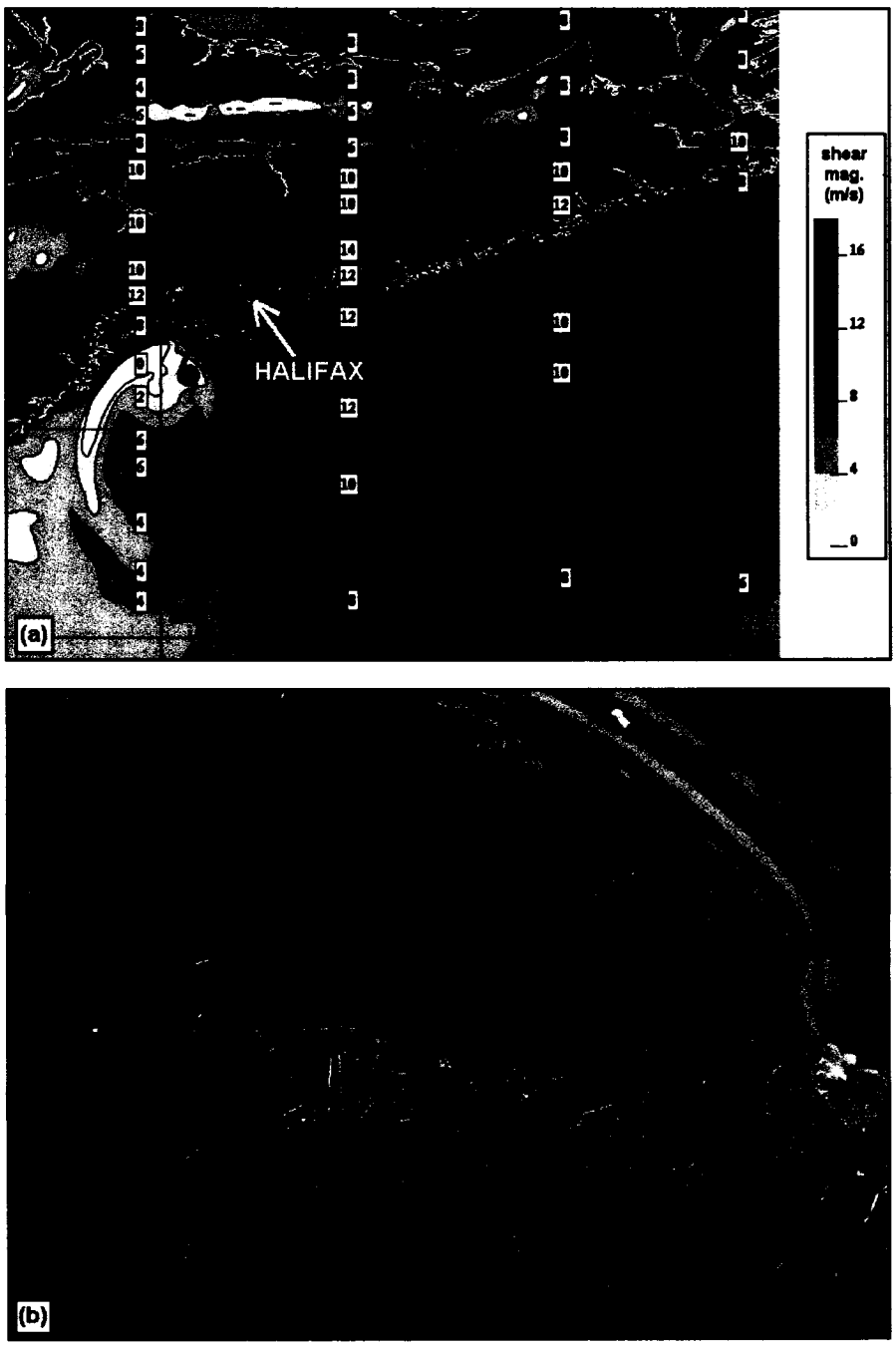

Figure 20. Model-simulated low-level wind shear and characteristic tree damage during Hurricane Juan. Wind shear magnitude between 50 and 300 m elevation from the JUAN control simulation is shown in (a) and a photograph of softwood forest blow-down is shown in (b) within the high wind shear region. The contour interval in (a) is every 2 m s^{-1} and the coastline is delineated by the thin white contour. The center of the storm is shown by the hurricane symbol southwest of Halifax.

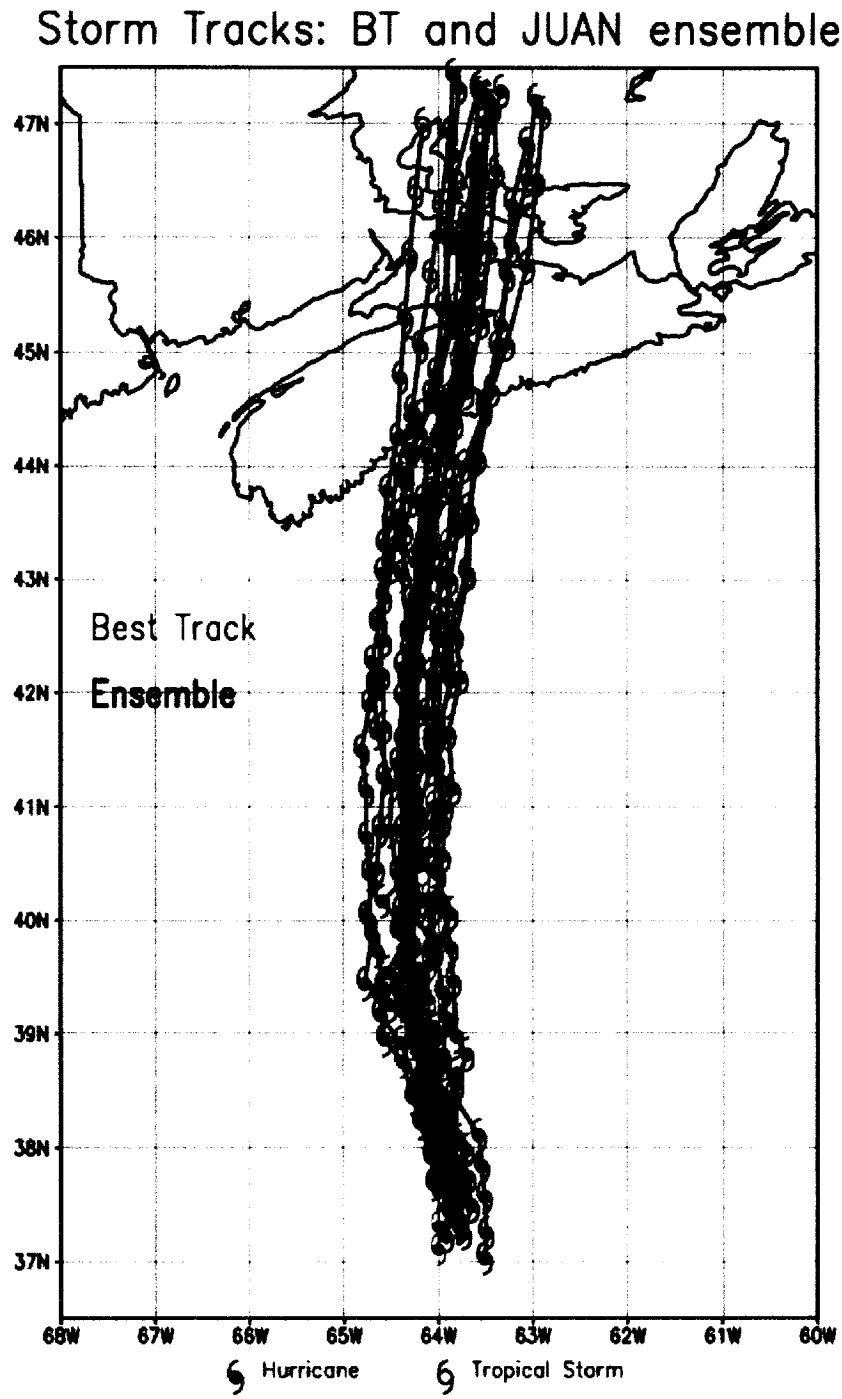

Figure 21. Ensemble of storm tracks from the Hurricane Juan simulations. Storm tracks of all ensemble members (including control) from the JUAN set of simulations is shown in black, including the best track (BT) in red. Track positions are every hour for the 24-hour period from 06/28 to 06/29 September.

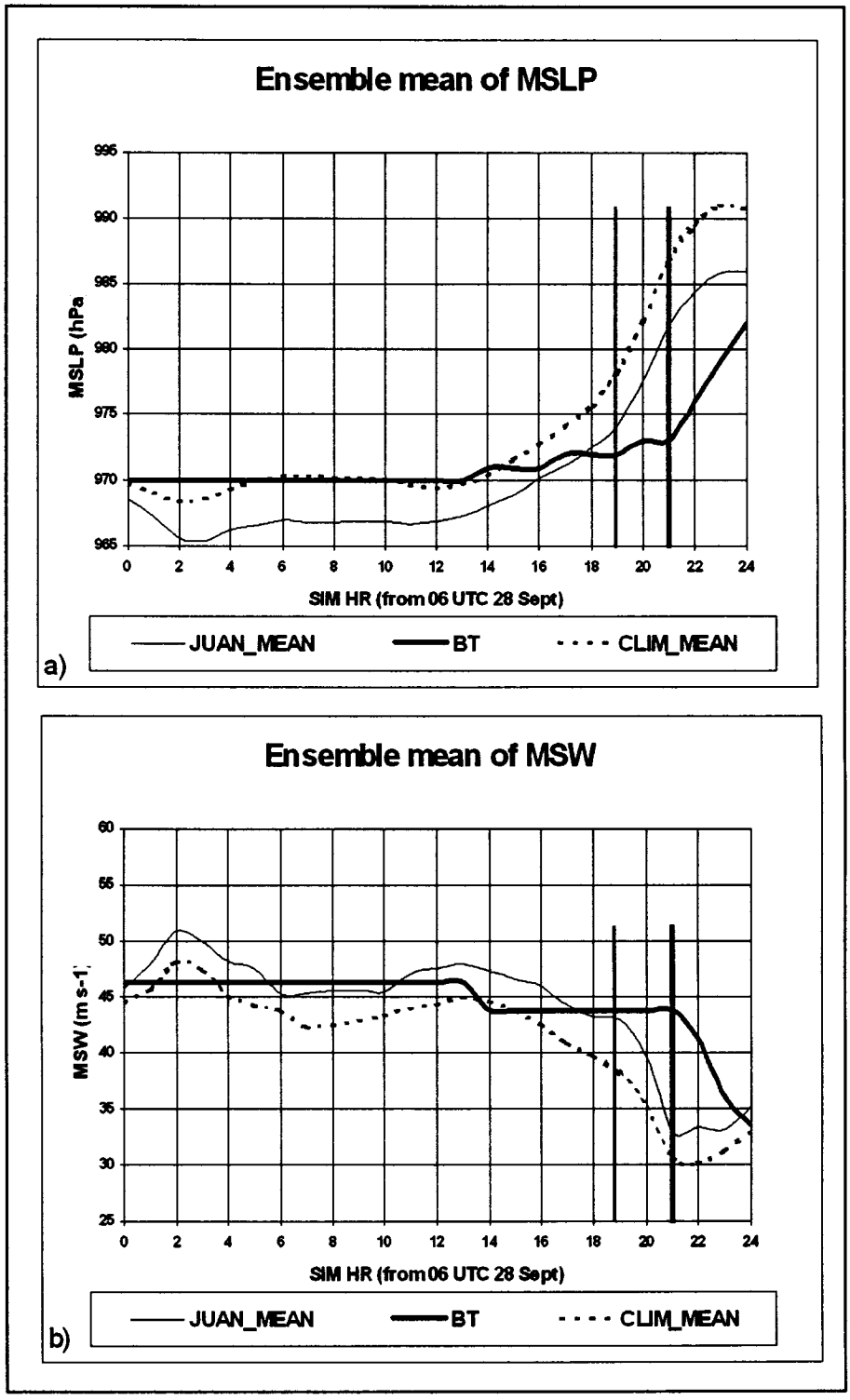

Figure 22. Time traces of ensemble means for Hurricane Juan. Runs include the JUAN and CLIM groups of simulations: (a) minimum sea level pressure (MSLP) and (b) maximum surface wind speed (MSW). Mean time of simulated landfall is shown by the thin vertical lines and time of best track landfall is shown by the thick vertical lines.

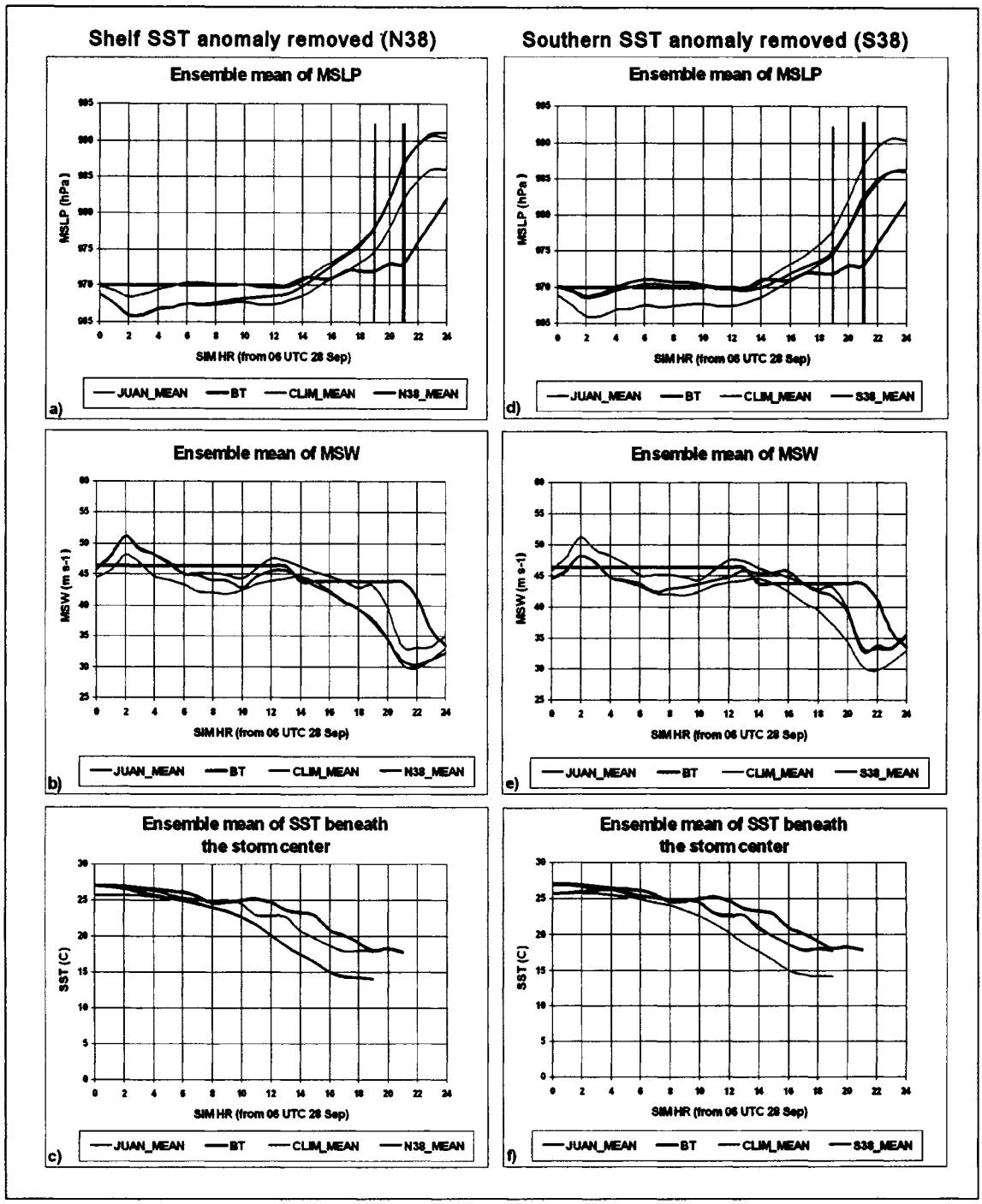

Figure 23. Results from the sea surface temperature anomaly removal experiments for Hurricane Juan. Time traces of the 6-member (plus control) sub-ensemble means for the simulations where the shelf sea surface temperature (SST) anomaly is removed (blue curves, N38) is shown on the left-hand side, and where the southern SST anomaly is removed (blue curves, S38) is on the right-hand side. Results are compared with the sub-ensemble means from the JUAN (red) and CLIM (green) groups, with best track (black). N38: (a) minimum sea level pressure (MSLP), (b) maximum surface wind speed (MSW), and (c) SST beneath the storm center (defined by the location of the MSLP); (d)-(f) same as (a)-(c) except for S38. Mean of simulated landfall time is indicated in panels (a) and (d) by the thin vertical lines and observed landfall time is indicated by the thick vertical lines.

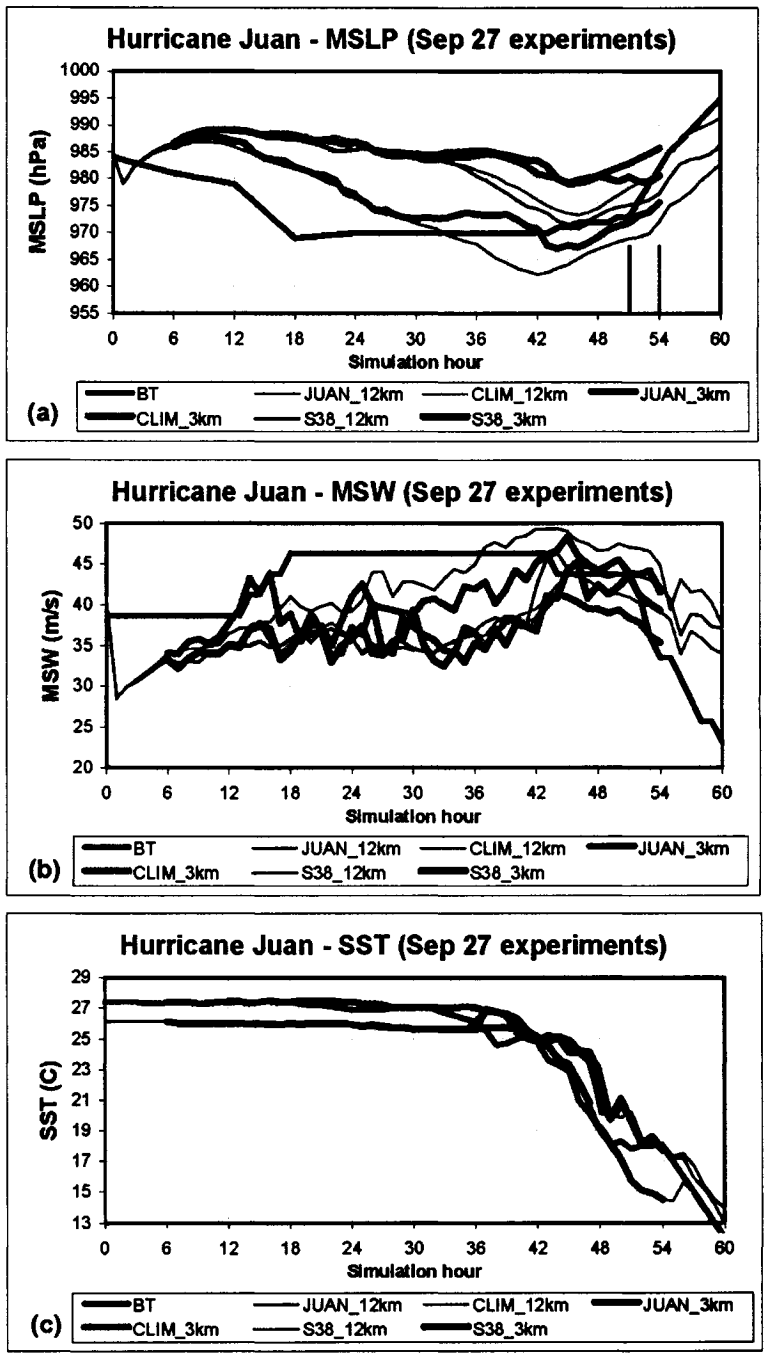

Figure 24. Model results for the 12 km and 3 km extended integrations for Hurricane Juan initiated on 27 September: (a) evolution of minimum sea level pressure (MSLP) for the 12 km control (JUAN) (thin red line), 12 km climatology-SST (CLIM) (thin green line), 12 km S38 (described in text) experiment (thin blue line), 3 km JUAN (thick red line), 3 km CLIM (thick green line), 3 km S38 (thick blue line), and the best track (black line); (b) maximum surface winds (MSW); and (c) sea surface temperature (SST) beneath the storm center (defined by the location of the MSLP) as a function of model simulation time (hours). The vertical bars in (a) denote the approximate model landfall time (blue) and observed landfall time (black).

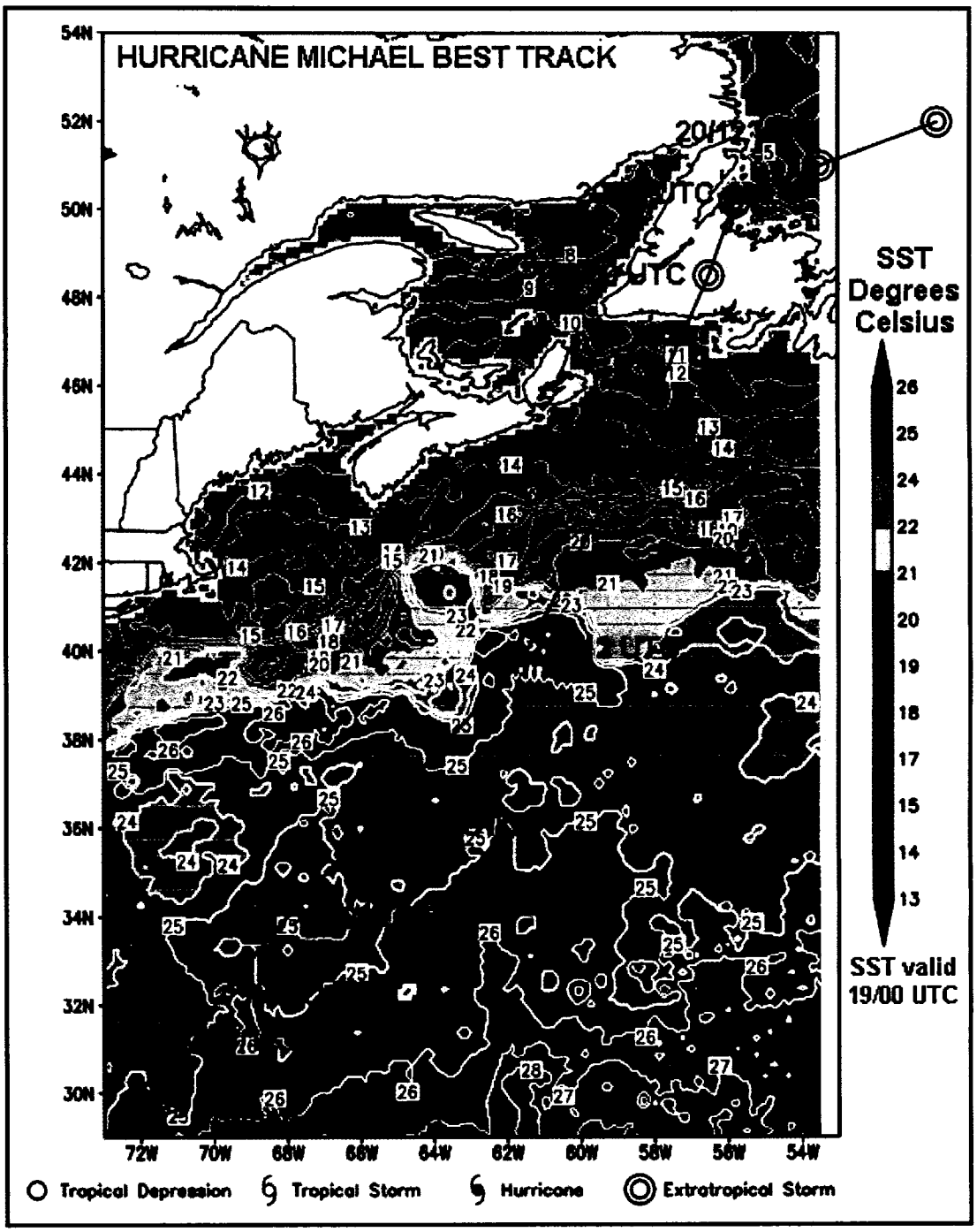

Figure 25. Best track for Hurricane Michael with sea surface temperatures. Sea surface temperatures (contours every 1°C) are valid at 00 UTC 19 October, 2000.

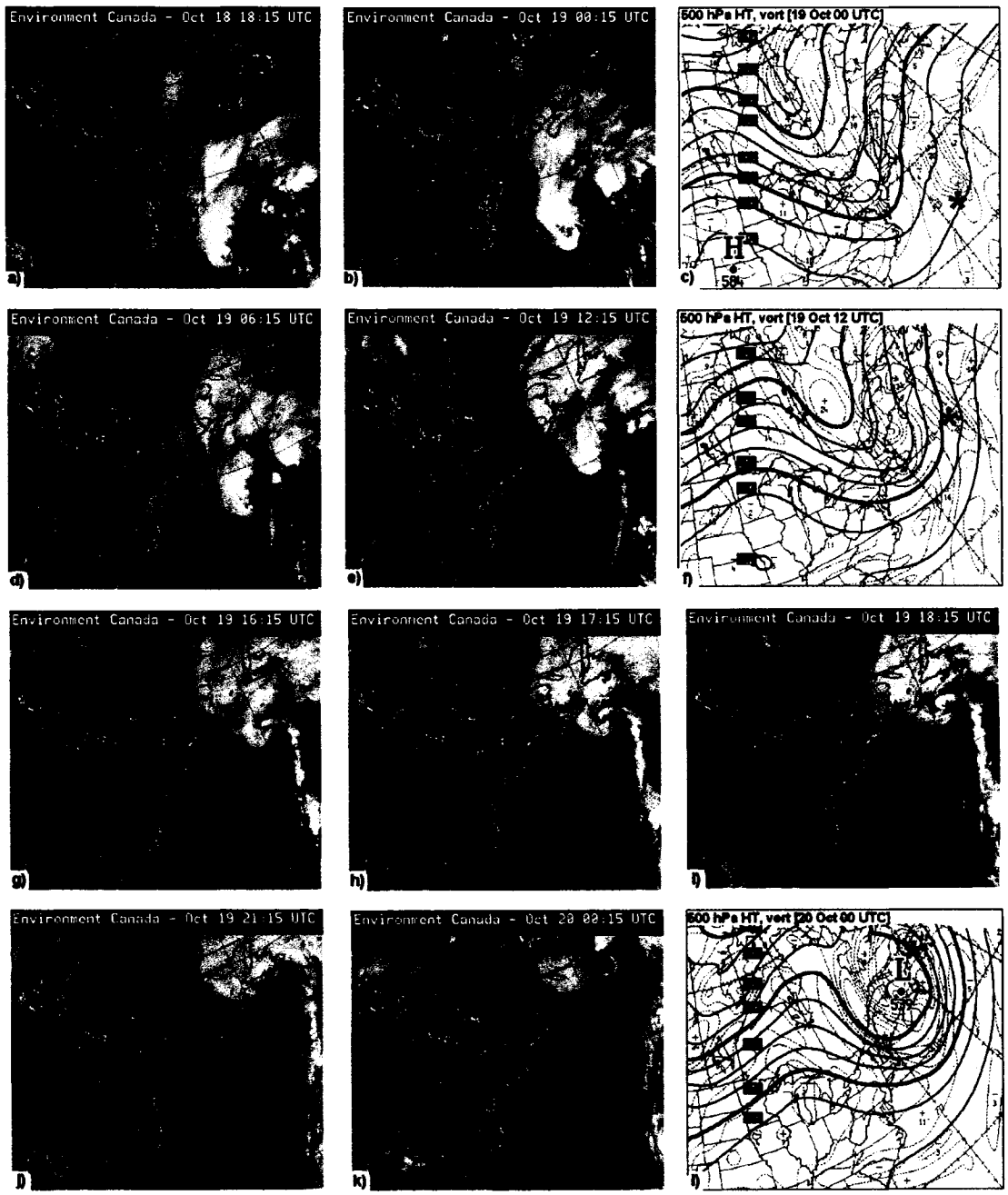

Figure 26. Evolution of GOES infrared satellite, 500-hPa geopotential height and absolute vorticity analyses during the extratropical transition of Hurricane Michael, October 2000. The location of the hurricane surface center is shown in the 500-hPa panels by the large black asterisk.

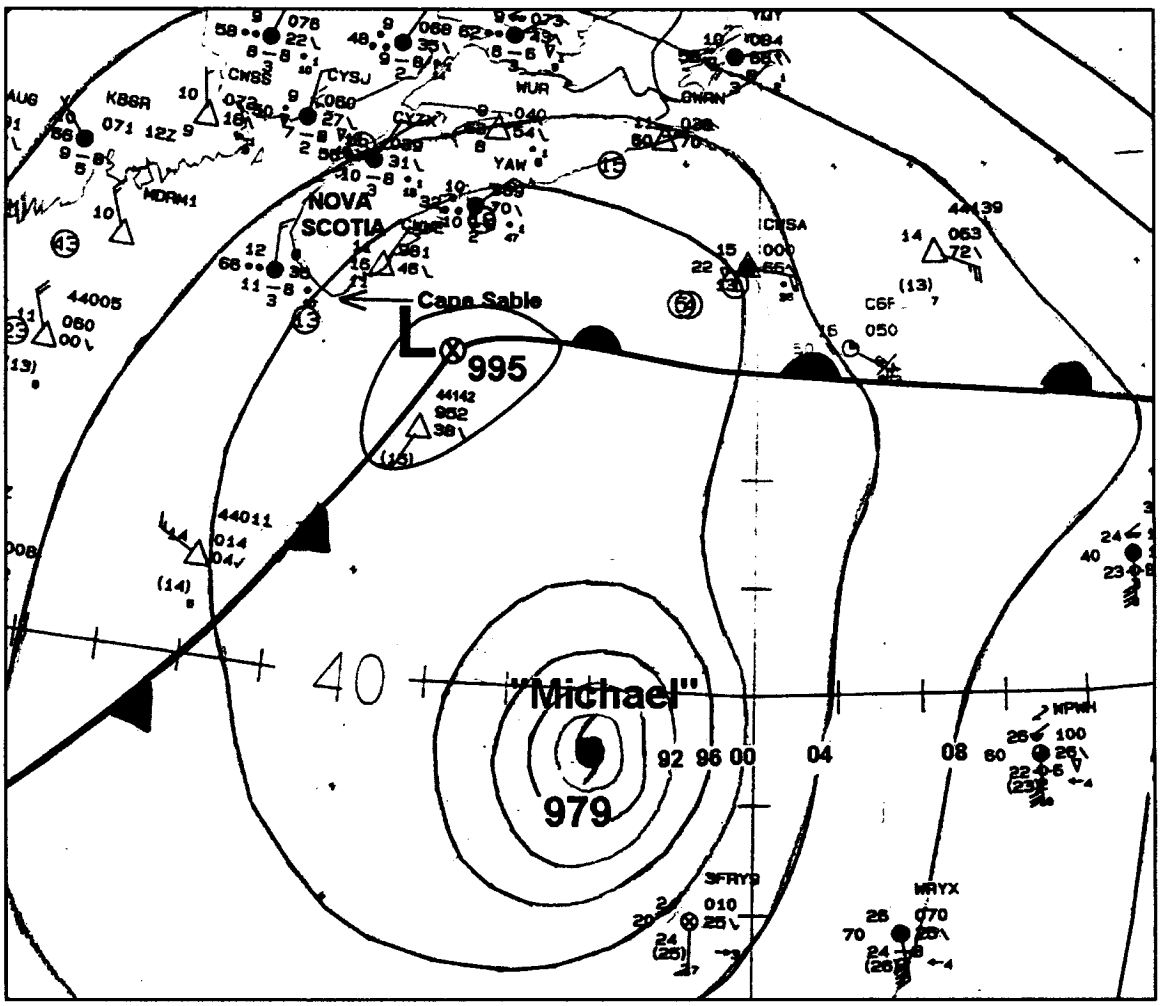

Figure 27. Manually drawn sea level pressure analysis of Hurricane Michael and the baroclinic cyclone. Valid time is 12/19, 2000. Sea level pressure contours are drawn every 4 hPa. Standard synoptic weather data plots are also shown.

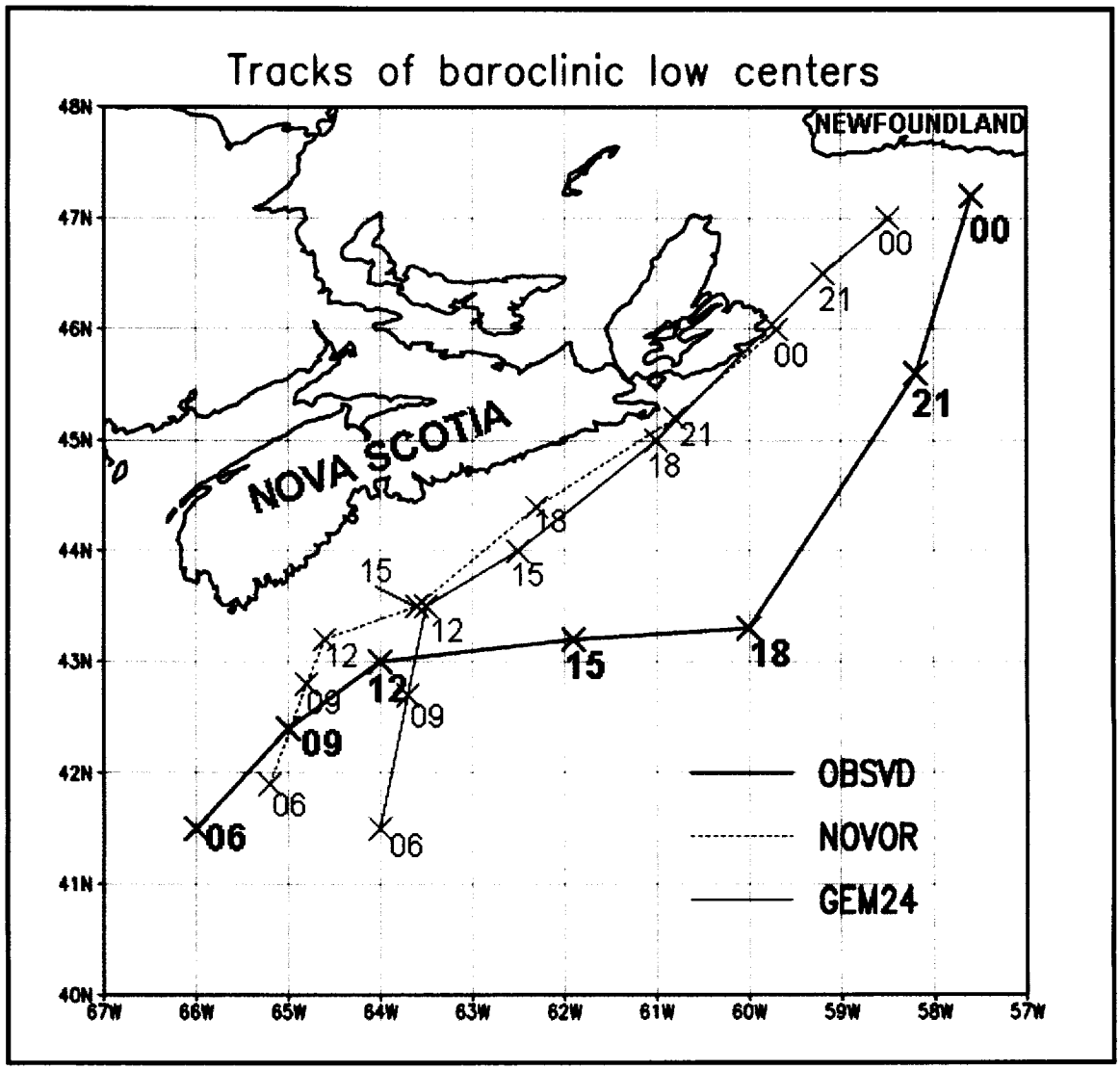

Figure 28. Evolution of the baroclinic cyclone associated with Hurricane Michael. Shown are the tracks of the baroclinic cyclone center from observations (thick solid), the operational GEM model (thin solid), and the no-vortex version of the MC2 model (dashed) every three hours from 06 UTC 19 October to 00 UTC 20 October 2000.

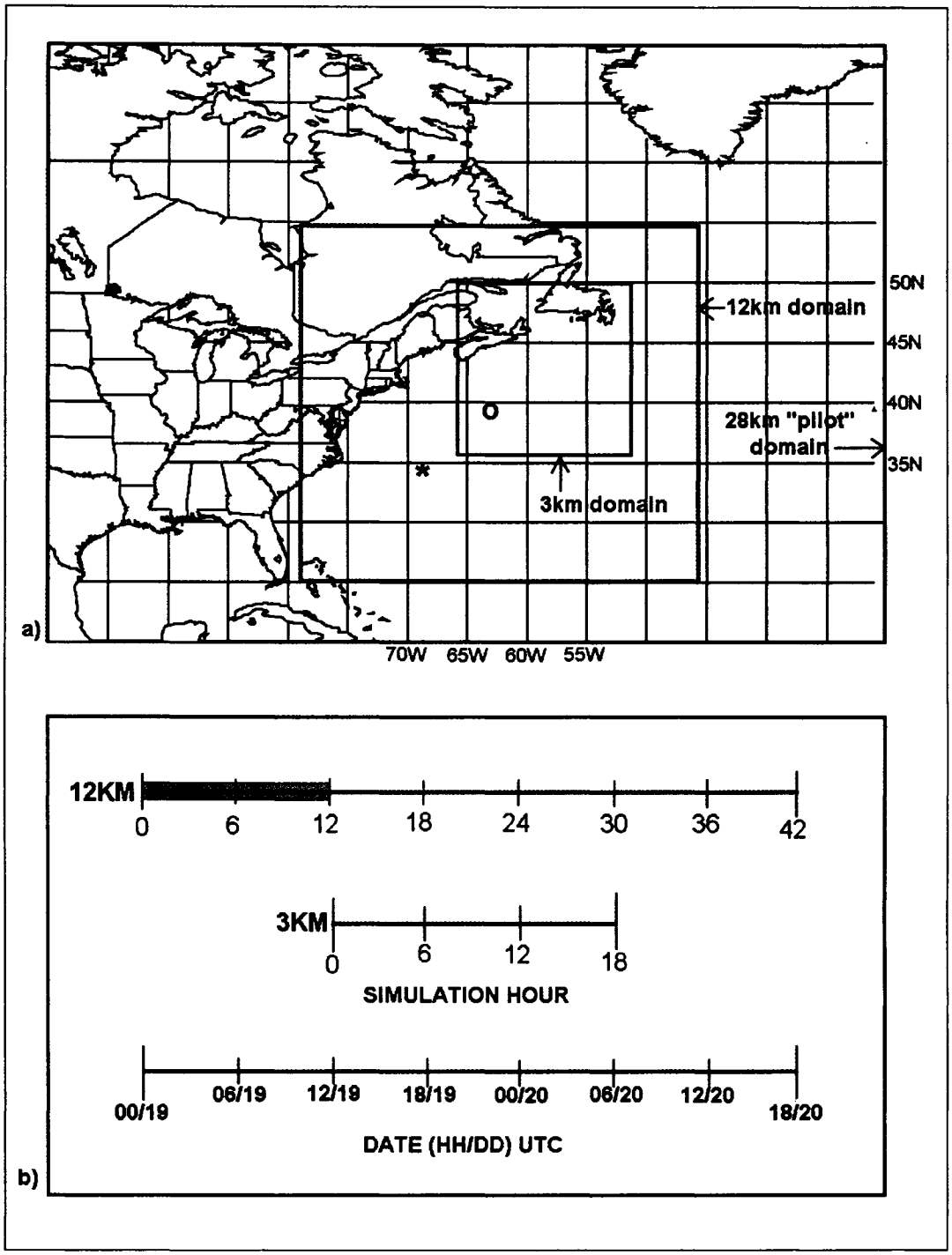

Figure 29. Layout for the Hurricane Michael model experiments: (a) grid configuration and (b) timelines for the model integrations. The asterisk in (a) marks the storm center at time-zero of the 12 km control simulations and the open circle marks the mean position of the storm at time-zero of the 3 km control simulations. The grey region on the 12 km timeline in (b) denotes the 12-hour model adjustment period.

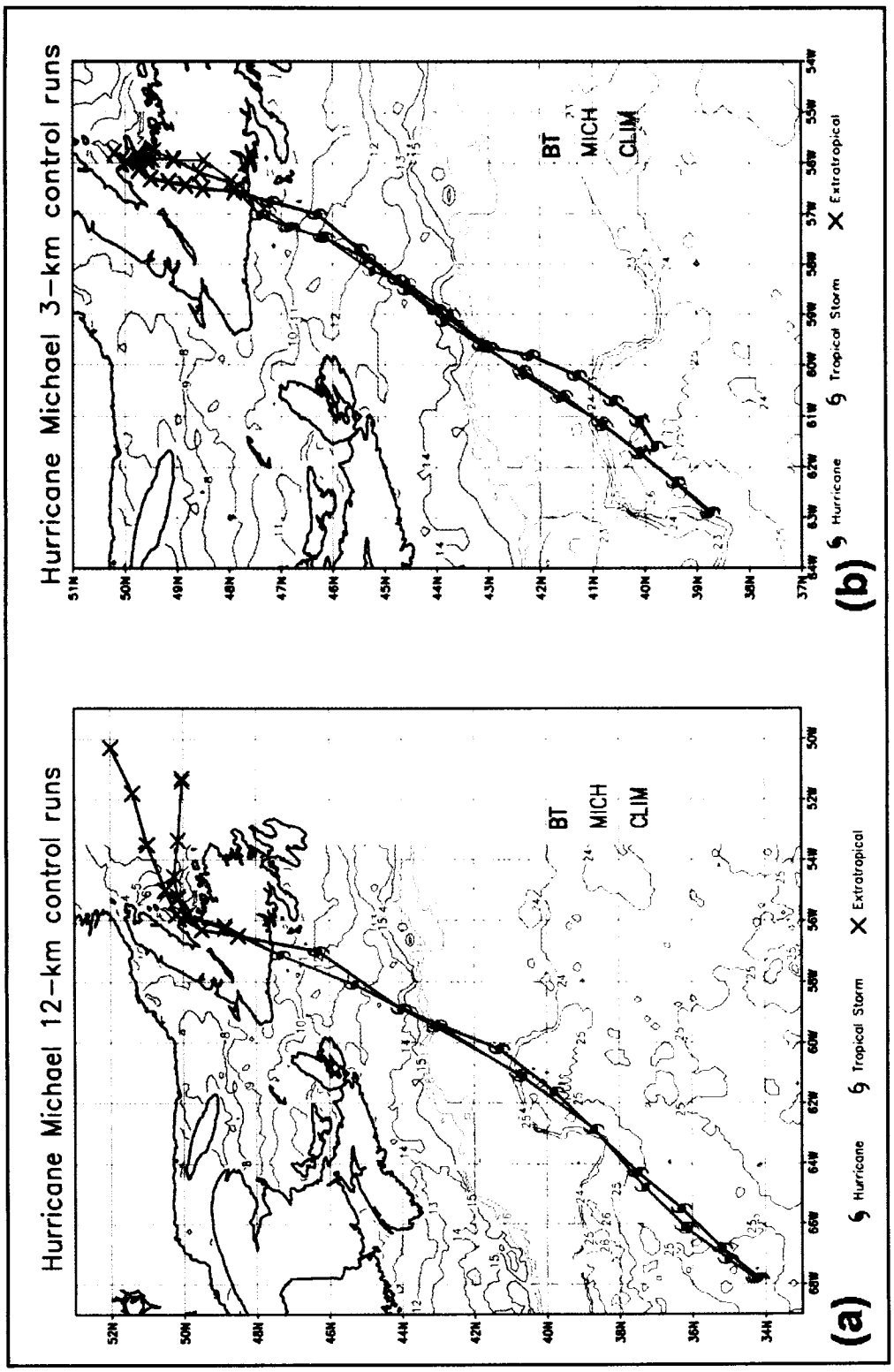

Figure 30. Simulated storm tracks for Hurricane Michael. Storm tracks are from the 12 km control runs of the model (a) and the 3 km control runs (b). Black curve denotes the best track (BT), red is the observed-SST control run (MICH) and green is the climatology-SST run (CLIM). Track nodes are every three hours in (a) from 00/19 to 18/20 and every hour in (b) from 12/19 to 06/20. Observed (CLASS) SST (every 1°C) is also shown.

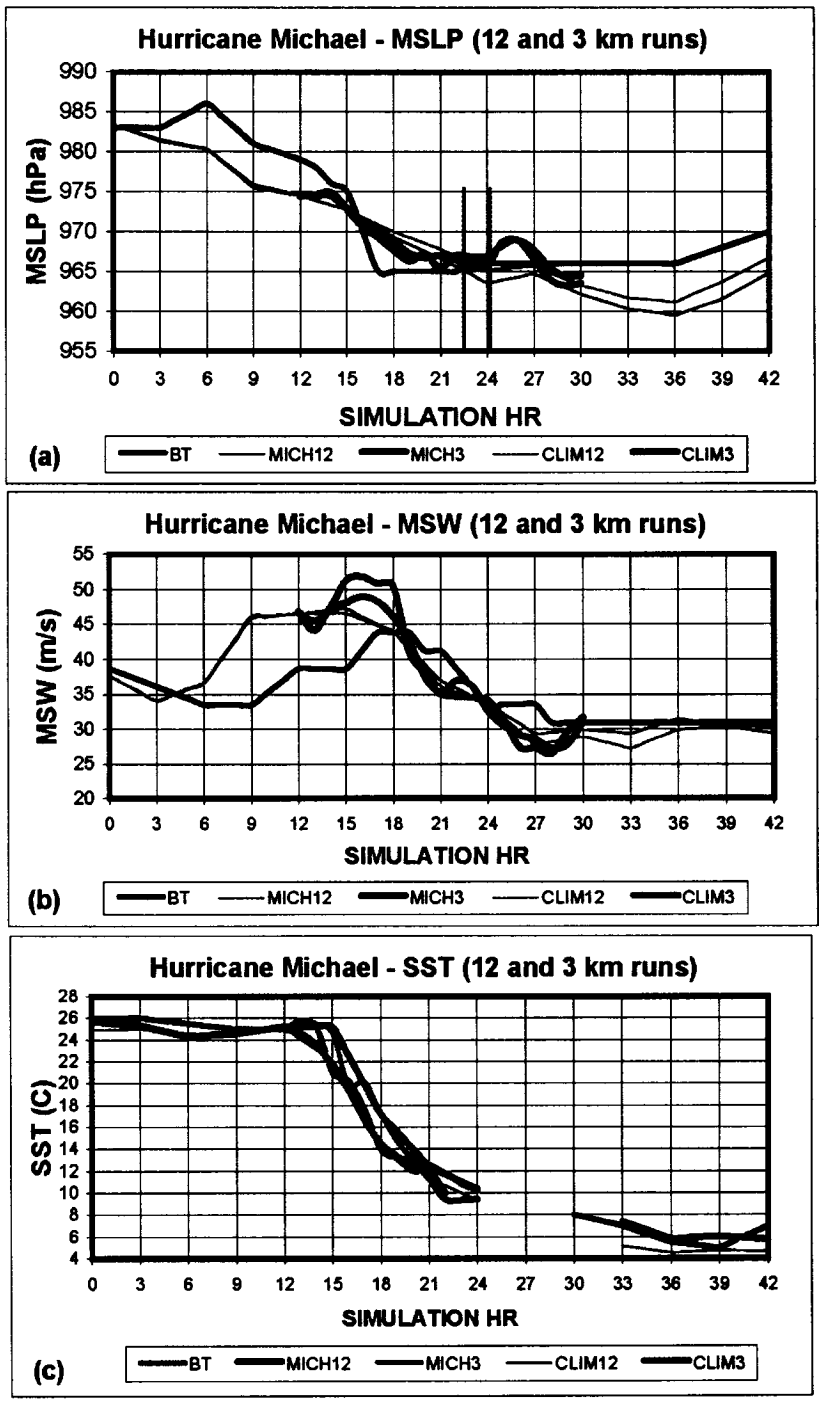

Figure 31. Time traces from the Hurricane Michael control simulations. Model results are for the 12 km control (MICH12 and CLIM12) and 3 km control (MICH3 and CLIM3) simulations: (a) evolution of minimum sea level pressure (MSLP) for MICH12 (thin red line), CLIM12 (thin green line), MICH3 (thick red line), CLIM3 (thick green line) and the best track (black line); (b) maximum surface winds (MSW); and (c) sea surface temperature (SST) beneath the storm center (defined by the location of the MSLP) as a function of model simulation time (hours). The vertical bars in (a) denote the approximate model landfall time (blue) and observed landfall time (black).

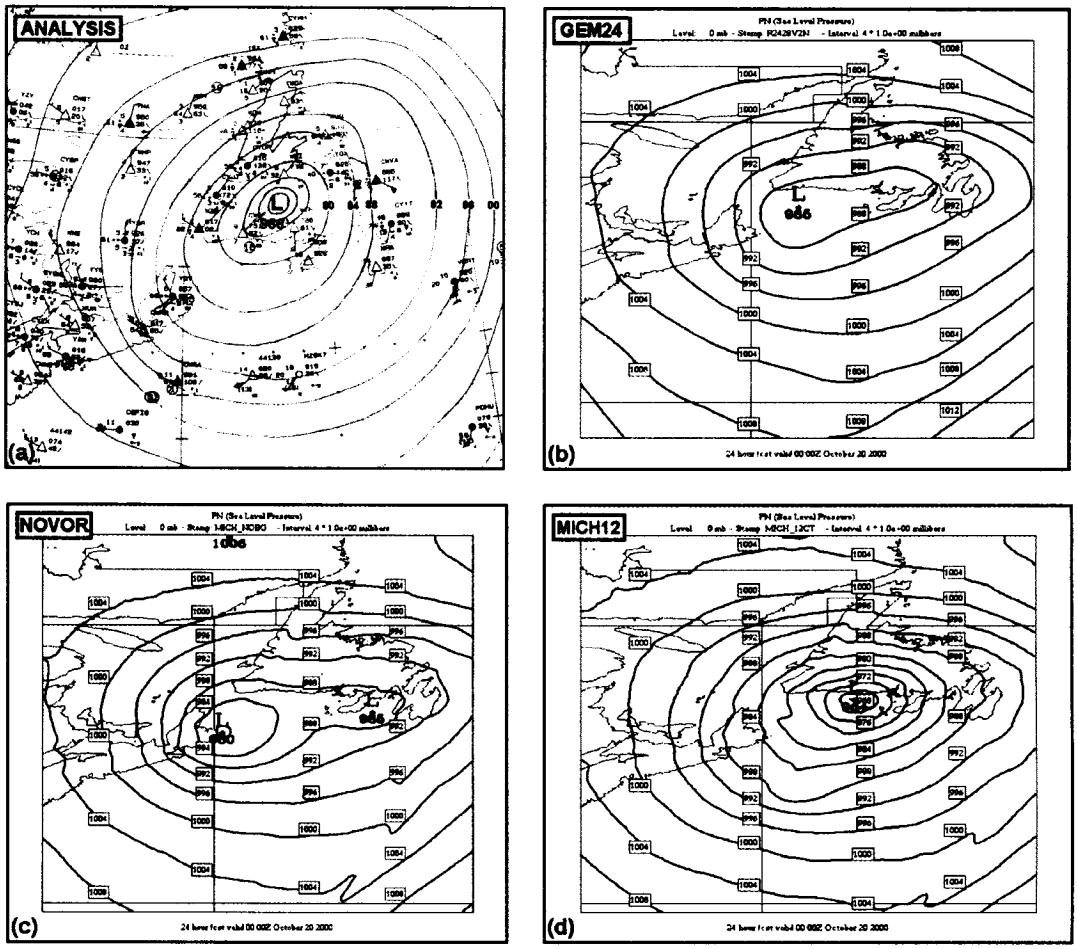

Figure 32. Comparison of sea level pressure between various model results and observations for Hurricane Michael near landfall. Shown is the sea level pressure (every 4 hPa) valid at 00 UTC 20 October based on (a) manually drawn (subjective) analysis, (b) 24-hour GEM regional forecast, (c) 24-hour "no-vortex" simulation of the 12 km MC2 model, and (d) 24-hour simulation of the control run of the MC2 model with vortex insertion employed (MICH12). Standard synoptic weather plots are shown in (a).

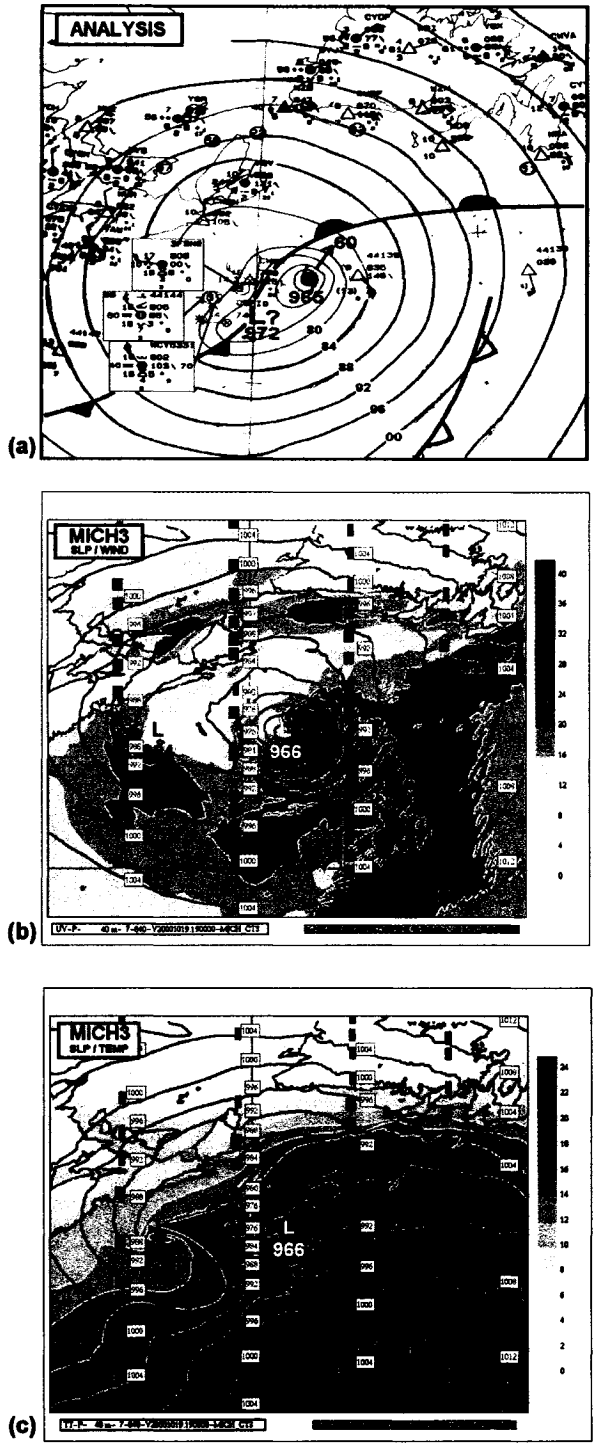

Figure 33. Comparison of sea level pressure, surface winds, and surface temperature between model and observations for Hurricane Michael in mid-transition. Manually drawn (subjective) sea level pressure analysis (every 4 hPa) valid at 18/19 (a) is compared with 3 km model control simulation (MICH3) (b) valid at 19/19 showing sea level pressure (solid grey contours) and surface (40 m) wind speed (shaded) every 4 m s^{-1} and model-simulated surface (40 m) temperatures (shaded every 2°C) (c) valid for the same time. The estimated position of the baroclinic cyclone in (a) is shown by "L?" and is also marked in (b) and (c).

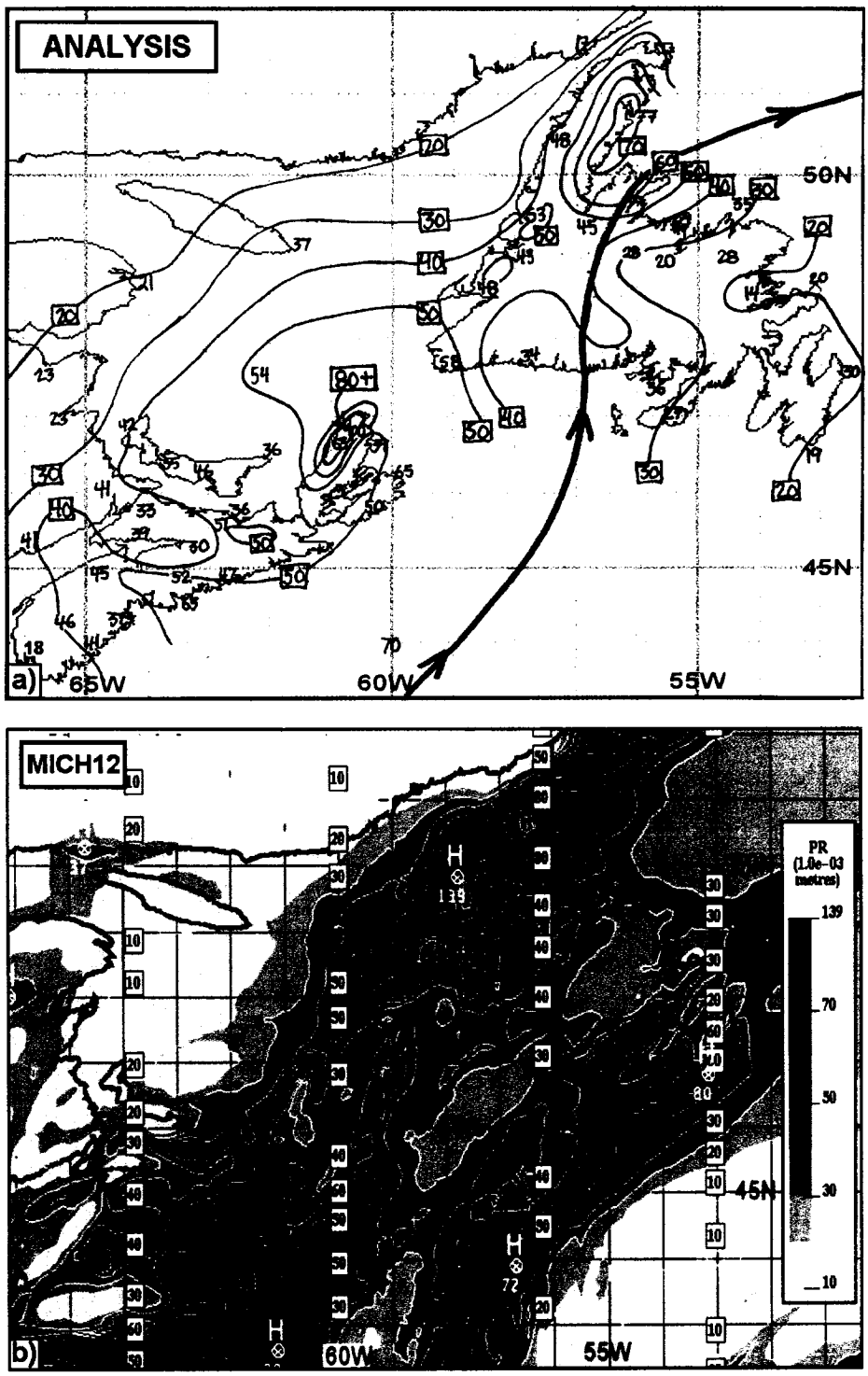

Figure 34. Observed and simulated rainfall during the extratropical transition of Hurricane Michael: (a) subjective analysis of storm total rainfall (contours drawn every 10 mm) and (b) storm total rainfall from the MICH12 control simulation (contours also drawn every 10 mm). Actual rainfall amounts at various stations are marked in (a) with contour labels contained in a small box. The actual storm track is shown by a bold line in (a). More data was used to construct the analysis than is shown in the figure.

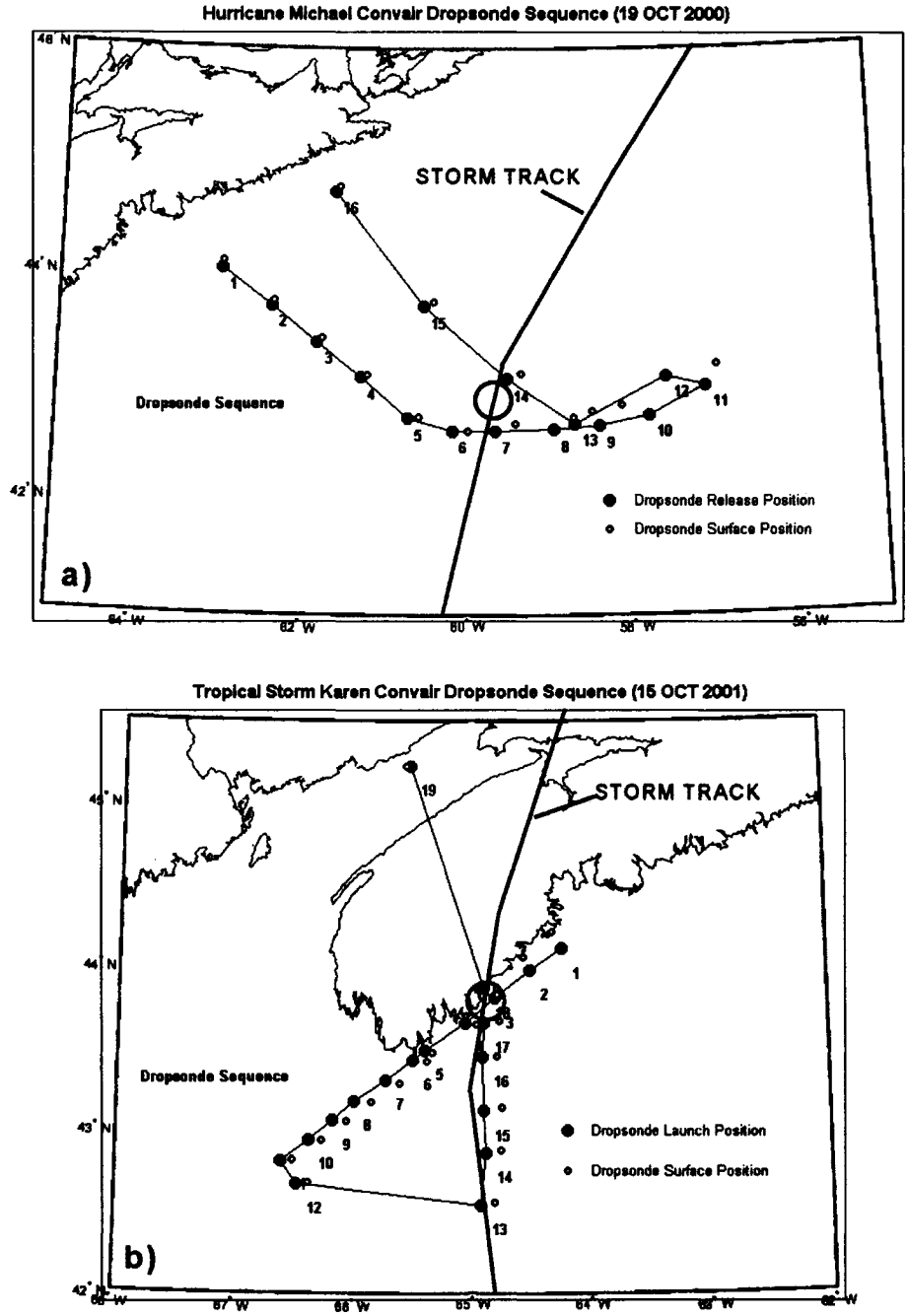

Figure 35. Sequence of dropsondes deployed from the Convair 580 aircraft during Hurricane Michael (a) and Tropical Storm Karen (b). The individual sondes are numbered to the lower right of their release position. The approximate storm position corresponding to the cross sections discussed in the text is indicated with a large open circle.

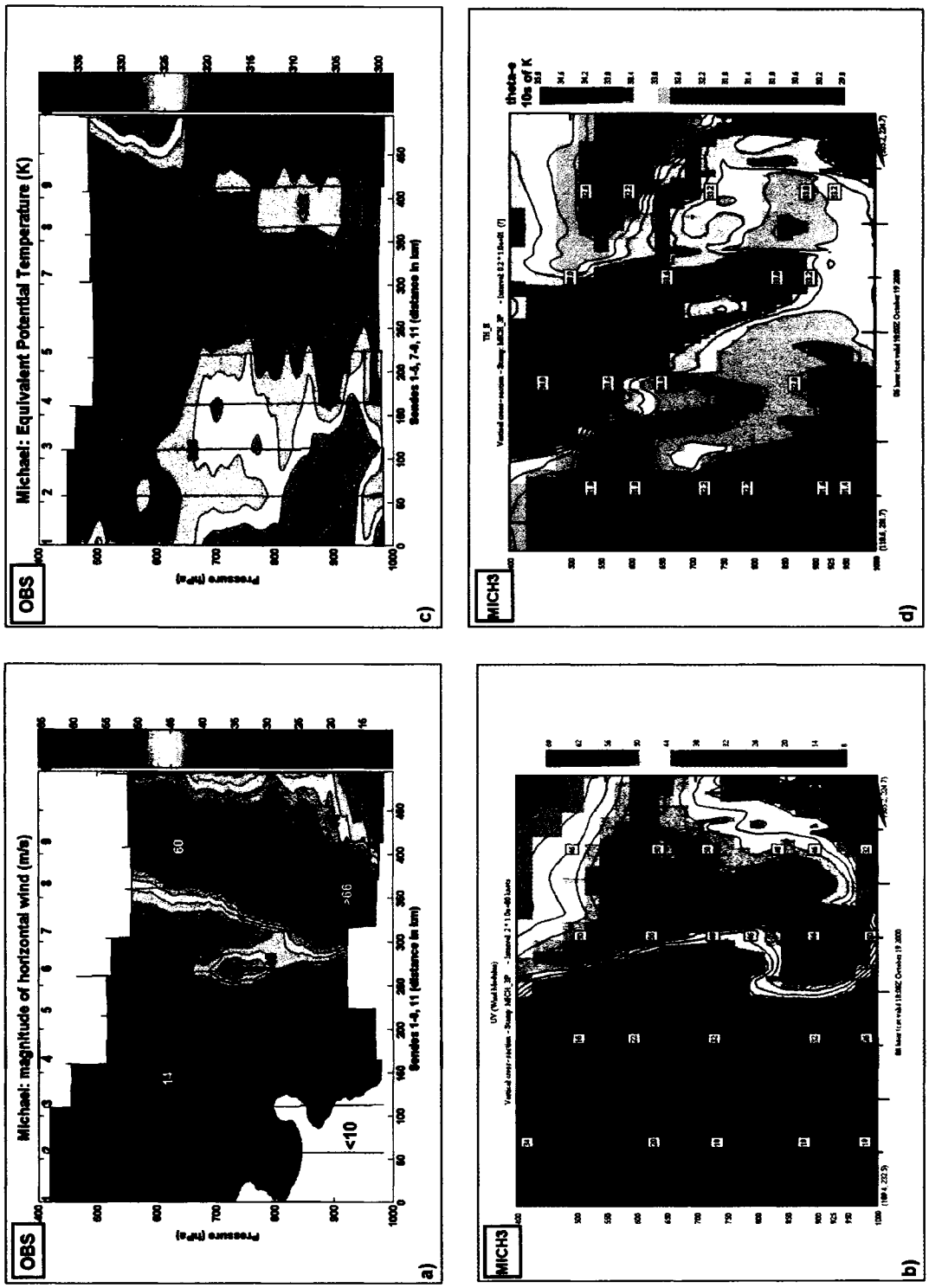

Figure 36. Observed and simulated vertical cross sections of wind speed and equivalent potential temperature through Hurricane Michael during mid transition. Panel (a) – horizontal wind speed magnitude from dropsonde data and (b) output of wind speed from the control run of the model (MICH3) every 2 m s^{-1} as a function of pressure and distance. The horizontal scale in (a) is the same as (b). Panel (c) – equivalent potential temperature from dropsonde data (every 2 K) and (d) output of equivalent potential temperature from the MICH3 control run in tens of Kelvin. The location of dropsondes in (a) and (c) are shown by vertical lines and are numbered.

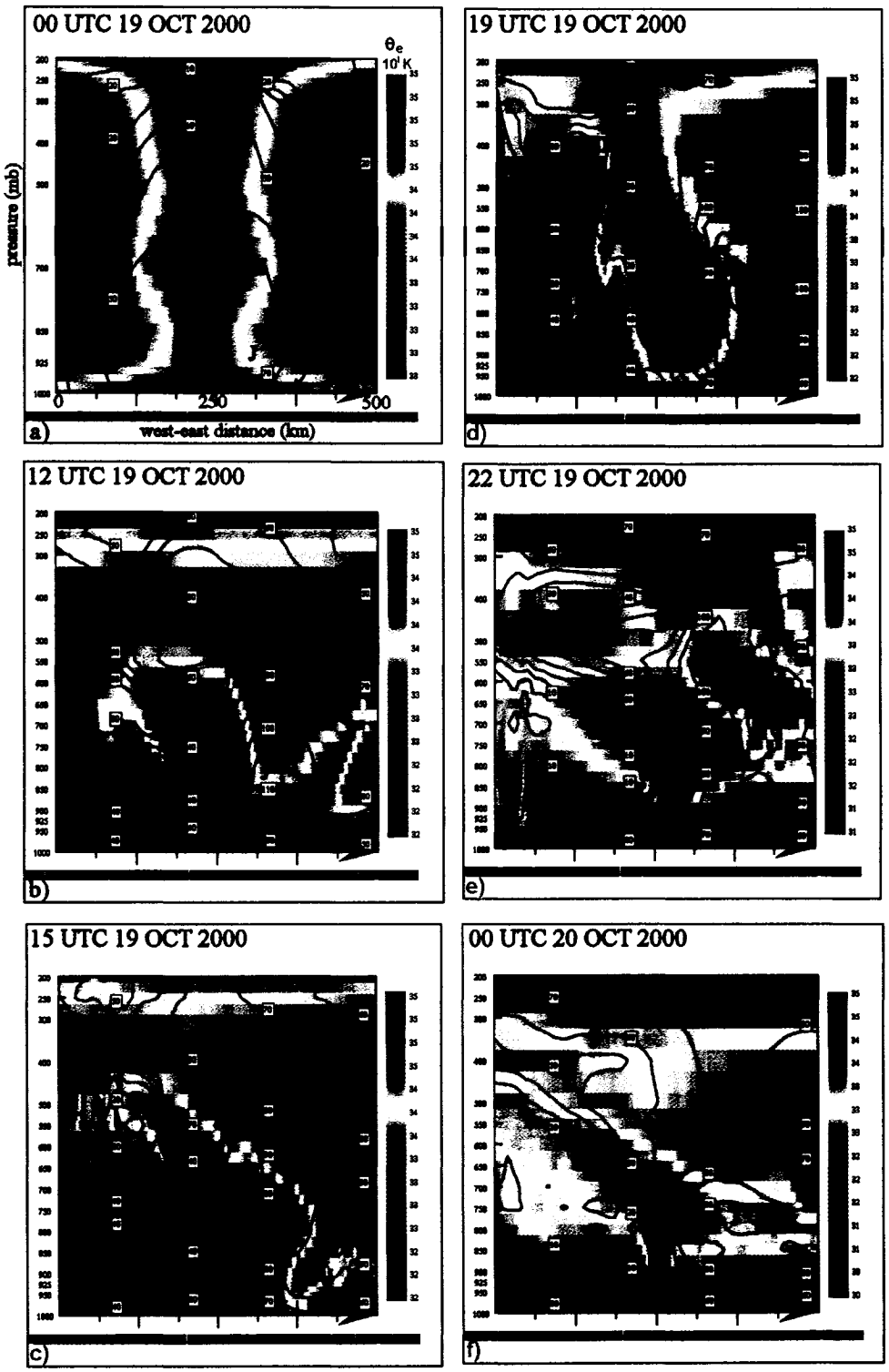

Figure 37. Time series of simulated vertical cross sections of equivalent potential temperature and wind speed for Hurricane Michael. Equivalent potential temperature is denoted by the colored field and horizontal wind speed magnitude is denoted by solid contours every 10 knots (1 knot = 0.515 m s^{-1}) from the 3 km control simulation (MICH3) at selected times during extratropical transition. The cross sections are taken along a west to east line through the storm center. Panel (a) shows the structure of the synthetic vortex at 00/19.

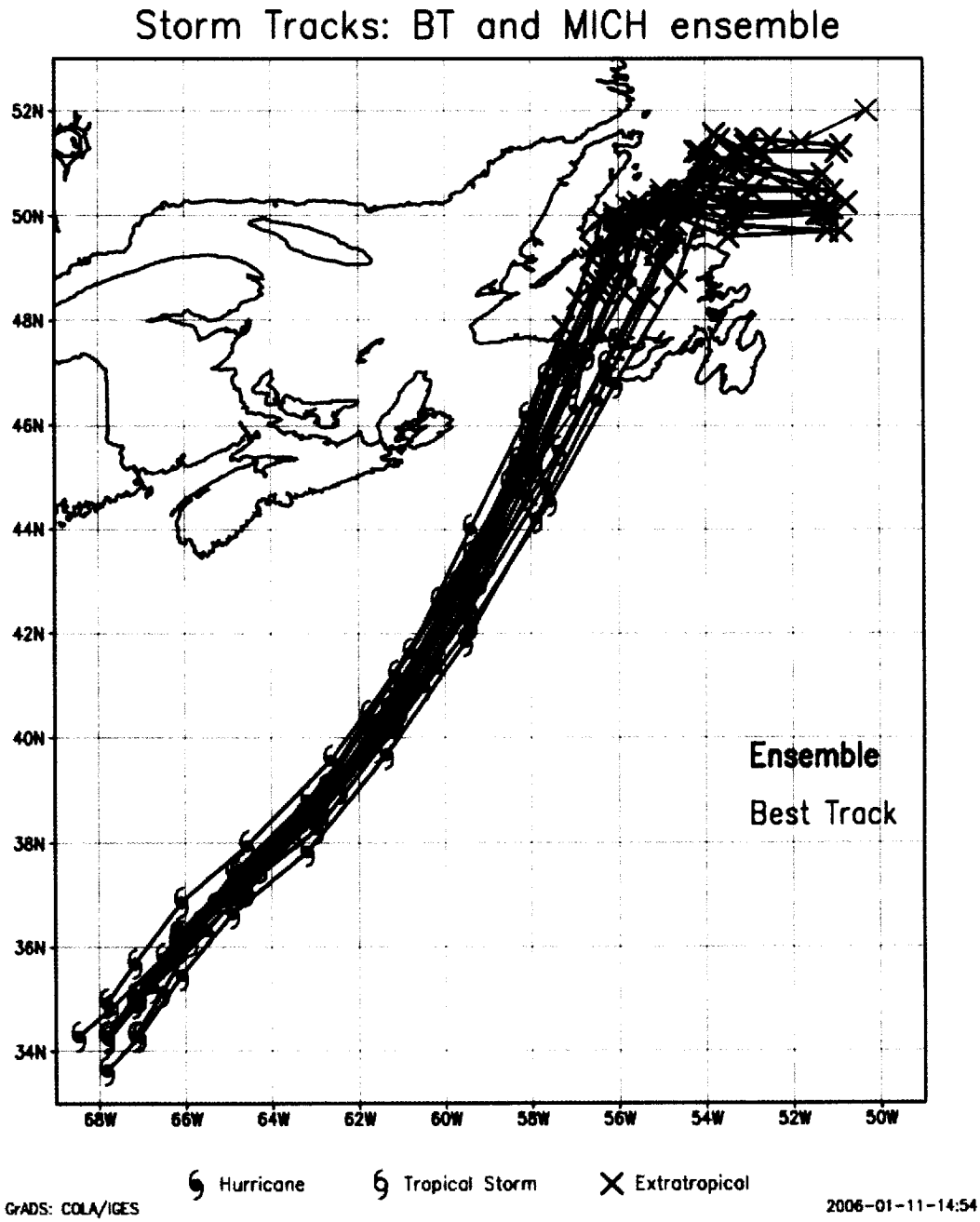

Figure 38. Ensemble of storm tracks from the Hurricane Michael simulations. Storm tracks for all ensemble members (including control) from the set of simulations in Table 3 (black), plus the best track (BT) (red) are shown. Track positions are every three hours for the 42-hour period from 00/19 to 18/20 October, 2000.

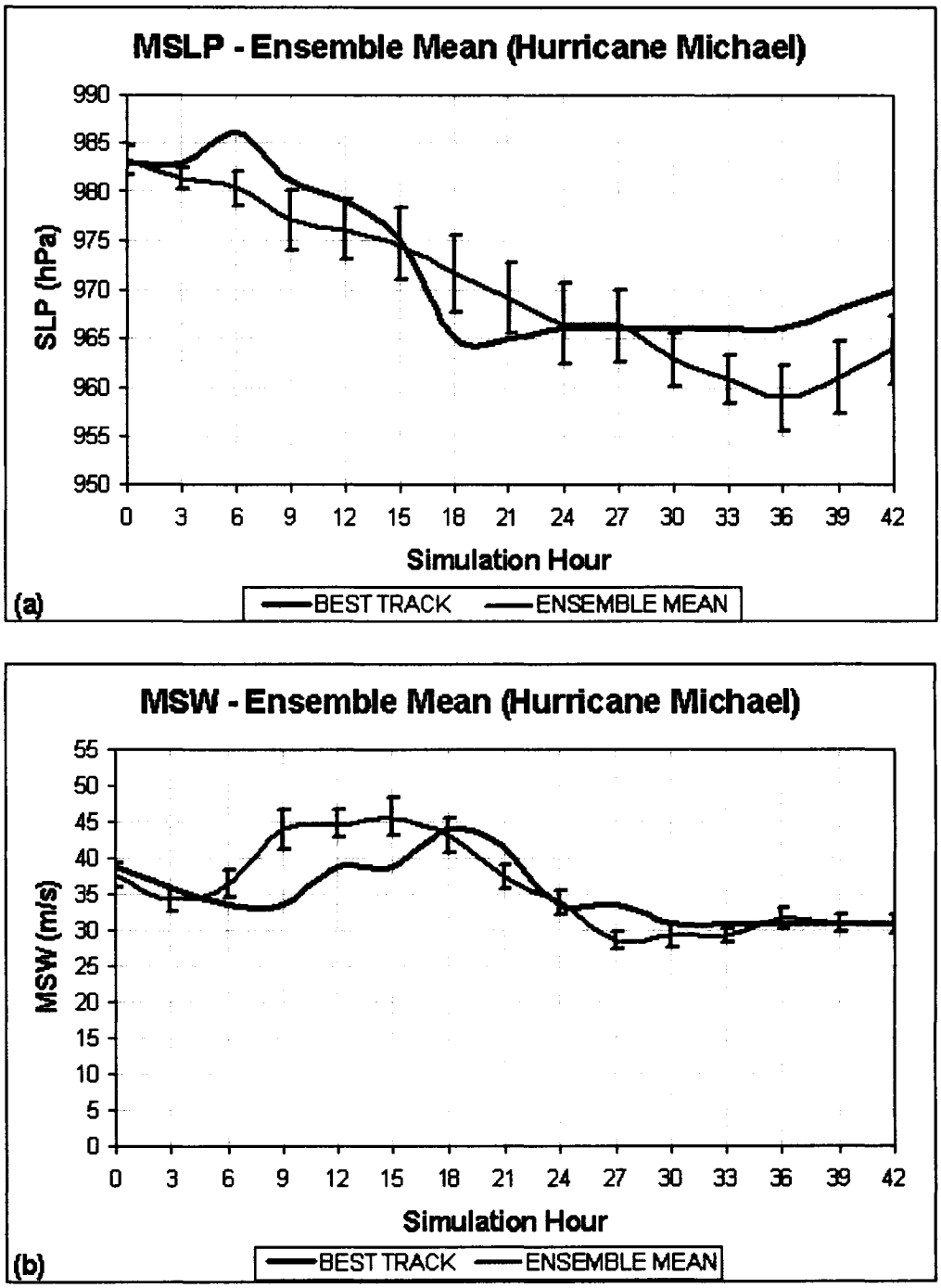

Figure 39. Time traces of ensemble means for Hurricane Michael. Minimum sea level pressure (a) and maximum surface wind traces (b) for the ensemble mean (thin curve) and the best track (thick curve) are indicated. Vertical range bars denote the one-standard deviation values from the ensemble.

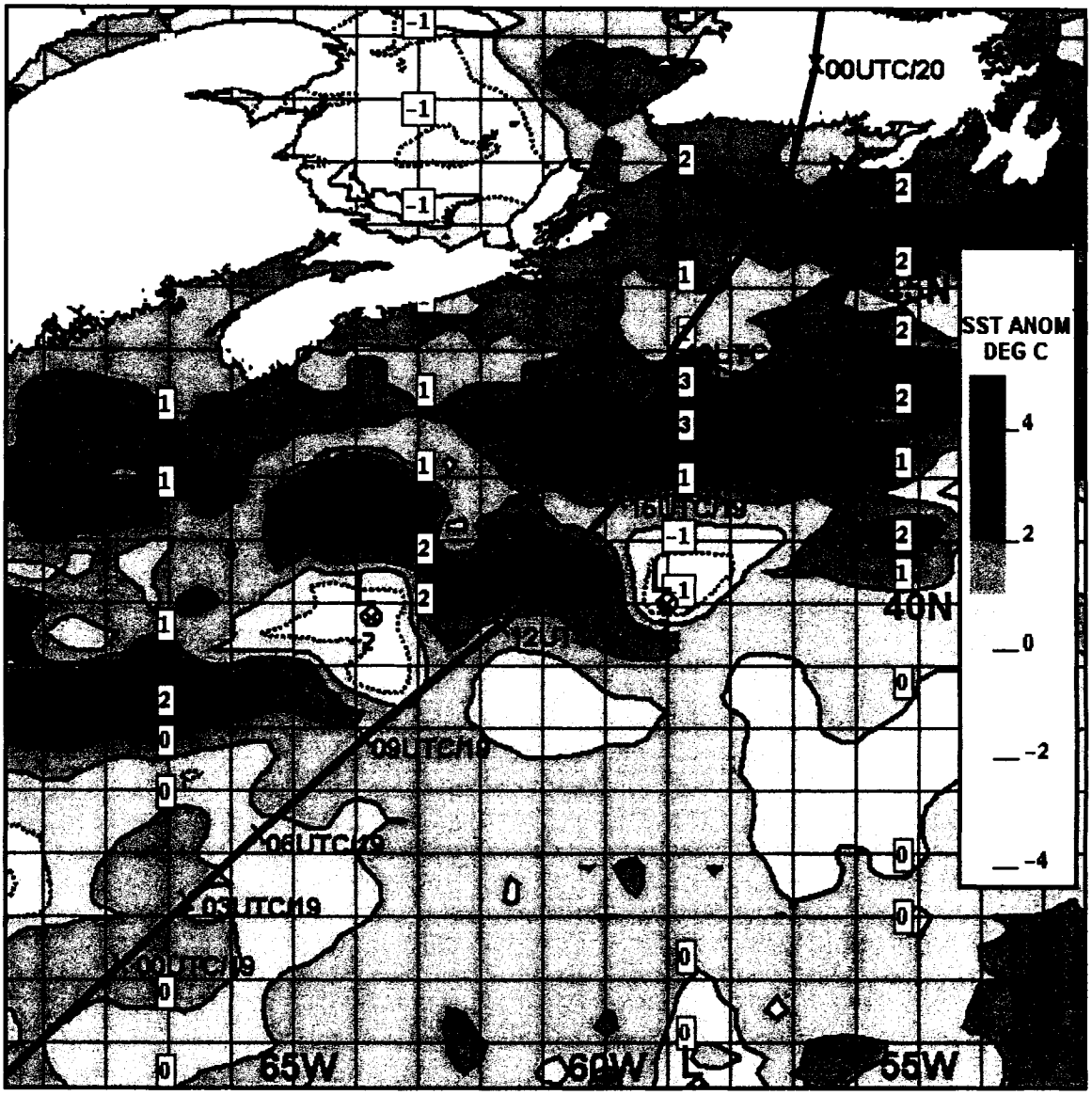

Figure 40. Sea surface temperature anomaly during the extratropical transition of Hurricane Michael. Sea surface temperature field (contours every 1°C) is valid at 00 UTC 19 October 2000. Negative anomaly is represented by dotted contours. Partial storm track for Hurricane Michael also shown.

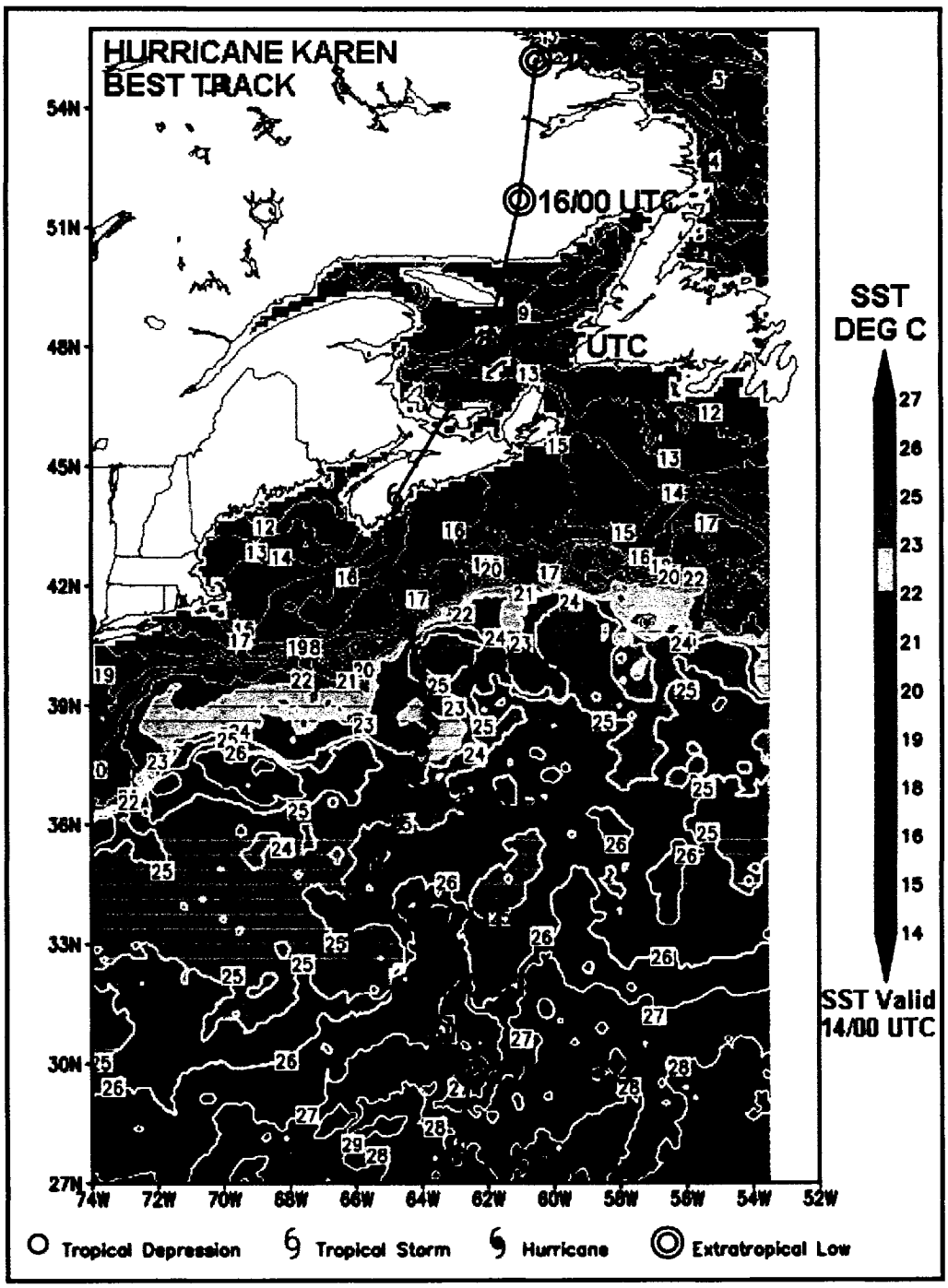

Figure 41. Best track for Hurricane Karen with sea surface temperatures. Sea surface temperatures (contours every 1°C) are valid at 00 UTC 14 October, 2001.

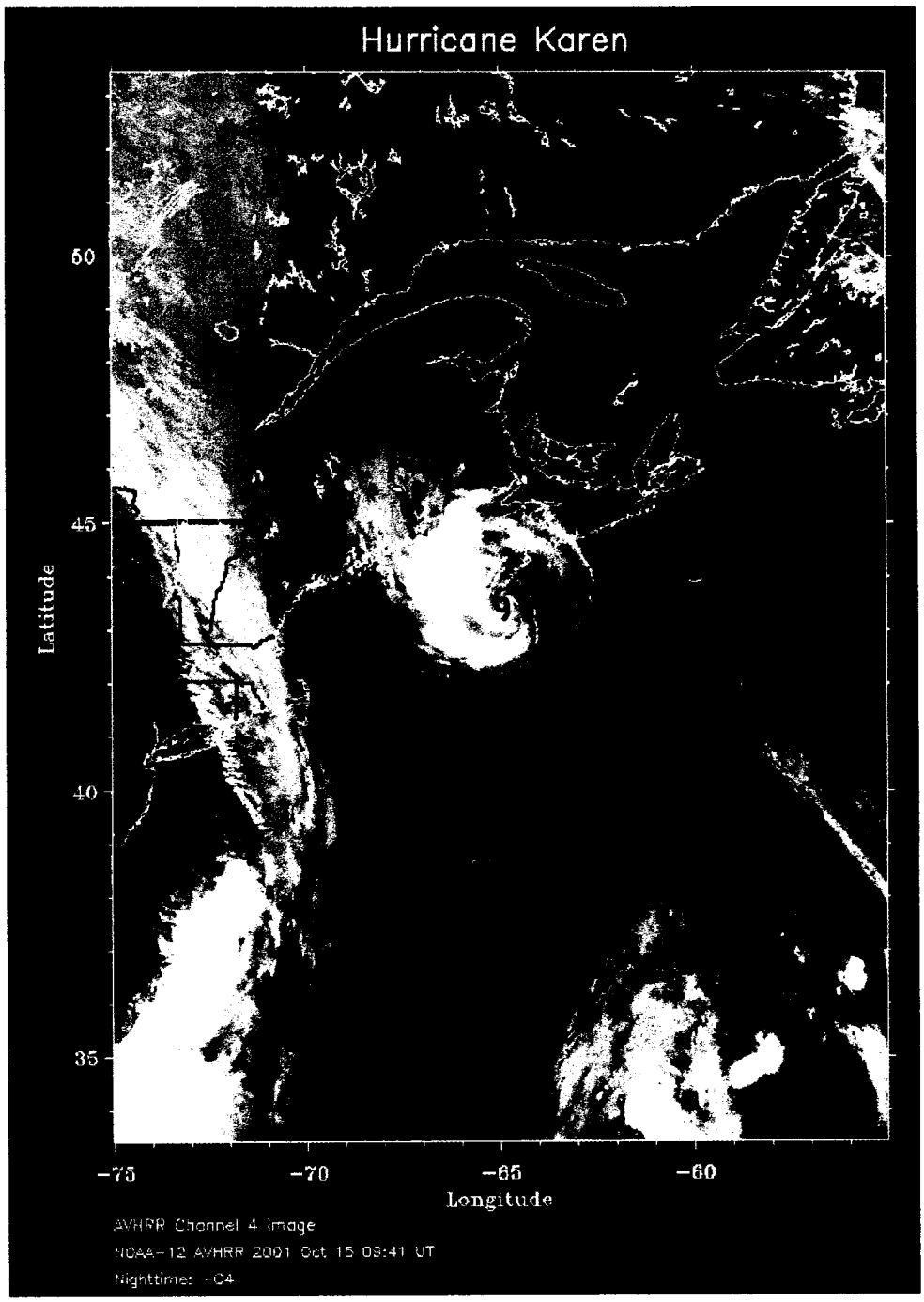

Figure 42. Infrared satellite image from the Advanced Very High Resolution Radiometer showing Tropical Storm Karen prior to landfall in Nova Scotia. Valid time of the image is 0941 UTC 15 October, 2001. The image is courtesy of the Johns Hopkins University Applied Physics Laboratory.

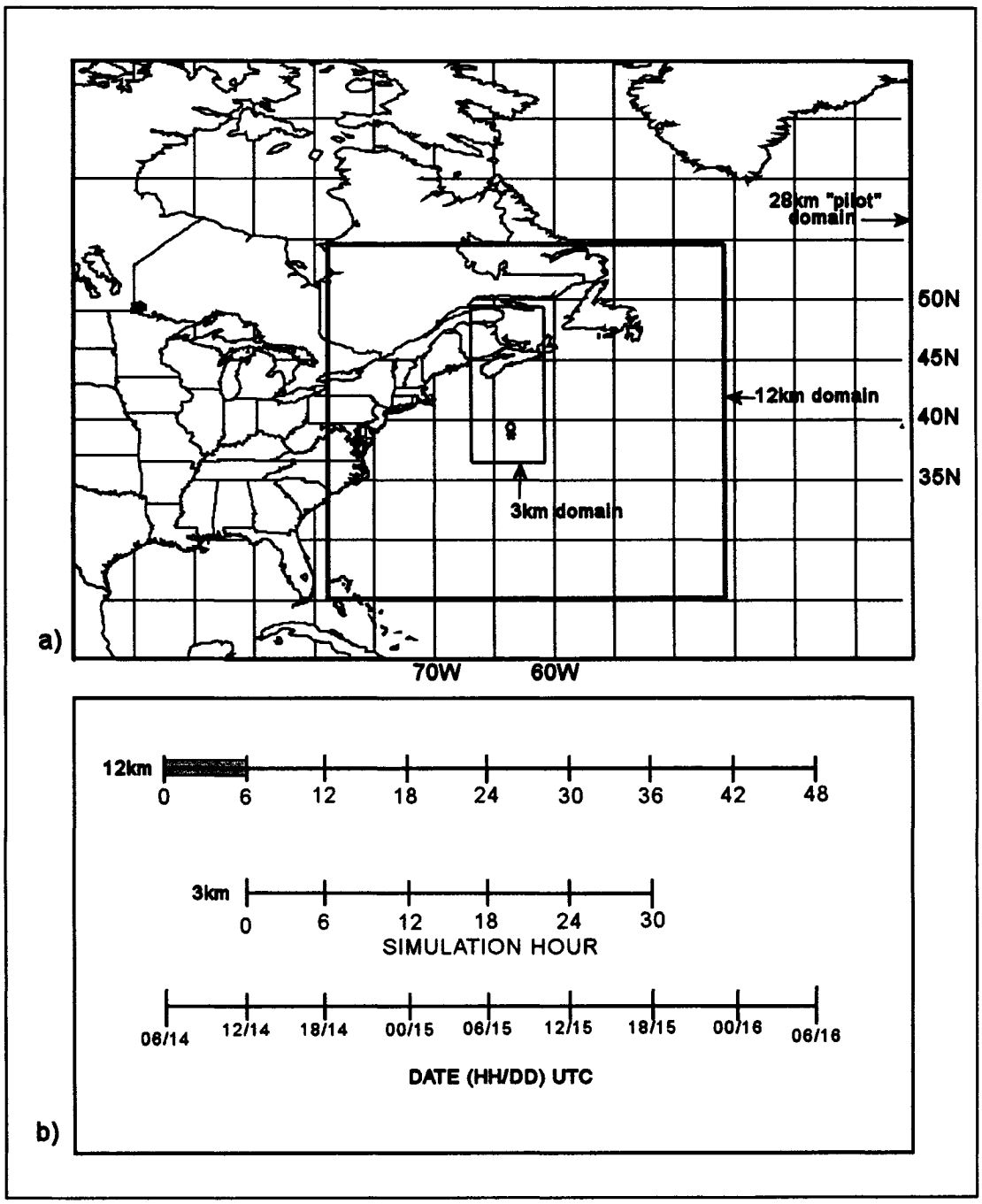

Figure 43. Layout for the model experiments for Hurricane Karen: (a) grid configuration and (b) timelines for the model integrations. The asterisk in (a) marks the storm center at time-zero of the 12 km control simulations and the open circle marks the mean position of the storm at time-zero of the 3 km control simulations. The grey region on the 12 km timeline in (b) denotes the 6-hour model adjustment period.

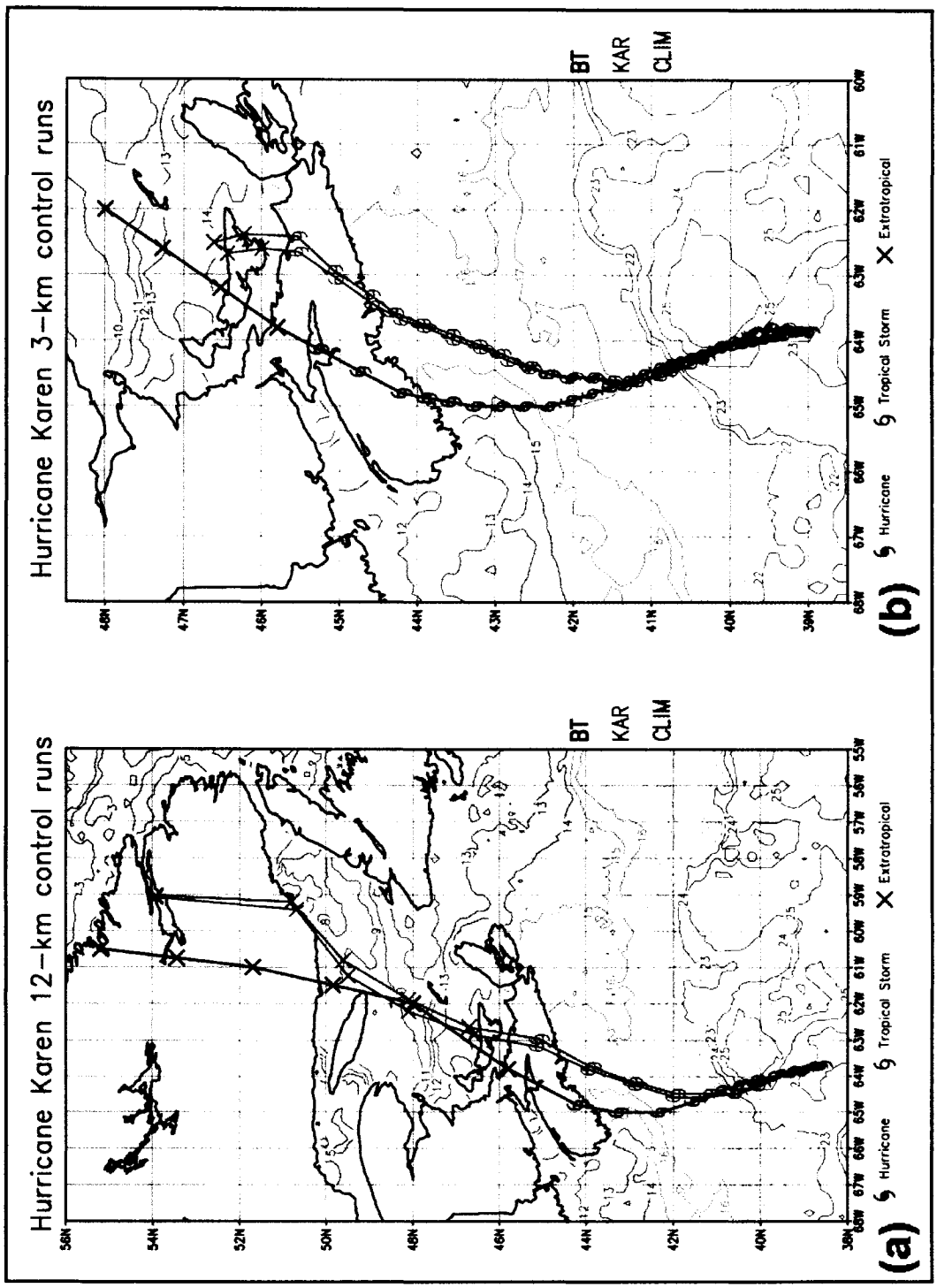

Figure 44. Simulated storm tracks for Hurricane Karen: (a) from the 12 km control runs of the model, and (b) the 3 km control runs. Black curve denotes the best track (BT), red is the observed-SST control run (KAR) and green is the climatology-SST run (CLIM). Track nodes are every three hours in (a) from 06/14 to 06/16 and every hour in (b) from 12/14 to 18/15. Observed (CLASS) SST (every 1°C) is also shown.

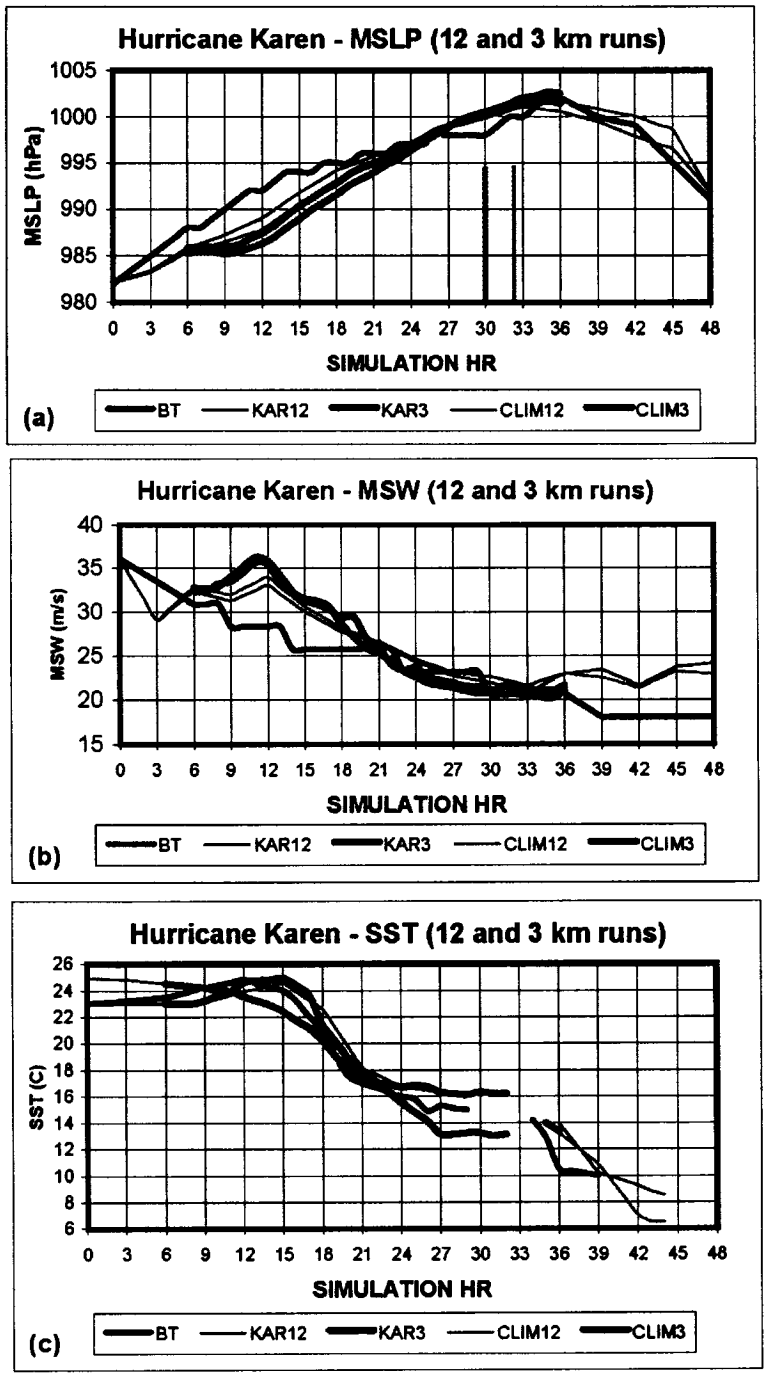

Figure 45. Time traces from the Hurricane Karen control simulations. Model results are for the 12 km control (KAR12 and CLIM12) and 3 km control (KAR3 and CLIM3) simulations: (a) evolution of minimum sea level pressure (MSLP) for KAR12 (thin red curve), CLIM12 (thin green curve), KAR3 (thick red curve), CLIM3 (thick green curve) and the best track (black curve); (b) maximum surface winds (MSW); and (c) sea surface temperature (SST) beneath the storm center (defined by the location of the MSLP) as a function of model simulation time (hours). The vertical bars in (a) denote the approximate model landfall time (blue) and observed landfall time (black).

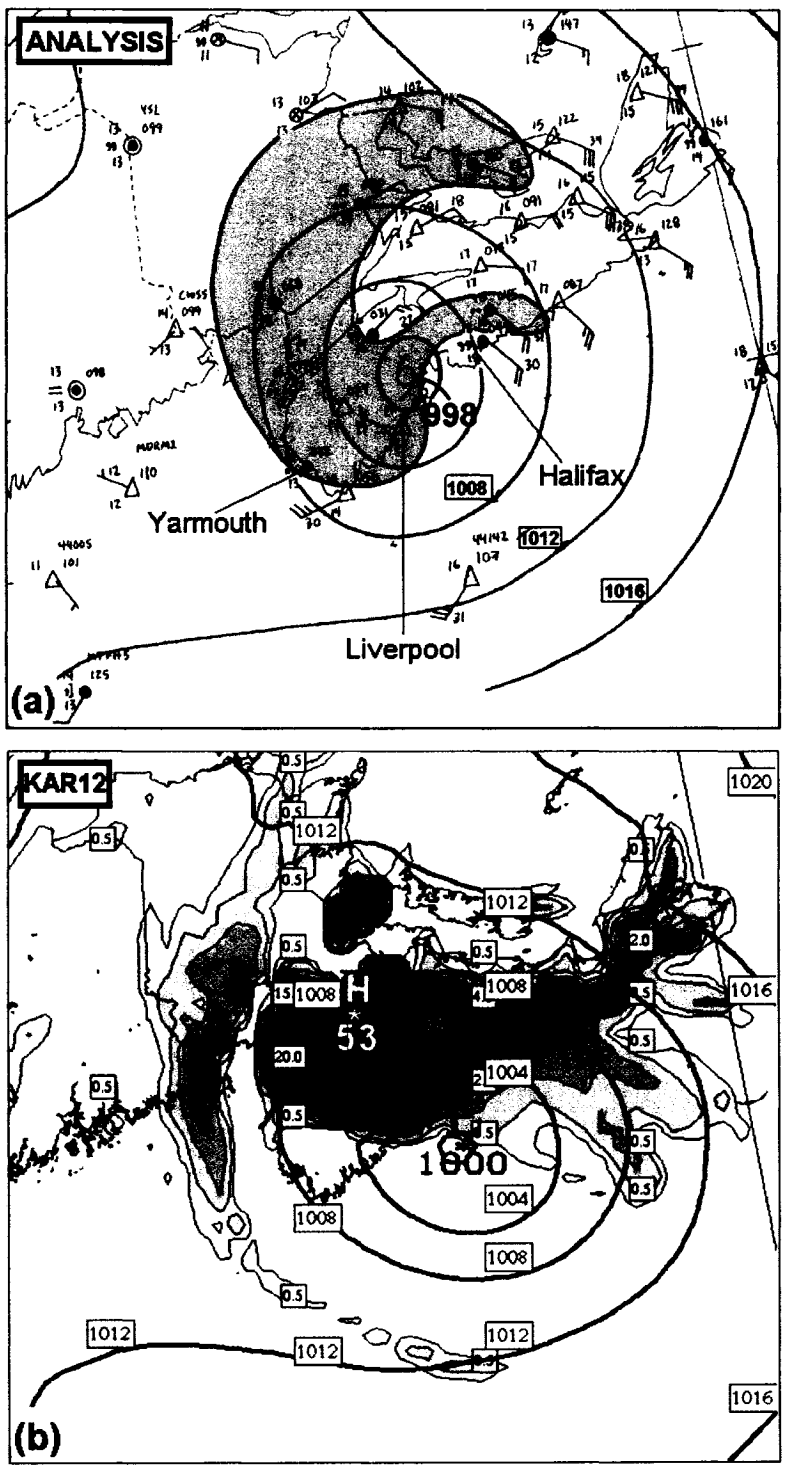

Figure 46. Comparison between observed and simulated sea level pressure and rain rate distribution for Tropical Storm Karen. Shown are the observed (a) and simulated (b) sea level pressure (solid contours every 4 hPa) with area of precipitation outlined in grey in (a) and simulated rainfall rate (10^{-4} mm s^{-1}) in (b). Valid time for both frames is 12/15 October. Conventional synoptic weather plots are shown in (a). The rainfall maximum of 53×10^{-4} mm s^{-1} is equal to 19 mm hr^{-1}.

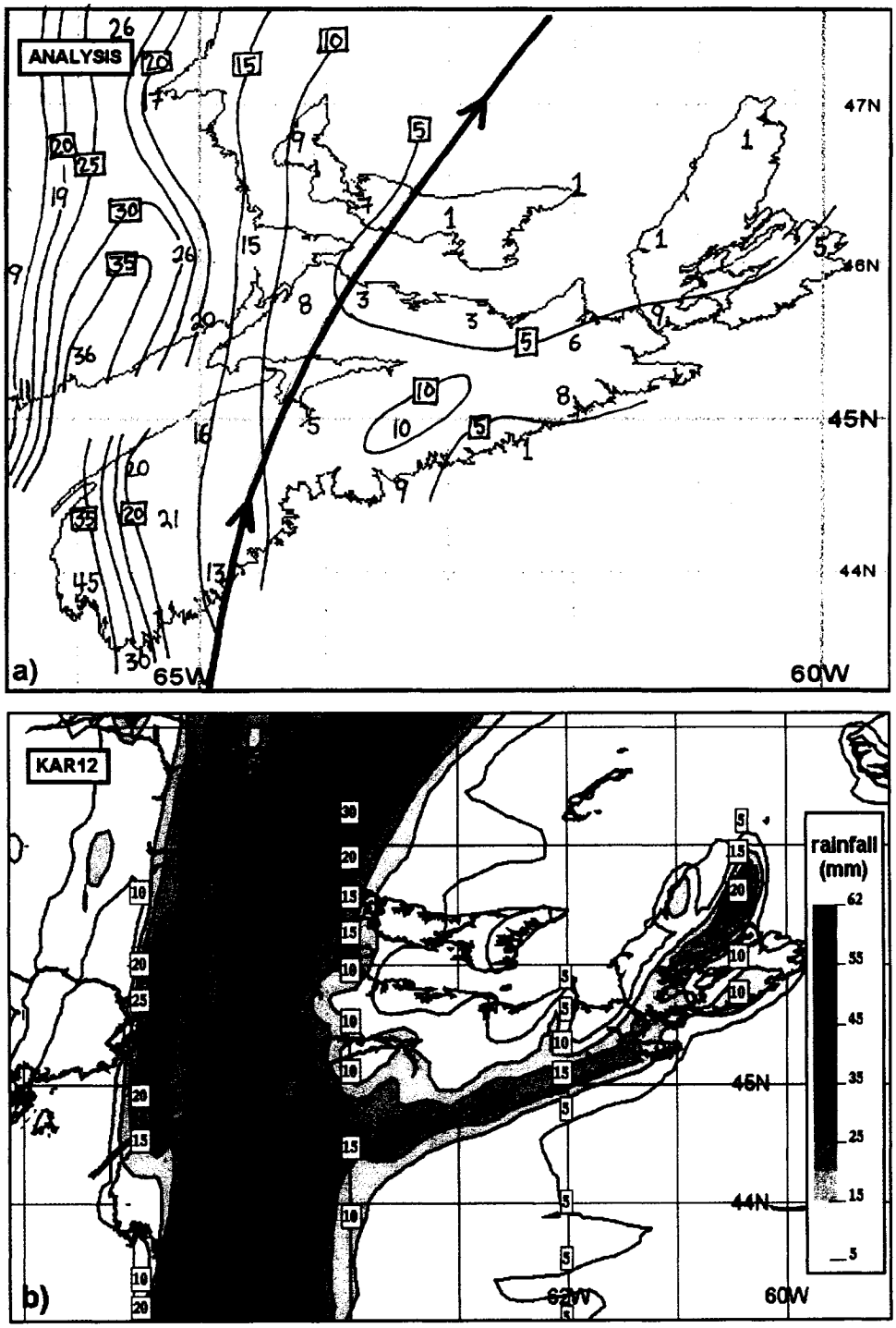

Figure 47. Observed and simulated rainfall during the extratropical transition of Tropical Storm Karen: (a) subjective analysis of storm total rainfall (contours drawn every 5 mm) and (b) storm total rainfall from the KAR12 control simulation (contours also drawn every 5 mm). Measured rainfall amounts at various stations are marked in (a) with contour labels contained in a small box. The actual storm track is shown by a bold line in (a).

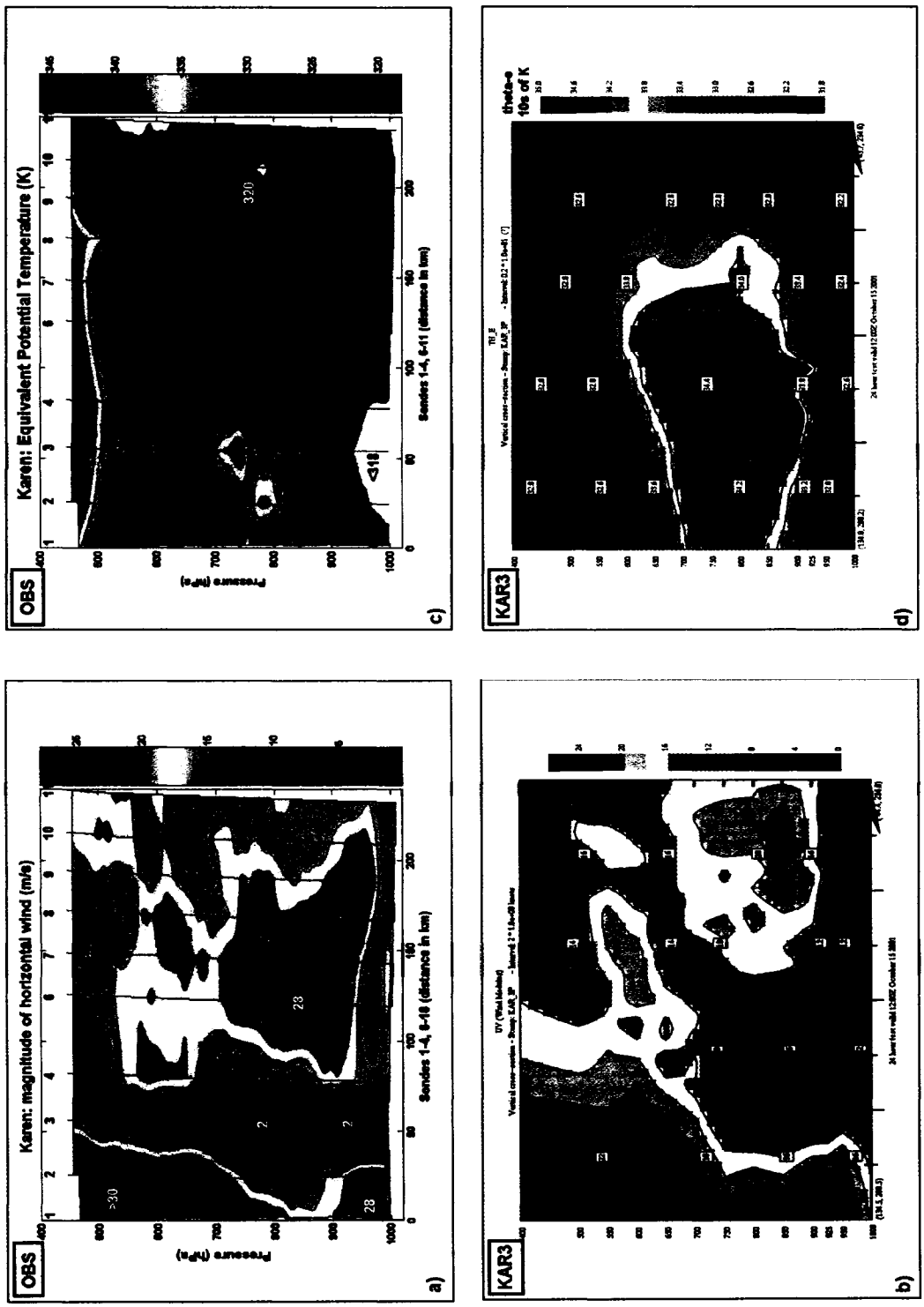

Figure 48. Observed and simulated vertical cross sections of wind speed and equivalent potential temperature through Tropical Storm Karen prior to landfall. Panel (a) – horizontal wind speed magnitude from dropsonde data and (b) output of wind speed from the control run of the model (KAR3) every 2 m s^{-1} as a function of pressure and distance. The horizontal scale in (a) is the same as (b). Panel (c) – equivalent potential temperature from dropsonde data (every 2 K) and (d) output of equivalent potential temperature from the KAR3 control run in tens of Kelvin. The location of dropsondes in (a) and (c) are shown by vertical lines and are numbered.

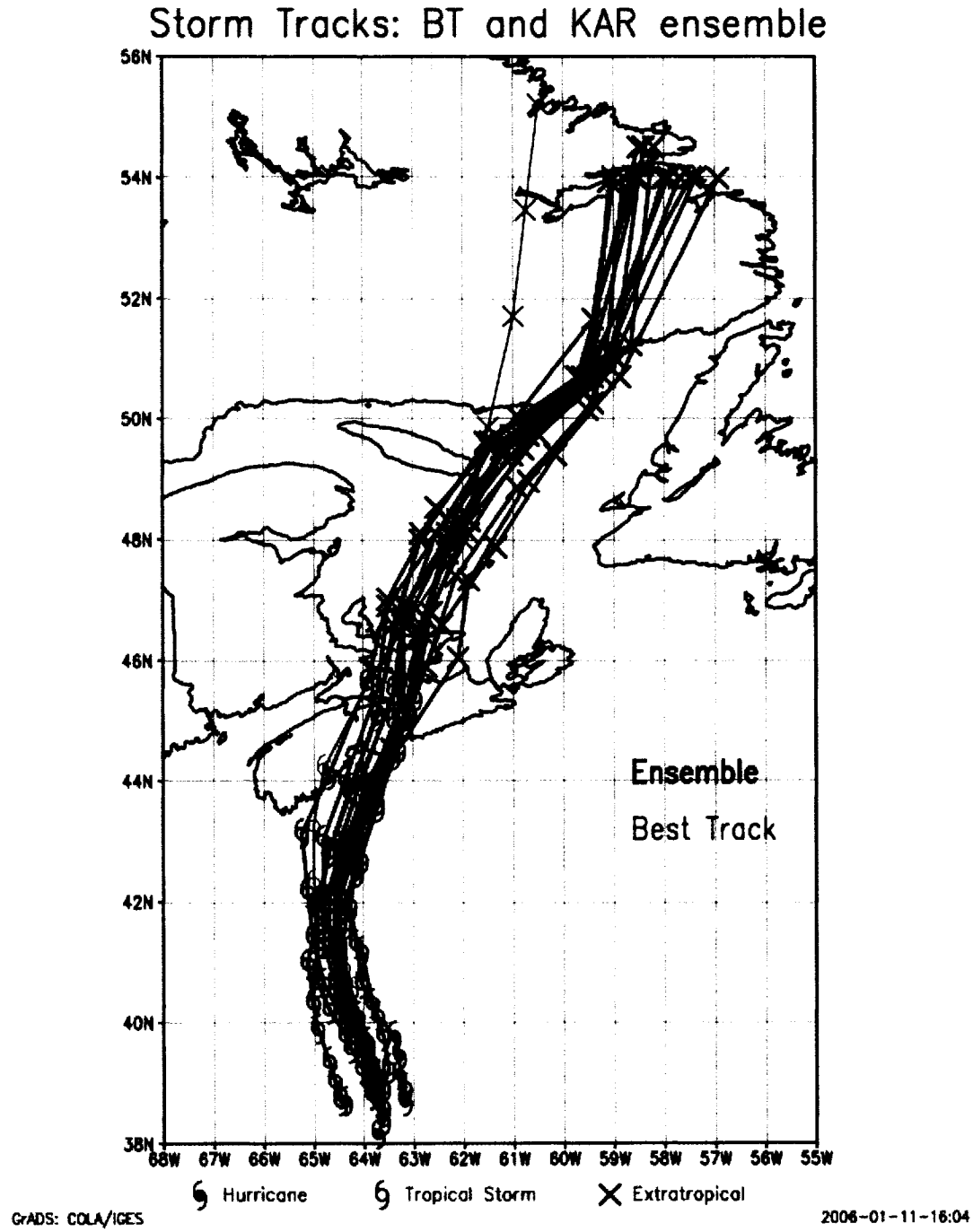

Figure 49. Ensemble of storm tracks from the Hurricane Karen simulations. Storm tracks for all ensemble members (including control) from the set of simulations in Table 4 (black), plus the best track (BT) (red) are indicated. Track positions are every three hours for the 48-hour period from 06/14 to 06/16 October, 2001.

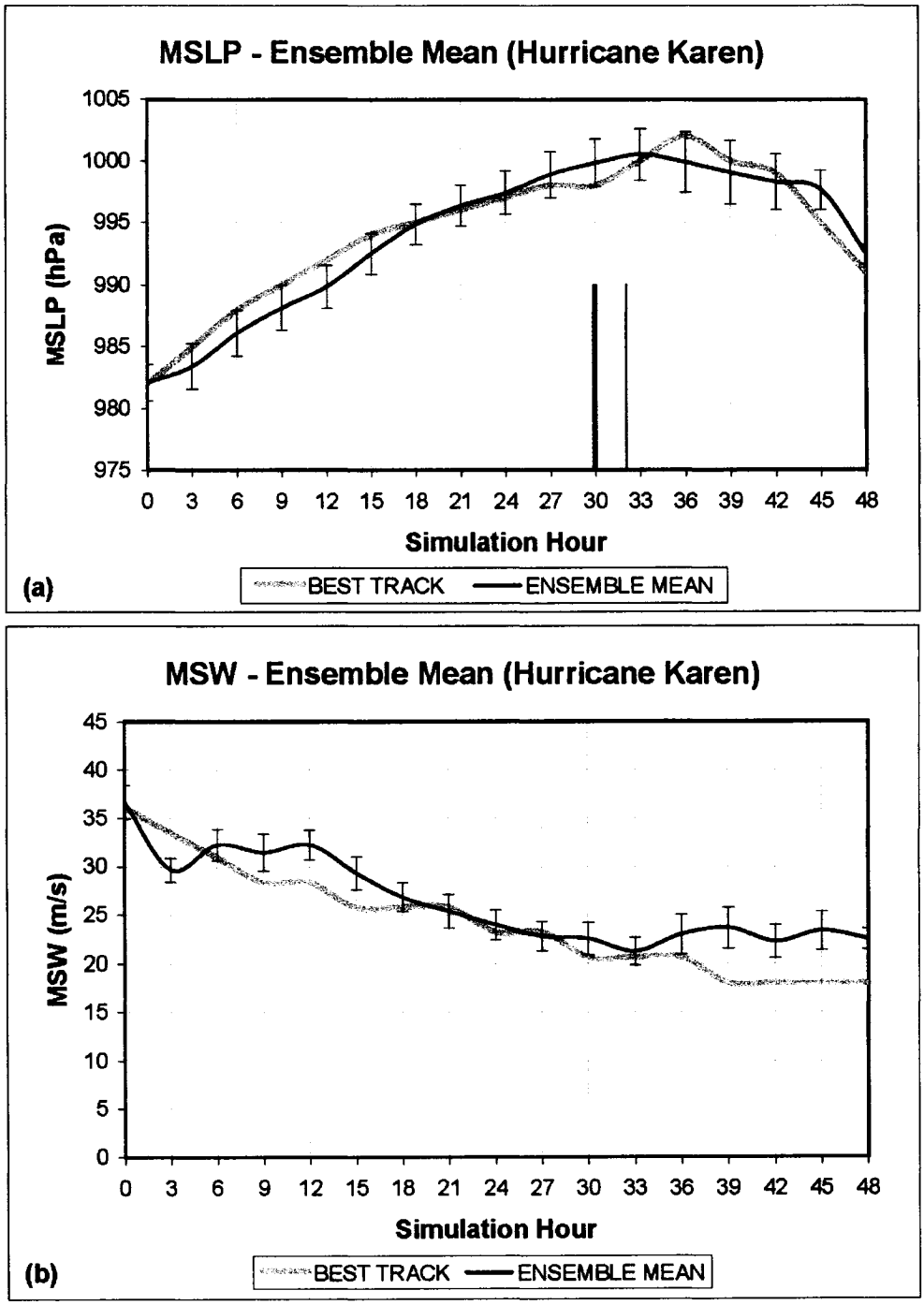

Figure 50. Time traces of ensemble means for Hurricane Karen. Minimum sea level pressure (a) and maximum surface wind traces (b) for the ensemble mean (black curve) and the best track (grey curve) are indicated. Vertical range bars denote the one-standard deviation values from the ensemble mean. The vertical bars in (a) denote the ensemble mean of landfall time (thin) and observed landfall time (thick).

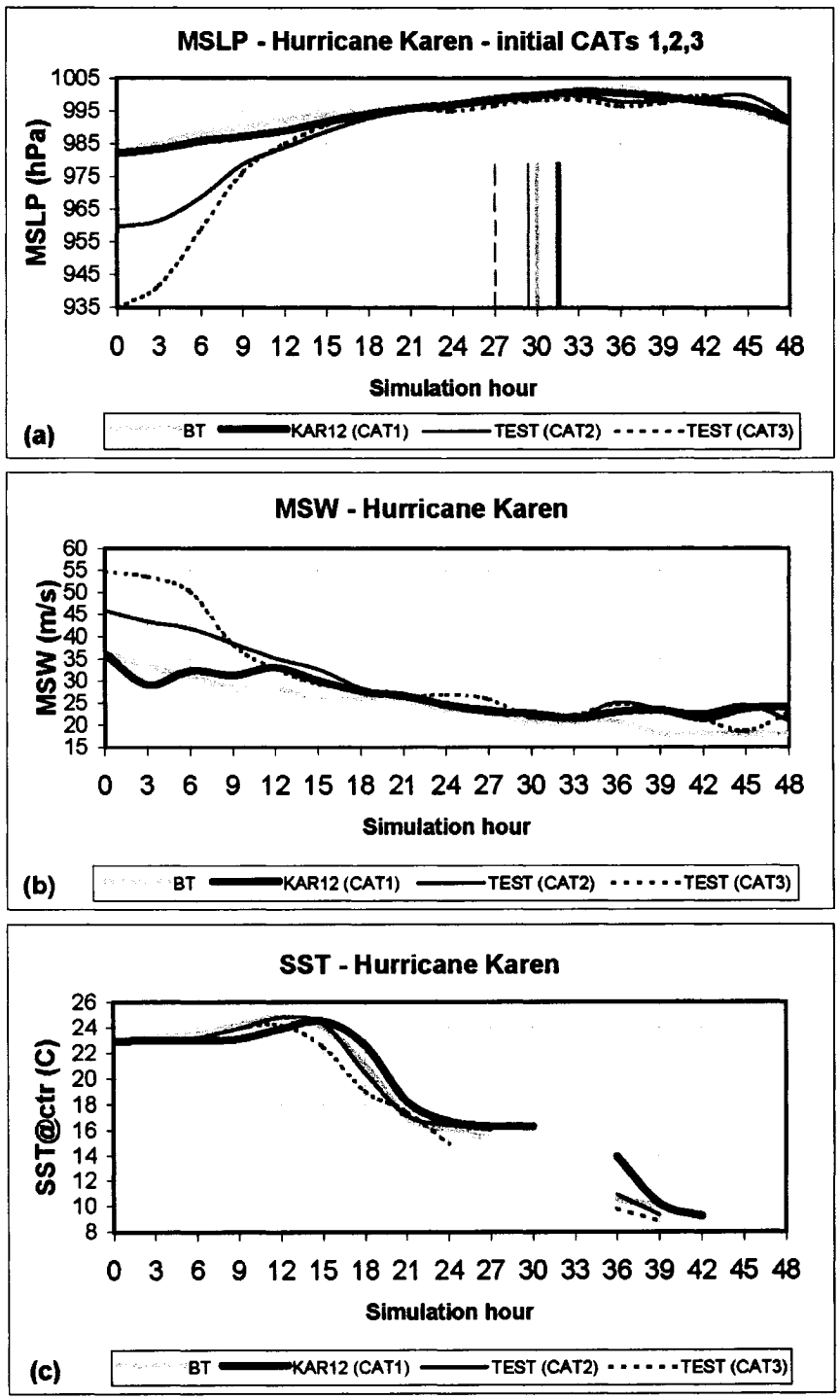

Figure 51. Modeling results for the initial intensity experiments for Hurricane Karen. Model results for the category-one control (KAR12), category-two test (CAT2), and category-three test (CAT3) simulations are shown: (a) evolution of minimum sea level pressure (MSLP) for KAR12 (thick black curve), CAT2 (thin black curve), CAT3 (thin dashed curve), and the best track (thick grey curve); (b) maximum surface winds (MSW); and (c) sea surface temperature (SST) beneath the storm center (defined by the location of the MSLP) as a function of model simulation time (hours). The vertical bars in (a) denote the approximate model landfall times (same line style as curves) and observed landfall time (grey).

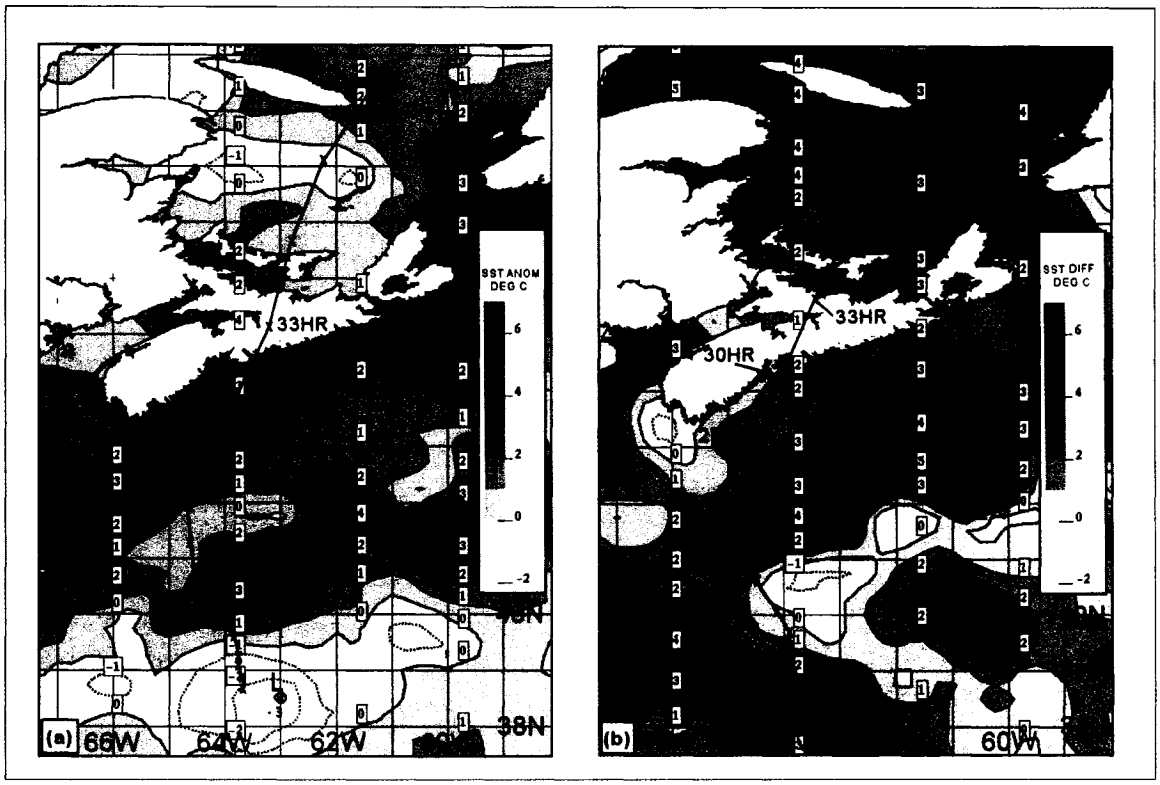

Figure 52. Sea surface temperature (SST) anomaly and difference fields for the Hurricane Karen SST sensitivity experiments. Shown is the sea surface temperature anomaly (against climatology) (a) valid at 00/14 October, and difference between SSTs during Hurricane Juan (28 September 2003) and Hurricane Karen (SST_{juan}-SST_{karen}) (b) every 1°C with values greater than 0°shaded. The KAR12 track is shown in (a) and the control track for the Juan-SST ensemble is shown in (b), with storm positions marked every 3 hours.

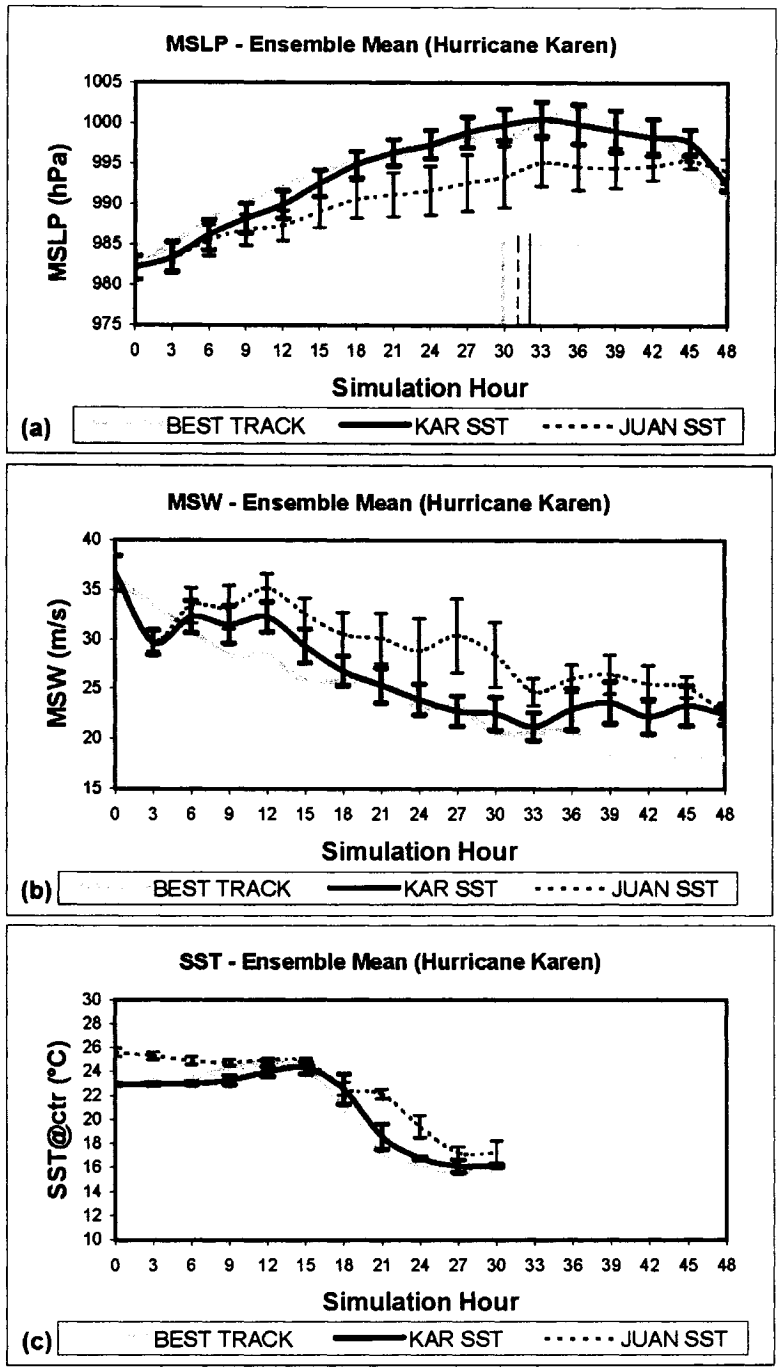

Figure 53. Model results for the SST sensitivity experiments for Hurricane Karen. Shown is the minimum sea level pressure (a), maximum surface wind (b), and storm-centered sea surface temperature (c), for the ensemble means of runs with SSTs from 14 October 2001 (KAR SST) (solid black curves) and with SSTs from 28 September 2003 (JUAN SST) (dashed black curves). The best track data are indicated by the grey curve. Vertical range bars denote the one-standard deviation values from the ensemble mean. The vertical bars in (a) denote the mean landfall time for the KAR SST ensemble (thin solid), JUAN SST ensemble (thin dashed), and observed landfall time (thick grey).

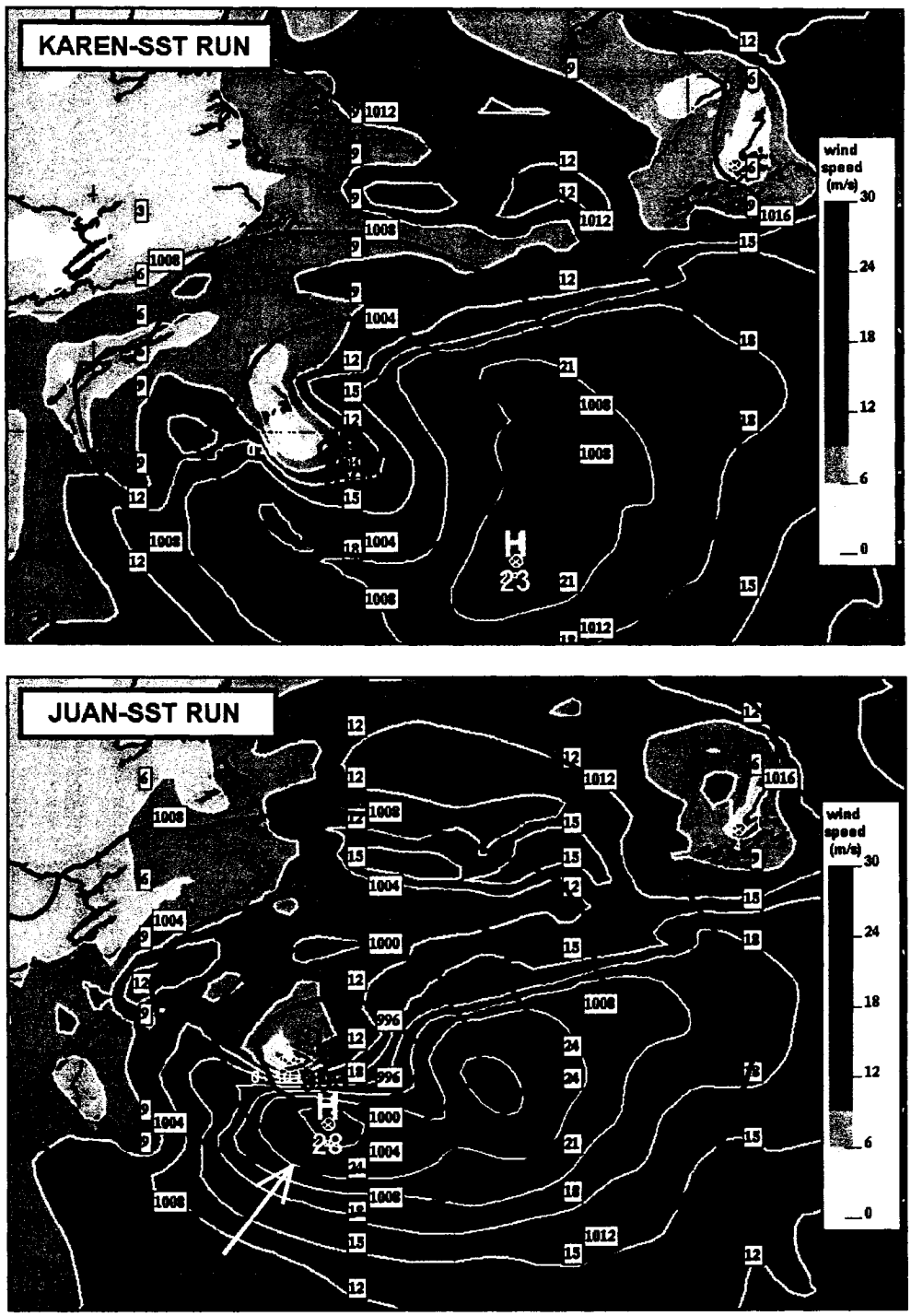

Figure 54. Sea level pressure and surface wind speeds for the SST sensitivity experiments for Hurricane Karen. Sea level pressure (thick black contours every 4 hPa) and surface wind speed (shaded field with white contours every 3 m s^{-1}) from (a) the Karen-SST and (b) the Juan-SST control simulations prior to landfall are displayed. The location of a low-level jet described in the text is indicated in (b).

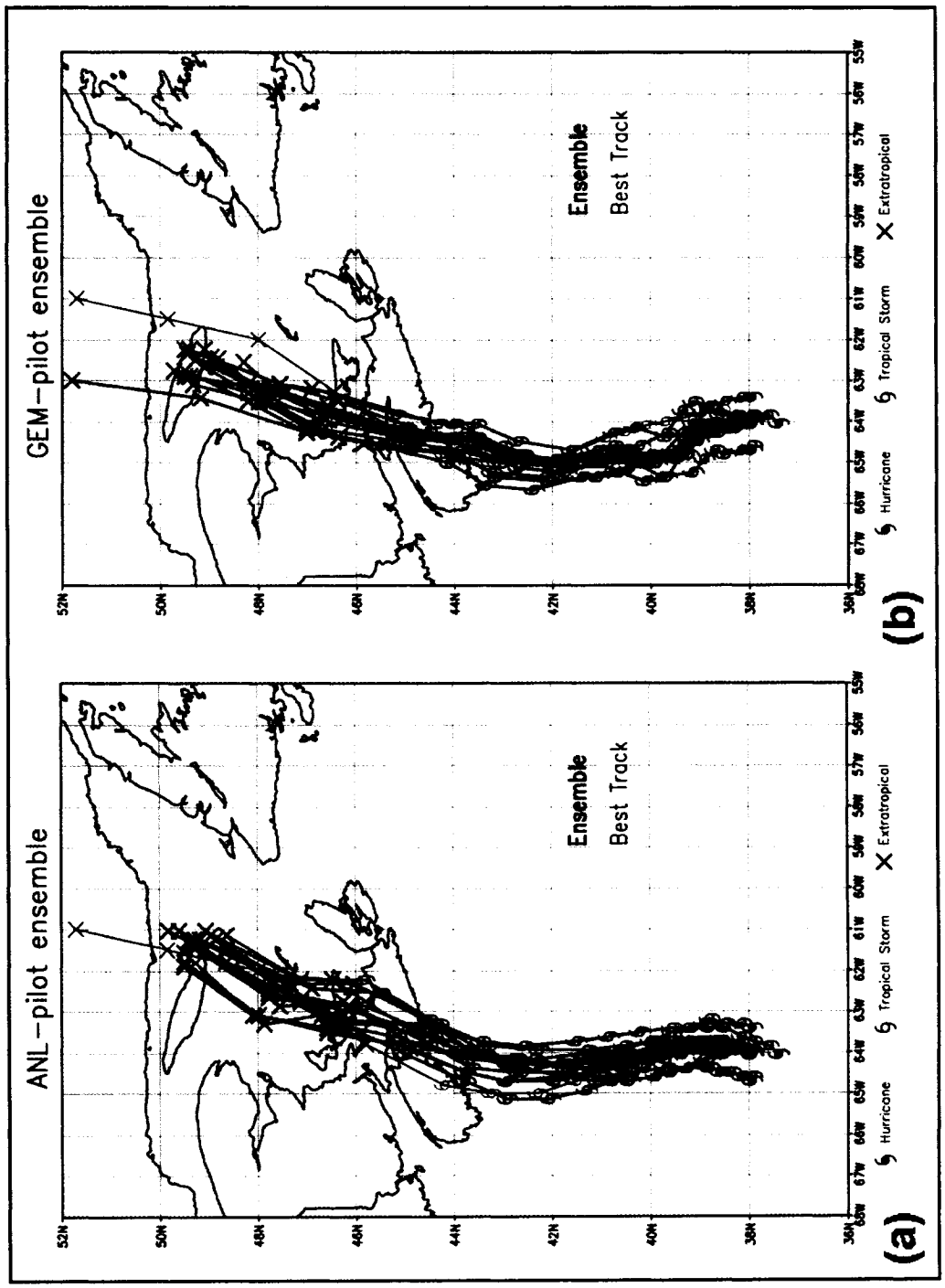

Figure 55. Simulated storm tracks from the boundary condition experiments for Hurricane Karen. Shown are the storm tracks for all members (including control) from the analyses-piloted Hurricane Karen ensemble (a), and the GEM-piloted ensemble (b), including the best track (red). Track positions are every three hours for the 48-hour period from 00/14 to 00/16 October, 2001.

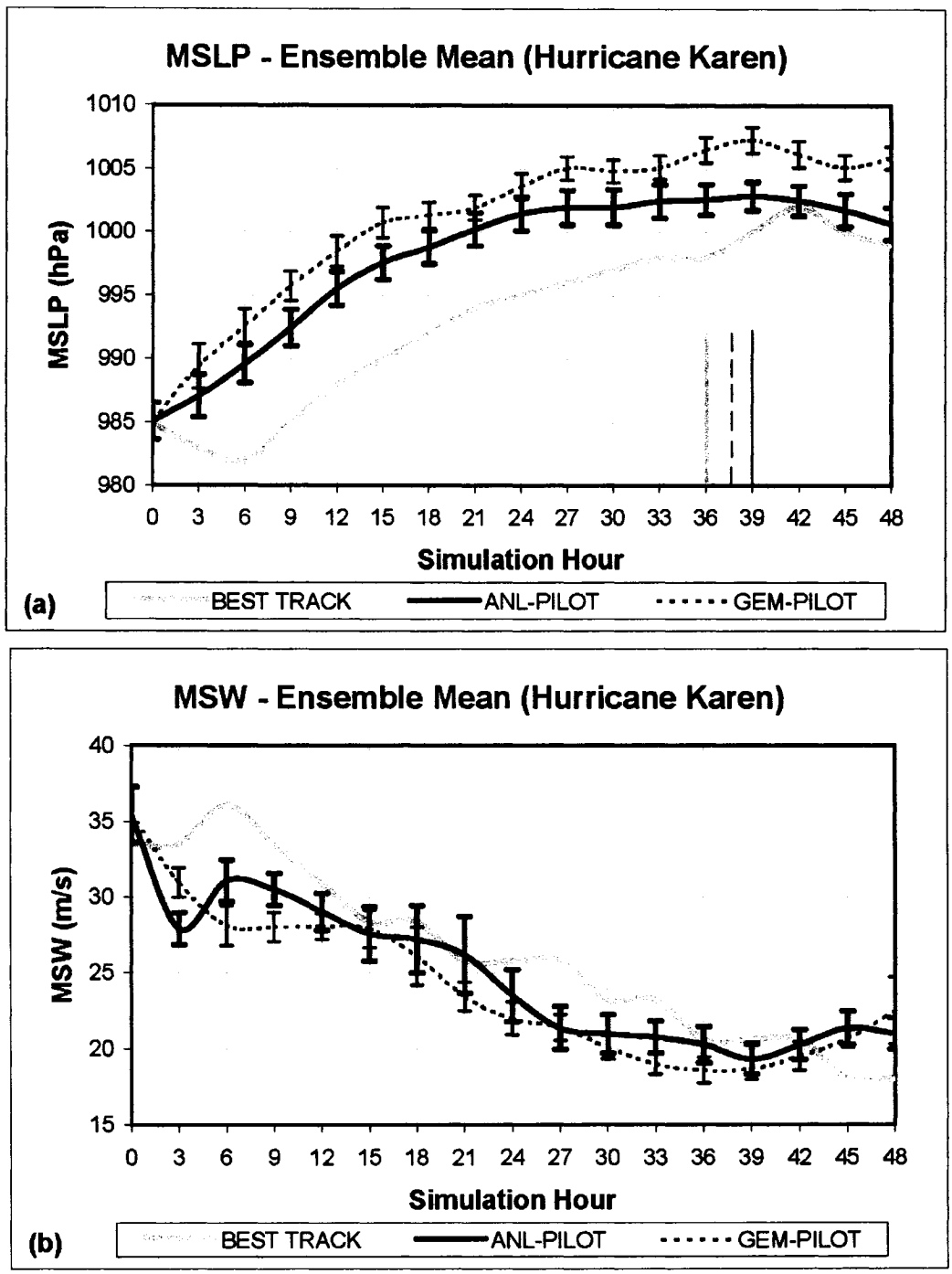

Figure 56. Ensemble mean time series from the boundary condition experiments for Hurricane Karen. Minimum sea level pressure (a), and maximum surface wind (b), for the ensemble means of runs piloted by analyses (ANL-PILOT) (solid black curves) and by GEM forecasts (GEM-PILOT) (dashed black curves) are shown. The best track data are indicated by the grey curve. Vertical range bars denote the one-standard deviation values from the ensemble mean. The vertical bars in (a) denote the mean landfall time for the ANL-PILOT ensemble (thin solid), GEM-PILOT ensemble (thin dashed), and observed landfall time (thick grey).

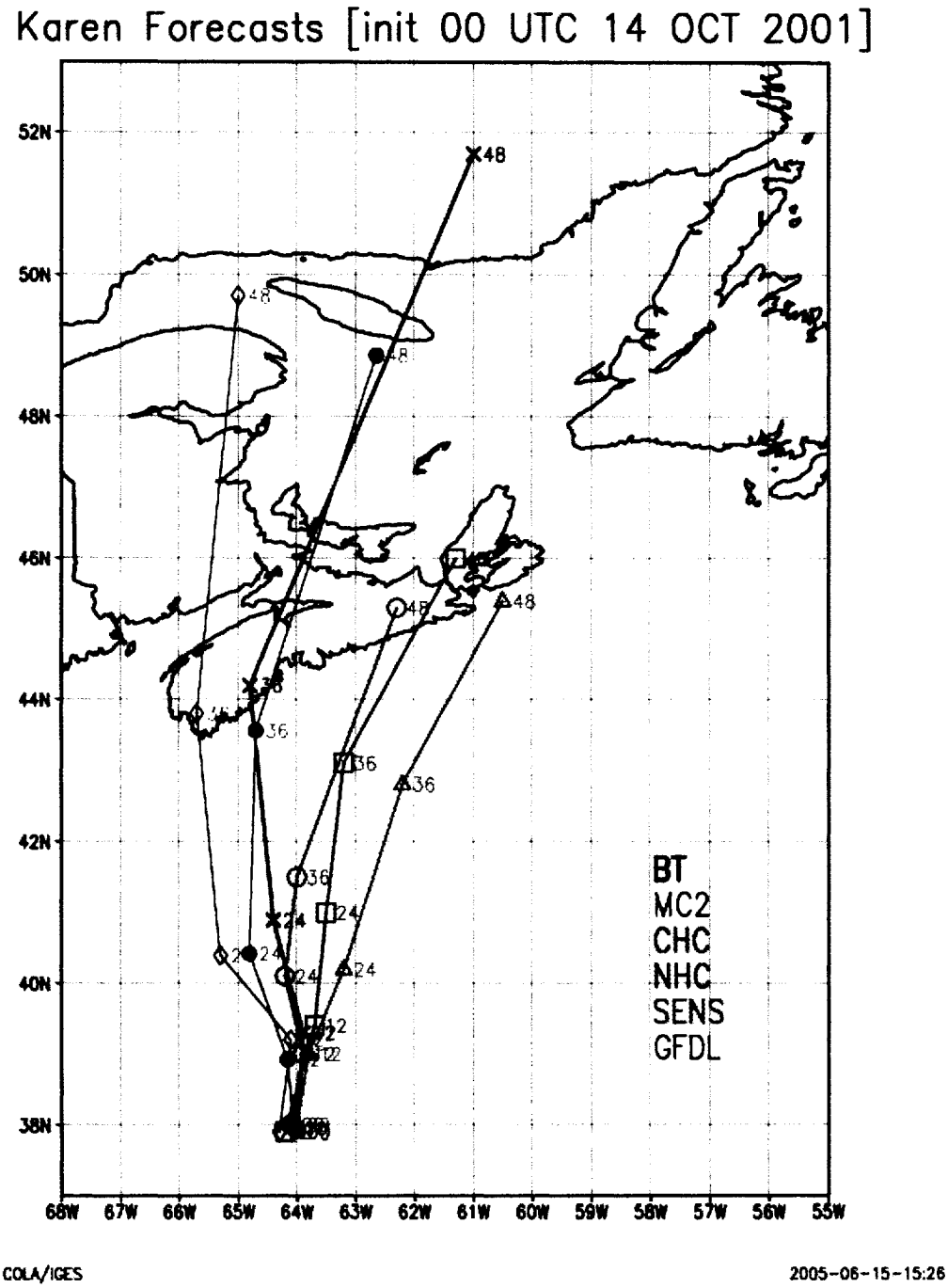

Figure 57. Operational and numerical track forecasts for Hurricane Karen. The time period spans 48 hours beginning 00/14. The acronyms in the legend are defined in the text.

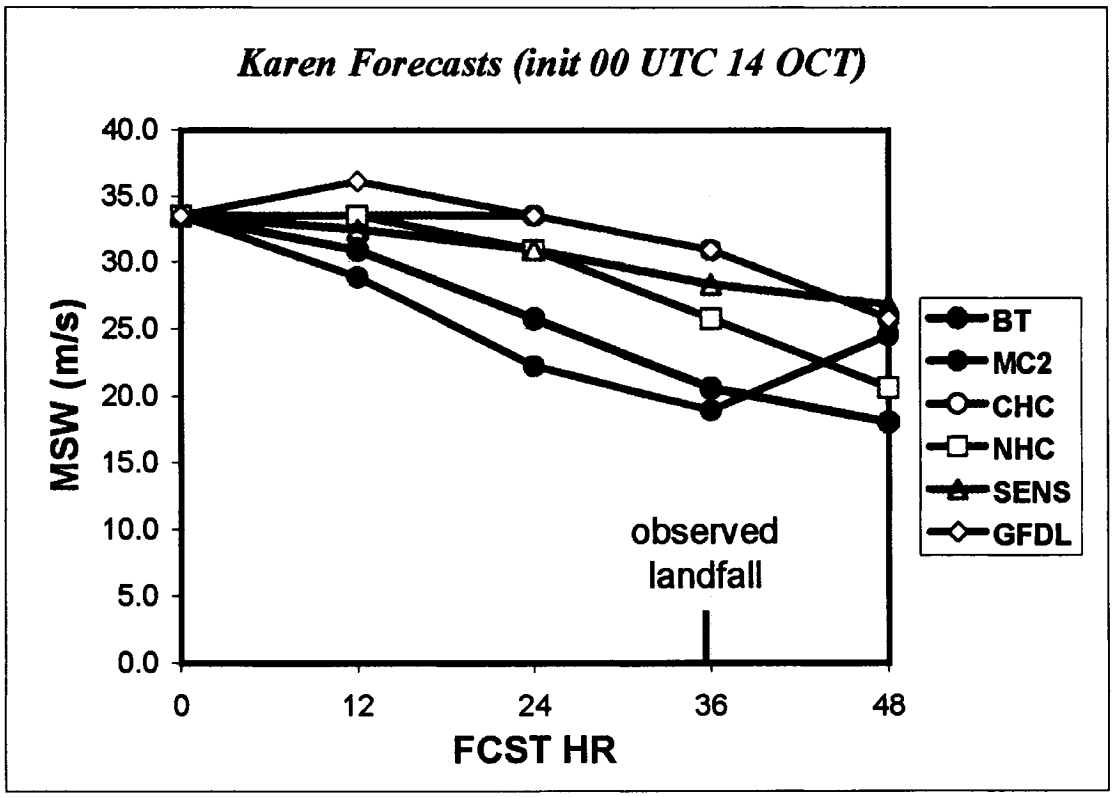

Figure 58. Operational and numerical intensity forecasts for Hurricane Karen. The time period spans 48 hours beginning 00/14. The acronyms in the legend are defined in the text.

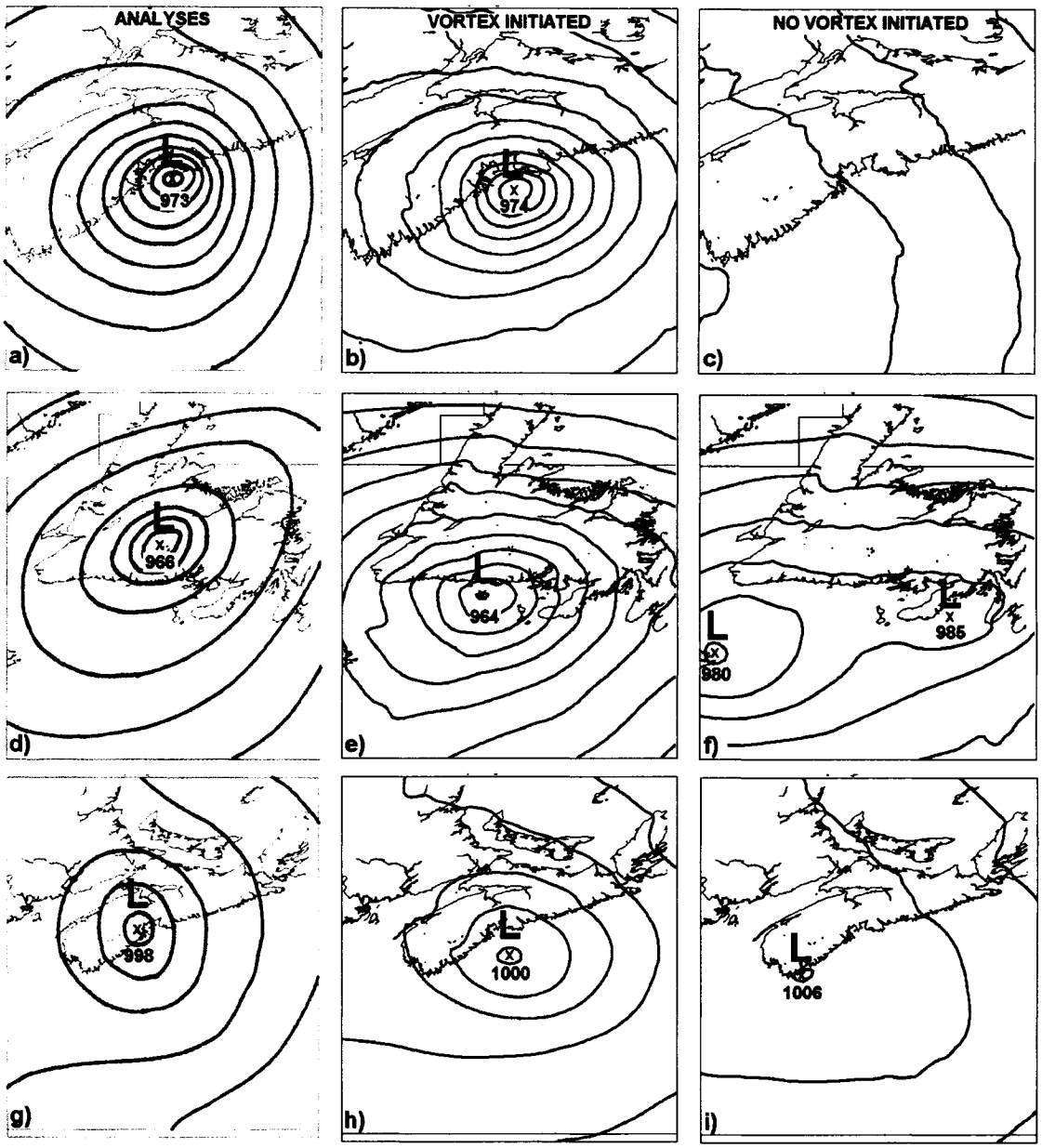

Figure 59. Summary of near-landfall sea level pressure patterns for storms in the study. The subjective analysis for Hurricane Juan is shown in (a), the control run of the model initiated with vortex insertion is shown in (b), and the model run without vortex insertion in the initial conditions is shown in (c). The same comparisons for Hurricane Michael (d-f) and Hurricane Karen (g-i) are also shown. The central pressure of the storm center is shown in hPa and contours of sea level pressure every 4 hPa.

REFERENCES

Abraham, J., W. Strapp., C. Fogarty, and M. Wolde, 2004: Extratropical transition of Hurricane Michael: an aircraft investigation. *Bul. Amer. Meteor. Soc.*, **85,** 323–1339.

Arnott, J. M., J. L. Evans, and F. Chiaromonte, 2004: Characterization of extratropical transition using cluster analysis. *Mon. Wea. Rev.*, **132,** 2916-2937.

Atallah, E. H., and L. F. Bosart, 2003: Extratropical transition and precipitation distribution: A case study of Hurricane Floyd '99. *Mon. Wea. Rev.*, **131,** 1063-1081.

Avila, L. A., 2003: Tropical cyclone report for Hurricane Juan: 24-29 September 2003. NCEP Rep., 14 pp. [Available online at: http://www.nhc.noaa.gov/2003juan.shtml]

Bender, M.A., and I. Ginis, 2000: Real-case simulations of hurricane-ocean interaction using a high-resolution coupled model: effects on hurricane intensity. *Mon. Wea. Rev.*, **128,** 917-946.

Benoit, R., J. Coté, and J. Mailhot, 1989: Inclusion of a TKE boundary layer parameterization in the Canadian regional finite-element model. *Mon. Wea. Rev.*, **117,** 1726-1750.

Benoit, R., M. Desgagné, P. Pellerin, S. Pellerin, S. Desjardins and Y. Chartier, 1997: The Canadian MC2: a semi-Lagrangian, semi-implicit wide-band atmospheric model suited for fine-scale process studies and simulation. *Mon. Wea. Rev.*, **125**, 2382-2415.

Bolton, D., 1980: The computation of equivalent potential temperature. *Mon. Wea. Rev.*, **108**, 1046-1053.

Bowyer, P. J., and A. W. MacAfee, 2005: The theory of trapped-fetch waves with tropical cyclones—an operational perspective. *Wea. and Forecasting*, **20**, 229–244.

Chouinard, C., J. Mailhot, H. L. Mitchell, A. Staniforth, and R. Hogue, 1994: The Canadian regional data assimilation system: Operational and research applications. *Mon. Wea. Rev* ., **122**, 1306-1325.

Colle, B. A., 2003: Numerical simulations of the extratropical transition of Floyd (1999): structural evolution and responsible mechanisms for the heavy rainfall over the northeast United States. *Mon. Wea. Rev.*, **131**, 2905–2926.

Cote, J., S. Gravel, A. Methot, A. Patoine, M. Roch, and A. Staniforth, 1998: The operational CMC-MRB Global Environmental Multiscale (GEM) model. Part I: Design considerations and formulation. *Mon. Wea. Rev.*, **126**, 1373–1395.

Cressman, G. P., 1959: An operational objective analysis system. *Mon. Wea. Rev.*, 87, 367–374

Davidson, N. E., J. Wadsley, K. Puri, K. Kurihara, and M. Ueno, 1993: Implementation of the JMA typhoon bogus in the BMRC tropical prediction system. *J. Met. Soc. Japan*, **71**(4), 437-467.

Davis, C. A., and L. F. Bosart, 2003: Baroclinically induced tropical cyclogenesis. *Mon. Wea. Rev.*, **131**, 2730–2747.

Dvorak, V. F., 1975: Tropical cyclone intensity analysis and forecasting from satellite imagery. *Mon. Wea. Rev.*, **103**, 420–464.

Elsner, J. B., and A. B. Kara, 1999: *Hurricanes of the North Atlantic: Climate and Society*, Oxford, New York, 488 pp.

Emanuel, K. A., C. DesAutels, C. Holloway and R. Korty, 2004: Environmental control of tropical cyclone intensity. *J. Atmos. Sci.*, **61**, 843–858.

Emanuel, K. A., 2005: Increasing destructiveness of tropical cyclones over the past 30 years. *Nature*, **436**, 686-688.

Evans, J. L., and R E. Hart, 2003: Objective indicators of the onset and completion of extratropical transition for Atlantic tropical cyclones. *Mon. Wea. Rev.*, **131**, 909-925.

Fogarty, C. T., and J. R. Gyakum, 2005: A study of extratropical transition in the western North Atlantic Ocean, 1963-1996. *Atmosphere-Ocean*, **43**(2), 173-191.

Fogarty, C. T., R. J. Greatbatch, and H. Ritchie, 2006: The role of anomalously warm sea surface temperatures on the intensity of Hurricane Juan (2003) during its approach to Nova Scotia. *Mon. Wea. Rev.*, in press.

Franklin, J. L., M. L. Black, and K. Valde, 2003: GPS dropwindsonde wind profiles in hurricanes and their operational implications. *Wea. and Forecasting*, **18**, 32–44.

Fritsch, J. M., and C. F. Chappel, 1980: Numerical prediction of convectively driven mesoscale pressure systems. Part I: Convective parameterization. *J. Atmos. Sci.*, **37**, 1722-1733.

Fujita, T., 1952: Pressure Distribution within a Typhoon. *Geophys. Mag.*, **23**, 437-451.

Geshelin, Y., J. Sheng, and R. J. Greatbatch, 1999: Monthly mean climatologies of temperature and salinity in the western North Atlantic. Can. Tech. Rep. Hydrogr. Ocean. Sci. 153: vi+62 pp.

Hart, R. E., and J. L. Evans, 2001: A climatology of the extratropical transition of Atlantic tropical cyclones. *J. Climate*, **14**, 546–564.

Jones, S. C., P. A. Patrick, J. Abraham, L. F. Bosart, P. J. Bowyer, J. L. Evans, D. E. Hanley, B. N. Hanstrum, R. E. Hart, F. Lalaurette, M. R. Sinclair, R. K. Smith, and C. Thorncroft, 2003: The extratropical transition of tropical cyclones: forecast challenges, current understanding, and future directions. *Wea. and Forecasting*, **18**, 1052–1092.

Kaplan, J., and M. DeMaria, 2001: On the decay of tropical cyclone winds after landfall in the New England area. *J. Appl. Meteor.*, **40**, 280–286.

Katsaros, K. B., E. B. Forde, P. Chang, and W. T. Liu, 2001: QuikSCAT's SeaWinds facilitates early identification of tropical depressions in 1999 hurricane season. *Geophys. Res. Lett.*, 28, 1043–1046.

Kain, J. S., and J. M. Fritsch, 1990: A one-dimensional entraining/detraining plume model and its application in convective parameterization. *J. Atmos. Sci*, **47**, 2784-2802.

Klein, P. M., P. A. Harr, and R. L. Elsberry, 2002: Extratropical transition of western North Pacific tropical cyclones: midlatitude and tropical cyclone contributions to reintensification. *Mon. Wea. Rev.*, **130**, 2240–2259.

Klein, P. M., P. A. Harr, and R. L. Elsberry, 2000: Extratropical transition of western North Pacific tropical cyclones: An overview and conceptual model of the transformation stage. *Wea. Forecasting*, **15**, 373-395.

Kong, F., and M. K. Yau, 1997: An explicit approach of microphysics in MC2. *Atmosphere-Ocean*, **35**, 257-291.

Kuo, H. L., 1974: Further studies on the parameterization of the influence of cumulus convection on large-scale flow. *J. Atmos. Sci.*, **31**, 1232-1240.

Ma, S., H. Ritchie, J. R. Gyakum, J. Abraham, C. Fogarty, and R. McTaggart-Cowan, 2003: A study of the extratropical reintensification of former Hurricane Earl using Canadian Meteorological Centre regional analyses and ensemble forecasts. *Mon. Wea. Rev.*, **131**, 1342–1359.

Malkin, W., and G. C. Holzworth, 1954: Hurricane Edna, 1954. *Mon. Wea. Rev.*, **82**, 267-279.

McAdie, C. J., and M. B. Lawrence, 2000: Improvements in tropical cyclone track forecasting in the Atlantic Basin, 1970–98. *Bul. Amer. Meteor. Soc.*, **81**, 989–997.

McTaggart-Cowan, R., J. R. Gyakum, and M. K. Yau, 2001: Sensitivity testing of extratropical transitions using potential vorticity inversions to modify initial conditions: Hurricane Earl case study. *Mon. Wea. Rev.*, **129**, 1617–1636.

———, ———, and ———, 2004: The impact of tropical remnants on extratropical cyclogenesis: Case study of Hurricanes Danielle and Earl (1998). *Mon. Wea. Rev.*: **132**, 1933–1951.

McTaggart-Cowan, R., E. Atallah, J. R. Gyakum, and L. F. Bosart, 2005a: Hurricane Juan (2003). Part II: Forecasting and numerical simulation. *Mon. Wea. Rev.*, in press.

———, ———, ———, and ———, 2005b: Hurricane Juan (2003). Part I: A diagnostic lifecycle study. *Mon. Wea. Rev.*, submitted.

Monin, A. S., and A. M. Obukhov, 1954: Basic laws of turbulent mixing in the surface layer of the atmosphere. *Tr. Geofiz. Inst. Akad. Nauk SSSR*, **151**, 163-187.

Price, J. F., 1981: Upper ocean response to a hurricane. *J. Phys. Oceanogr.*, **11**, 153–175.

Ritchie, E. A., and R. L. Elsberry, 2003: Simulations of the extratropical transition of tropical cyclones: Contributions by the midlatitude upper-level trough to reintensification. *Mon. Wea. Rev.*, **131**, 2112–2128.

Shearman, R. J., 1989: The mathematical representation of wind profiles over the sea. WMO/Tech. Doc. 311, 7 pp.

Simpson, R.H. and H. Riehl (1981): *The Hurricane and Its Impact.* Louisiana State Univ. Press, Baton Rouge (IBSN 0-8071-0688-7), 398 pp.

Stewart, S. R., 2000: Tropical cyclone report for Hurricane Michael: 17-19 October 2000. NCEP Rep., 13 pp. [Available online at: http://www.nhc.noaa.gov/2000michael.html].

Stewart, S. R., 2001: Tropical Cyclone Report for Hurricane Karen: 12-15 October 2001. NCEP Rep., 13 pp. [Available online at: http://www.nhc.noaa.gov/2001karen.html].

Stull, R. B., 1988: *An Introduction to Boundary Layer Meteorology.* Kluwer Academic Pub. (paperback). 666 pp.

Tremblay, A. A., W. Yu, and R. Benoit, 1996: An explicit cloud scheme based on a single prognostic equation. *Tellus.*, **48A**, 483–500.

Williford, C. E., T. N. Krishnamurti, R. C. Torres, S. Cocke, Z. Christidis, and T. S. Vijaya Kumar, 2003: Real-Time multimodel superensemble forecasts of Atlantic tropical systems of 1999. *Mon. Wea. Rev.*, **131**, 1878–1894.

Wolde, M., D. Marcotte, J. Jordan, J. Aitken, J. Abraham, and J. W. Strapp, 2001: The first Canadian experience with research flight operations in hurricane extratropical transition. *Can. Aeronaut. Space J.*, **47**, 179-189.

Zhang, D.-L., and C. Q. Kieu, 2005: Shear-forced vertical circulations in tropical cyclones. *Geophys. Res. Lett.*, **32,** L13822, doi:10.1029/2005GL023146.